Master's thesis

NTNU
Norwegian University of Science and Technology
Faculty of Engineering
Department of Marine Technology

Robert Hanssen

Spatial variations in wave conditions at aquaculture sites

Master's thesis in Marine Technology
Supervisor: Pål Lader
February 2020

NTNU
Norwegian University of
Science and Technology

Robert Hanssen

Spatial variations in wave conditions at aquaculture sites

Master's thesis in Marine Technology
Supervisor: Pål Lader
February 2020

Norwegian University of Science and Technology
Faculty of Engineering
Department of Marine Technology

NTNU
Norwegian University of
Science and Technology

Preface

This Master Thesis has been completed at the Norwegian University of Science and Technology during the autumn semester of 2019. It is a compulsory part of the Master of Science degree, and corresponds to 100 % of the workload of a semester. The Master Thesis is based on measurements done by Synnøve Risting Stemsrud in cooperation with SINTEF Ocean in 2018 for her Master Thesis.

I wish to express my gratitude towards my supervisor, Pål Lader, professor in Aquaculture Technology at the Department of Marine Technology, NTNU, for the guidance provided. I would also like to thank Eirik Svendsen and Jan Tore Fagertun at SINTEF Ocean AS for providing me with relevant data and advice. In addition, I would like to thank Stein Erik Sakshaug and Kyrre Vikestad at Aquastructures AS for helpful advice during this semester.

Abstract

The objective of this Master Thesis is to investigate spatial variations of wave conditions within an aquaculture site and try to determine whether spatial variations might have an effect on the reliability of site surveys done in Norway today. To do this, acceleration measurements of two different fish cages at a fish farm at Hosenøyan will be used to estimate the fish cage elevation responses during the period of measurement. This is done by integrating the measured accelerations twice to estimate the position of the fish cage. The resulting position estimates will further be compared to the incident waves recorded during the period of the measurements, using data from a wave buoy in close vicinity of the fish farm. The resulting data will be analysed and discussed in terms of the significant elevation response, the elevation period and the estimated wave directions. In addition, the validity of linear transfer functions will be investigated. The objective is to determine whether a fish cage can be used as a wave buoy to estimate the local wave conditions at the fish farm using linear transfer functions.

The main findings of this Master Thesis are that spatial variations seem to be present, even though the differences between the two fish cages are relatively small. However the differences seem to grow larger as the surrounding conditions grows harsher, pointing towards that spatial variations may be significant for fish farms at more exposed locations. As for using a fish cage as a wave buoy, the analysis showed no indication that it could be done by applying linear transfer functions. However, for both the estimation of the elevation response of the two fish cages and for the linear transfer function analysis, many large sources of error affected the results, indicating that the results of this thesis may not be reliable themselves.

Abstrakt

Målet med denne Masteroppgaven er å undersøke romlig variasjon av bølgeforhold på et havbruksanlegg, og å prøve å finne ut om romlig variasjon kan ha en effekt på påliteligheten til lokalitetsundersøkelser slik de gjøres i Norge i dag. For å gjøre dette er akselerasjonsmålinger fra to ulike merder på et havbruksanlegg på Hosenøyan brukt til å estimere merdeelevasjonene i måleperioden. Dette er gjort ved å dobbelintegrere akselerasjonsmålingene to ganger for å estimere posisjonen til merdene ved hver måling. Posisjonsestimatene vil videre bli sammenlignet med data fra en nærliggende bølgebøye. Resultatene vil bli analysert og diskutert med tanke på signifikant merdeelevasjon, periode og bølgeretning. I tillegg vil validiteten av å bruke lineære transferfunksjoner bli undersøkt. Her er målet å undersøke om en merd kan brukes som en bølgebøye for å estimere de lokale bølgeforholdene ved å bruke lineære transferfunksjoner.

Hovedfunnene fra denne Masteroppgaven er at romlig variasjon ser ut til å være til stede, selv om forskjellene på de to merdene som er undersøkt er relativt små. Likevel peker resulatene på at disse forskjellene ser ut til å bli større når bølgeforholdene merdene blir utsatt for blir større, noe som indikerer at romlig variasjon kan være signifikant for havbruksanlegg ved mer utsatte områder. Når det gjelder å bruke en merd som en bølgebøye viser analysen ingen indikasjon på at det kan gjøres ved å bruke lineære transferfunksjoner. For både kalkulasjonen av merdeelevasjonene og den lineære transferfunksjonsanalysen er det viktig å poengtere at resultatene er påvirket av mange store feilkilder, noe som kan indikere på at resultatene i denne Masteroppgaven ikke er pålitielige.

Contents

List of Figures

List of Tables

Nomenclature

Symbol	Description	Unit
A_c	Wave crest height	[m]
A_t	Wave trough height	[m]
A_w	Water plane area	$[m^2]$
A_{33}	Added mass in heave	[kg]
B_{33}	Dampening coefficient in heave	$[^{kg}/_{s}]$
C_{33}	Restoring coefficient in heave	$[^{kg}/_{s^2}]$
E	Wave action	$[^{J}/_{m^2}]$
F	Force	[N]
F_e	Effective fetch length	[m]
H	Wave height	[m]
K_r	Refraction coefficient	[-]
K_s	Shoaling coefficient	[-]
M	Mass	[kg]
N	Number of samples	[-]
R	Reflection coefficient	[-]
$S(\omega)$	Wave spectrum	[-]
T	Elevation period	[s]
U	Wind/current velocity	$[^{m}/_{s}]$
α	Angle between wave crest and depth contours	[rad]
ϵ	Error	[-]
η	Fish cage elevation response	[m]
λ	Wave length	[m]
ω	Wave frequency	$[^{rad}/_{sec}]$
ρ	Density	$[^{kg}/_{m^3}]$
θ	Wave direction	[rad]
ζ	Wave elevation	[m]
a	Cross-section radius of a torus	[m]
c	"Large" radius of a torus	[m]

Symbol	Description	Unit
c/c_g	Wave phase/group velocity	$[^m/_s]$
d	Depth	[m]
f	Frequency	[Hz]
g	Gravitational acceleration	$[^m/_{s^2}]$
k	Wave number	$[^{rad}/_m]$
m_n	Spectral moment	[-]
w_a	Amplitude of vertical motion	[m]

Abbreviations

DC . . . . . Direct current

DFT . . . . . Direct Fourier Transformation

FFT . . . . . Fast Fourier Transformation

HDPE . . . . . High Density Polyethylene

IFT . . . . . Inverse Fourier Transformation

IMU . . . . . Inertial Measuring Unit

MEMS . . . . . Micoelectromechanical system

RAO . . . . . Response Amplitude Operator

Chapter 1

Introduction

Seafood has for a long time been an integral part of Norwegian export, and today it is the second largest export only surpassed by oil and gas. By the year 2050 it is estimated by Olafsen et al. (2012) that Norway will produce around 5 million tons of seafood. This will lead to an estimated revenue of about 550 billion kr., roughly six times larger than the revenue today. For the seafood production to reach the estimated levels, it must be expanded and developed. Today the industry is experiencing challenges such as sea lice and fish disease, in addition to a lack of available fish farm locations. The solution for the latter may be to relocate the fish farms to more exposed locations.

Today, a site survey is required before a fish farm can be installed at a location. The site surveys are to be done according to the NYTEK regulations and NS 9415, the standard providing the procedure and criteria for site survey's in Norway. According to Sakshaug (2018), wave measurements are not a common method to use in the aquaculture industry, as the regulations proposes to use wave calculations instead. The sites are required to have a wave calculation for eight compass sectors, and the calculations should indicate wave conditions with a 10 year and 50-year return period. The wave calculations are either based on effective fetch length method or numerical calculations based on wind and bathymetric terrain models.

However, if wave measurements are done, they are usually done at one single point of the site. The main topic of this Master Thesis is to attempt to determine whether one measuring point is enough to reliably describe the wave conditions at an aquaculture site, and discuss whether spatial variations of wave conditions within the site should be considered.

The area of which the aquaculture sites covers is getting larger and larger, possibly covering areas up to 2-3 km^2 according to Stemsrud (2018). Due to the lack of available

sheltered areas, there is a trend in the aquaculture industry of the recent decade that new fish farm sites are relocating to more exposed locations. In exposed areas, the fish farms will be affected by larger environmental forces. If spatial variations are present at sheltered areas, they may be more significantly present at exposed locations. With the current regulations being made while most of the fish farms were located at relatively sheltered areas, the question is raised whether the regulations remain reliable at more exposed areas, and that spatial variations should be considered.

1.1 Background and previous results

As stated, the wave estimations for a specific area are most commonly done by measuring and evaluating wave elevations at one single point. This is the case for data acquisition for both extreme value analysis, and for short- and long-term statistic evaluation. The point where the measurements are done are often determined based on information from a local expert of the area. This is according to NS 9415:2009 a valid way of determining the point where the wave exposure is assumed to be the strongest.

In the Master Thesis by Stemsrud (2018) a literature study was done about the topic of spatial variations of met-ocean phenomena. Below, some of her findings are mentioned and commented, in addition to other comments on the topic:

- Bruserud & Haver (2017) states that it is important to assess and quantify all types of uncertainties related to the estimated environmental design conditions if possible, as they will impact both the accuracy and the reliability of the extreme environmental forces of a marine structure.

- In a paper by Forristal (2011) a point was made that the maximum wave crest from a grid of wave measurements is larger than a single-point average maximum. According to the paper, the difference between multidimensional and single-point estimates would decrease as the waves became long-crested, but even then, the area maximum was 10 percent greater than point-extremes. In addition, it was proven that linear theory agrees well with measurements in a wave basin.

- When analyzing space-time wave extremes, Barbariol et al. (2015) stated that estimations of wave extremes should be done by assuming a multidimensional wave field for short crested waves. The difference between wave extremes and significant wave height (H_s) was reduced by increasing wind speeds and by depth-induced shoaling. H_s would increase as waves travelled to shallower waters, which counteracted extreme wave heights. An important note from this paper was the fact that

when enlarging the area analyzed, the difference between maximum wave height and H_s was increased. As the current trend in aquaculture is that the sites grow larger, Stemsrud (2018) points out that this effect can possibly be expected to be significant in future site surveys.

- Faltinsen & Shen (2017), in a paper describing the wave and current effects on floating fish farms, also points out that many realizations of a sea state are required to obtain reliable estimates of extreme values in a stochastic sea. They further state that many net cages operate in close vicinity, which raises questions about spatial variations of the current and wave environment as well as hydrodynamic interaction between the net cages. For instance, upstream cages modify the incident current to downstream cages.

Despite thorough searching in this literature study, no actual experiment of the spatial variations of the wave or current conditions at an aquaculture site has been found. Nevertheless, there are a sufficient number of papers that suggests this topic being investigated further.

Previous work and results by Stemsrud (2018)

The acceleration data this thesis is based on were obtained by Synnøve Risting Stemsrud for her Master Thesis in 2018. Due to practical issues related to the full-scale measurements, her work was not finished, and only effects of filtering and spatial variation of energy content in linear acceleration were analyzed. Despite this, some preliminary results were found involving spatial variation in wave energy, by analyzing the results in a power spectrum:

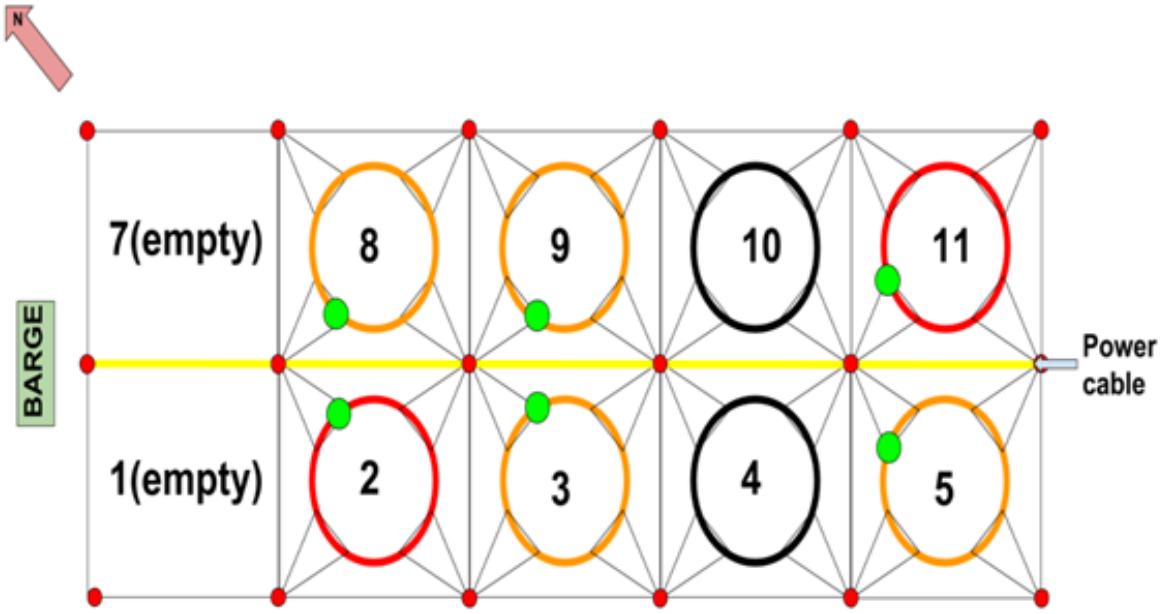

Figure 1.1.1: Illustration and numbering of the fish farm investigated by Stemsrud (2018). IMU position are marked with green dots

- The overall mean energy content in spectra of the fish cages were dissimilar
- Fish cage 9 had a magnitude of fluctuation deviant from fish cages 8, 5 and 3.
- Significant periodic peak values are seen for fish cage 8 and 9 and smaller periodic peaks are also visible for fish cage 3.

The results from Stemsrud (2018), indicates that that fish cage 3 and 5 had the wave spectra with lowest and second lowest energy content. This is the case even though they were the fish cages that the waves coming from South West would encounter first, which is the assumed direction of the main part of the waves. According to Stemsrud (2018), the bathymetry was reported to be relatively constant across the fish farm. This would imply that the wave height should not be significantly elevated when waves propagated from one end of the fish farm to the other due to shoaling.

Stemsrud (2018) draws no conclusion of the effects of spatial variations of the wave conditions from her preliminary results, but states that the measurements suggest that it should be investigated further. This Master Thesis will attempt to do that.

1.2 Problem description

The objective of this master thesis is to investigate spatial variations in wave conditions at an aquaculture site. If the spatial variations are significant, this could affect the reliability of site survey's as they are done today, where wave conditions are usually only determined at one point of the aquaculture site. To do this, acceleration measurements from two different fish cages at an aquaculture farm at Hosenøyan will be evaluated. Only measurements of the acceleration in heave will be analysed. In addition, the validity of using the fish cage as a wave buoy to estimate the wave conditions assuming linear transfer functions will be investigated. The following main tasks are to be done:

- Literature study on estimating the motion of the fish cages by integrating the acceleration measurements twice, and treatment of the resulting data due to noise and drift of the measurements and as a consequence of the integration.
- Determine the fish cage elevation response in heave η_3 and corresponding elevation period T_z which will be compared with wave buoy data of the same area. This is to be done both by calculating the zero-th moments of a wave spectrum and by estimating the parameters directly from the estimated fish cage elevation response data.
- Analysis and discussion of the elevation response estimates with regards to period, height and direction of the incident waves.
- Investigate the validity of linear transfer functions, by comparing the estimated fish cage elevation responses with data from the wave buoy.
- Make proposal for further work.

Chapter 2

Site surveys in Norwegian aquaculture

In this chapter, the laws and regulations in Norwegian aquaculture will be presented and discussed, with the focus being on investigating the procedures of a site survey in Norway. To do this, the general legislative structure will be investigated first, leading to the regulations relevant for site survey's of aquaculture sites. Some of the content of this chapter is based on the project thesis done in spring 2019.

2.1 Regulations in Norwegian aquaculture

2.1.1 The Aquaculture Act

Since the rapid development of Norwegian aquaculture started in the early 1970's, regulations were deemed necessary. As a consequence it was decided to implement a responsible licensing system in the industry. This lead to the Fish Farming Act being established. In January 1. 2006, the Fish Farming Act was replaced by the Aquaculture Act, made by the then called Ministry of Fisheries and Coastal Affairs, today referred to as the Ministry of Trade, Industry and Fisheries.

The Aquaculture act has four focus areas:

- Growth and innovation in the industry
- Simplification for the industry and public administration
- The environment
- Efficient land and area utilisation

According to Norwegian Ministry of Trade, Industry and Fisheries (2005a), the purpose of the Aquaculture act is to enhance the profitability and competitiveness of the aquaculture industry, while ensuring a sustainable development of the industry along the coast of Norway. The Norwegian Food Safety Authority ensures that Norwegian fish farming are in agreement with the relevant animal welfare regulations, in addition to help prevent the spread of fish-related diseases should a fish farm have an outbreak.

Obtaining aquaculture licenses

According to the Aquaculture Act, a license is required before any aquaculture activities can begin. The process of approving a license is a decision made by the relevant authorities, as described in Figure 2.1.1:

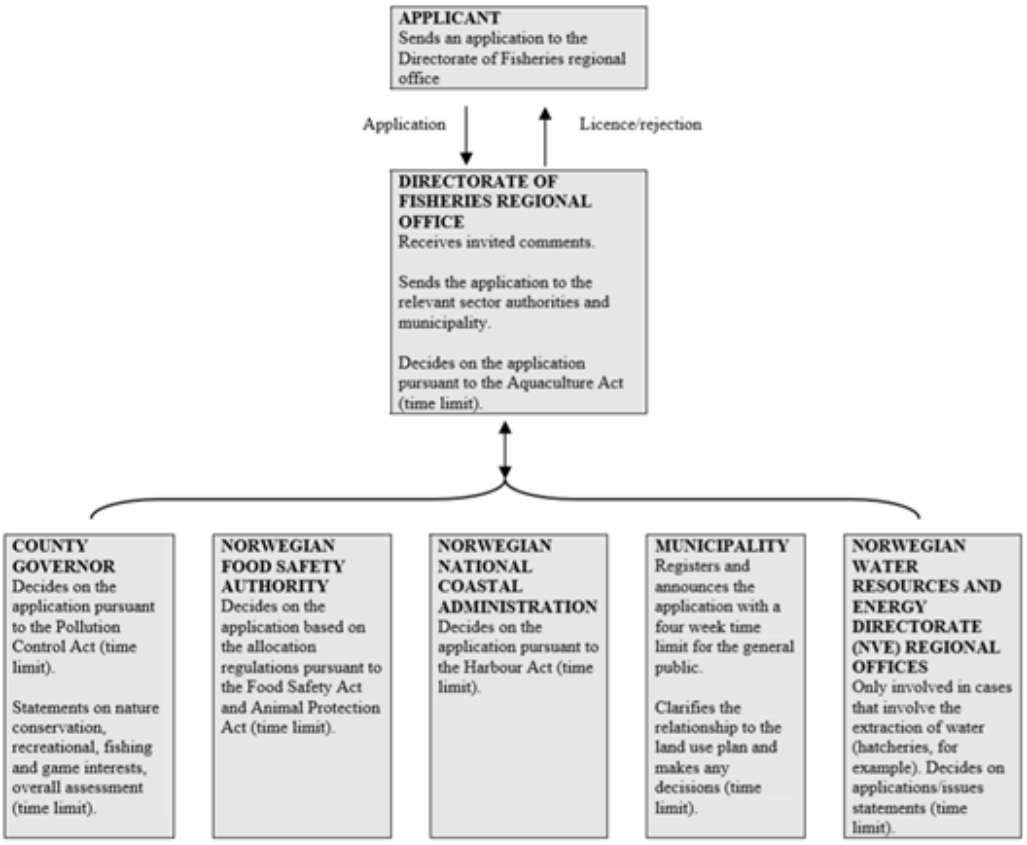

Figure 2.1.1: Processing of aquaculture applications. Source: Norwegian Ministry of Trade, Industry and Fisheries (2005a)

The applicant of the licence only have to send an application to the Directorate of Fisheries, Regional Office, who will then send the application to the other relevant authorities for processing of the application. The reason for this is according to Norwegian Ministry of Trade, Industry and Fisheries (2005a) to ensure optimal coordination of the application

process by ensuring that the individual applicant only has to deal with one government agency as far as this is possible. The fisheries authorities will ensure that decisions from the local municipality, as well as sector authorities like the environmental authorities (County Governor), Norwegian Food and Safety Authorities and Norwegian National Coastal Administration are filed. In the case of water extraction processes, which are needed for instance for land-based hatcheries, the Norwegian Water Resources and Energy Directorate will also be involved.

According to Norwegian Ministry of Trade, Industry and Fisheries (2005a), the aquaculture license can be viewed as a set of rights to produce specific species, in a specific quantity, at specific sites, but also with obligations to ensure that the regulations are being followed. The Ministry of Trade, Industry and Fisheries provides with the Aquaculture Act a licensing system where the individual licenses are combined with general regulations. This means that if the individual applicant have special circumstances that needs to be addressed, this can be regulated in detail for the individual applicant.

In addition, Norwegian Ministry of Trade, Industry and Fisheries (2005a) states that a license requirement is deemed necessary to make sure that the administration have control over the social and environmental considerations, optimal use of the coastal zone of Norway, and the distribution and scarcity considerations revolving the aquaculture industry.

Transferring of licences

The Aquaculture Act enlists the right to transfer aquaculture licenses, following a practice providing an opportunity for licences to be reallocated by application. This is provided that the allocation of the licence does not lead to change of the regulations of the previous owner. This is done by ensuring that the regulations and conditions of the previous holder still is regulatory for the new holder. In practice this means that this is a continuation of a licence rather than a new licence. Furthermore, Norwegian Ministry of Trade, Industry and Fisheries (2005a) states that the transfer of an aquaculture licence will in practice be viewed as the previous holder's request for a transfer, rather than the opportunity to transfer.

Transferring of licences can be done by a closed or open bidding round, indicating a marked determined payment. This usually means that obtaining an aquaculture licence through reallocation is much more expensive for an enterprise compared to getting a new licence granted by the Ministry of Trade, Industry and Fisheries.

2.1.2 The NYTEK regulations

The NYTEK regulations have been implemented since 2006 together with the technical standard NS 9415 to prevent the escape of fish, which is an important issue concerning Norwegian aquaculture. The objective of NYTEK, stated in Norwegian Ministry of Trade, Industry and Fisheries (2005b), is to prevent fish escapes by ensuring that the fish farms themselves and the fish farm equipment are according to NS 9415. The NYTEK regulations are issued by the Ministry of Fisheries and Coastal Affairs, which is the ministry that is responsible for making any amendments to the regulations.

The Directorate of Fisheries is responsible for the enforcement of the regulations, which according to Norwegian Ministry of Trade, Industry and Fisheries (2005b) can be divided in three main tasks in this context:

- Supervising that the requirements in the NYTEK regulations are followed. This is done primarily through system audits based on internal control.
- Answering questions concerning the interpretation of the regulations from industry, participants etc.
- Deciding on applications that due to special circumstances can not follow all the requirements in the regulations.

According to Norwegian Ministry of Trade, Industry and Fisheries (2005b), it is clearly stated in the NYTEK regulations that a site classification must be done in order to install a fish farm at the location. In the site classification the local wind, current and wave conditions are to be evaluated according to the procedures described in NS 9415 and the NYTEK regulations.

Certification and competent bodies

Norwegian Ministry of Trade, Industry and Fisheries (2005b) describes certification as a documentation from an independent third party (i.e. a certification body), confirming that a product or a management system is according to the governing requirements. The classification of the site governs the dimensions the main components of the fish farm shall have. Norwegian Accreditation accredits certification and inspection bodies, who performs inspections and certification according to the NYTEK regulations.

The procedure and criteria for classification are stated in NS 9415. Such classification shall be performed by a competent body, or an accredited inspection body. A competent

body is a body that can present the relevant professional qualifications to the client and be independent of the client. There is no requirement that the competent body shall be accredited or certified.

It is the fish farmers themselves who hire a competent body to classify the site, meaning that the fish farmers themselves must ensure that the body they hire meets the requirements for being a competent body.

2.2 Trends and challenges in Norwegian aquaculture

2.2.1 Economic trends

Since the start of the millennia, Norwegian aquaculture have experienced an increase in both production numbers, export value and the price of salmon, where the latter has changed according to Statistics Norway (2019) and Figure 2.2.1 from around 35 NOK/kg in the early 2000's to around 58 NOK/kg in 2019. However, since around 2016, the development has slowed down due to the challenges the aquaculture industry is facing today.

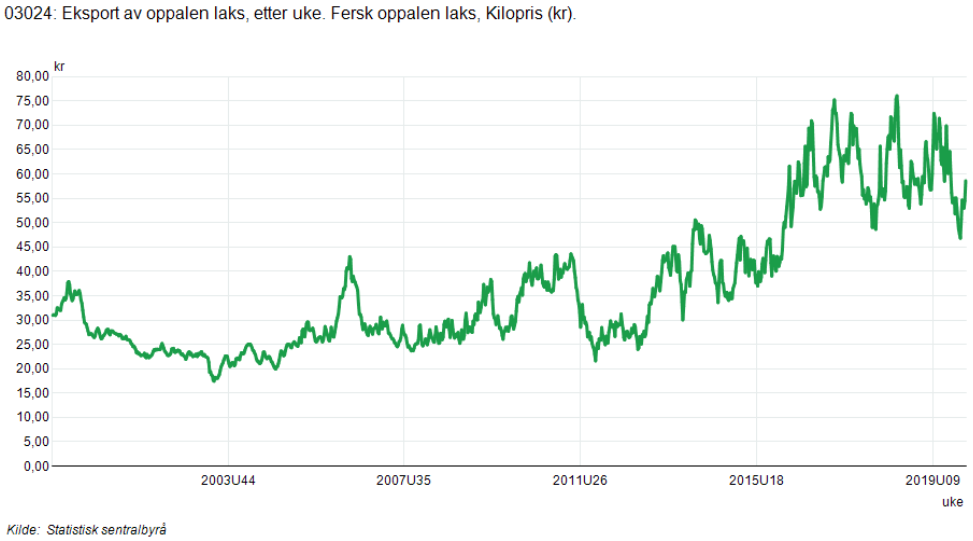

Figure 2.2.1: Weekly price/kg of fresh salmon from 2000 to 2019. Source: Statistics Norway (2019)

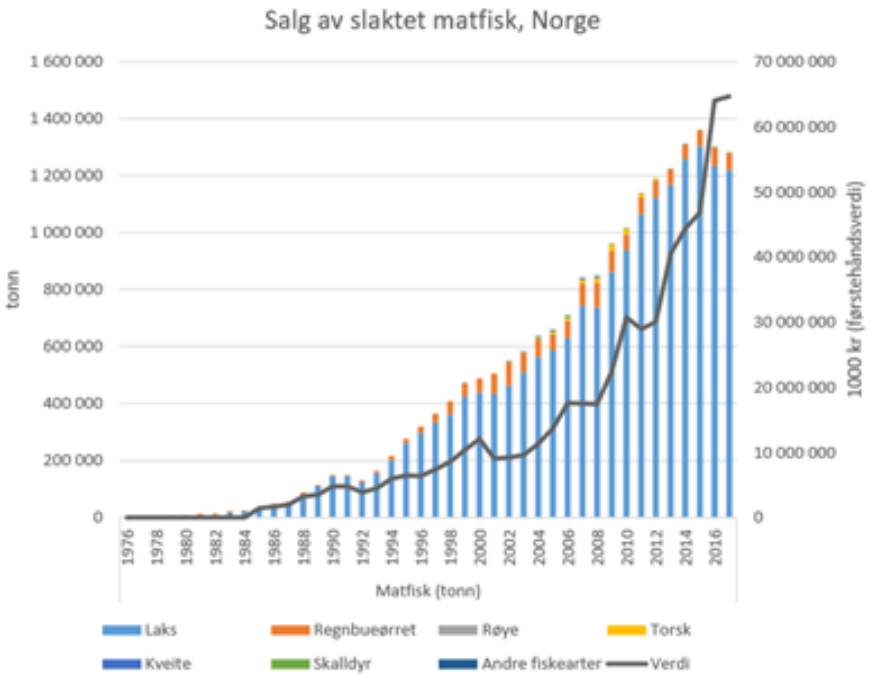

Figure 2.2.2: Sale of slaughtered fish in Norway from 1976 to 2017. Source: Ministry of Trade, Industry and Fisheries (2018)

Olafsen et al. (2012) estimated that by the year 2050 Norway will produce around 5 million tons of seafood. This will lead to an estimated revenue of about 550 billion kr., roughly six times larger than today. The estimate assumes that that the current challenges in aquaculture, for instance sea lice, fish disease and area issues are solved.

2.2.2 Research in the industry

Development licences

Due to the present challenges in Norwegian aquaculture regarding for instance fish disease, salmon lice and area issues, the Norwegian Ministry of Trade, Industry and Fisheries issued a temporary arrangement of development licences. According to Norwegian Directorate of Fisheries (2016), the idea was to encourage technological development of the aquaculture industry to cope with the aforementioned challenges. This arrangement was open for application from November 20 2015 to November 17 2017. In this time span, a total of 104 different projects were submitted, consisting of 898 licences. Hagen (2019) reported that only eleven different projects was approved, which consisted of 68 licences. Figure 2.2.3 displays some of the approved development projects.

Figure 2.2.3: Image of some of the approved development projects. Top left: "Ocean Farm 1" by Salmar, top right "Aquatraz" by Midt Norsk Havbruk, in the middle: "Egget" by Marine Harvest (MOWI)/Hauge Aqua, bottom left: "Havfarm 1" by Nordlaks, bottom right: "Arctic Offshore Farming" by NRS/Aker ASA. Source: (Ministry of Trade, Industry and Fisheries 2018)

Exposed/offshore aquaculture

One of the ideas to handle the area issue of the aquaculture industry could be to move the fish farms from sheltered areas towards more open ocean areas. These are areas exposed to harsher environmental conditions, in addition to making day to day operations more difficult. To solve the problems of aquaculture at such areas, SINTEF Exposed, a center for research and inovation for fish farming at exposed locations, was created. The research is divided into six subareas, according to SINTEF EXPOSED (2018):

- Autonomous systems and technologies for remote operations
- Monitoring and operational decision support
- Structures for exposed locations
- Vessel design for exposed operations
- Safety and risk management
- Fish behaviour and welfare

2.3 NS 9415:2009

NS 9415:2009 contains requirements for the physical design of the installation of a fish farm and the associated documentation. This includes calculation and design rules, as well as installation, operating and maintenance requirements. The purpose of the standard is, according to Standard Norway (2010), to reduce the risk of fish escape as a result of technical failure of the fish farm structure or in the form of unsatisfactory operation of the fish farm. To ensure this, the standard sets requirements for the aquaculture structure, as well as parameters used to indicate the natural conditions of the aquaculture site. Most relevant for this thesis is chapter 5 of NS 9415:2009, which describes the regulations and guidelines for site surveys. The chapter contains parameters and recommended methods for the survey in addition to descriptions of the environmental loads on an aquaculture site, based on topography and degree of exposure.

Due to the fact that a site surveys are required before any installations take place on an aquaculture site, it is important to have an understanding of how NS 9415:2009 is used to classify an aquaculture site. Despite that NS 9415:2009 have no requirement for evaluation of spatial variation of the environmental loads, it still forms the basis for any calculation that previously is done to evaluate a fish farm site. If spatial variations should have an impact on the reliability of site surveys, it is reasonable that this standard should be a reference point in order to determine what the degree the deviance might be.

2.3.1 Methods for estimating the wave conditions according to NS 9415

The environmental loads that affects a floating fish farm can be divided into wind loads, wave loads and current loads. The wave loads acts primarily on the floating collar and the upper parts of the net cage. The current load is estimated to cause the largest environmental load on the fish farm according to Fredheim & Langan (2009), where it acts on both the floating collar and the mooring grid below the surface, depending on the length of the mooring lines. The wind loads acts on the upper parts of the fish farm. According to F. Cardia and A. Lovatelli (2015), the following rough distribution of the loads on a typical mid-sized fish farm can be estimated:

- Wave loads accounts for approximately 20 to 25 % of the total forces.
- Current loads accounts for 70 to 75 % of total forces.
- Wind loads represents about 5 to 10 % of the total forces.

In this master thesis, the main focus will be the wave conditions of an aquaculture site. According to Stemsrud (2018), there are two different methods of calculating the wave conditions at an aquaculture site that stands out in site surveys today. These methods are the effective fetch length method and modelling the waves using SWAN. Below, the general idea of these methods will be described.

Effective fetch length method

To calculate the wind-induced waves, the NS 9415:2009 suggests calculation based on effective fetch length. According to chapter 5.4.2 in NS 9415:2009 by Standard Norway (2010), wind-induced waves shall be calculated based on wind data from meteorological stations and the effective fetch length F_e, most often measured on an electronic sea chart.

The calculation of the adjusted wind velocity U_A is done according to Equation 2.3.1 by using the wind velocity $U_{10}[^m/_s]$:

$$U_A = 0.71 \cdot U_{10}^{1.23} \tag{2.3.1}$$

Here, U_{10} refers to the average wind at 10 m height. Significant wave height H_s and peak period T_p as a function of effective fetch length F_e is then given as described in Equation 2.3.2:

$$\begin{aligned} H_s &= 5.112 \cdot 10^{-4} U_A F_e^{1/2} \\ T_p &= 6.238 \cdot 10^{-2} (U_A F_e)^{1/3} \end{aligned} \tag{2.3.2}$$

An example of calculating the effective fetch length is to apply Equation 2.3.3, as demonstrated in a site survey done by Noomas Sertifisering AS (2013) at Kråkøya in Trøndelag.

$$F_e = \frac{\sum_{i=-60}^{i=60} R_i \cos^2 \alpha_i}{\sum_{i=-60}^{i=60} R_i \cos^2 \alpha_i} \tag{2.3.3}$$

Here R_i is the fetch length per sector line for angle α_i between ± 60 degrees for each of the directions the wave is calculated for. In this case, the waves were calculated for every 45 degrees as required by Standard Norway (2010) in NS 9415:2009. The sector line angles are 6 degrees, which is well within the demands from NS 9415:2009 of angle openings of maximum ± 12 degrees.

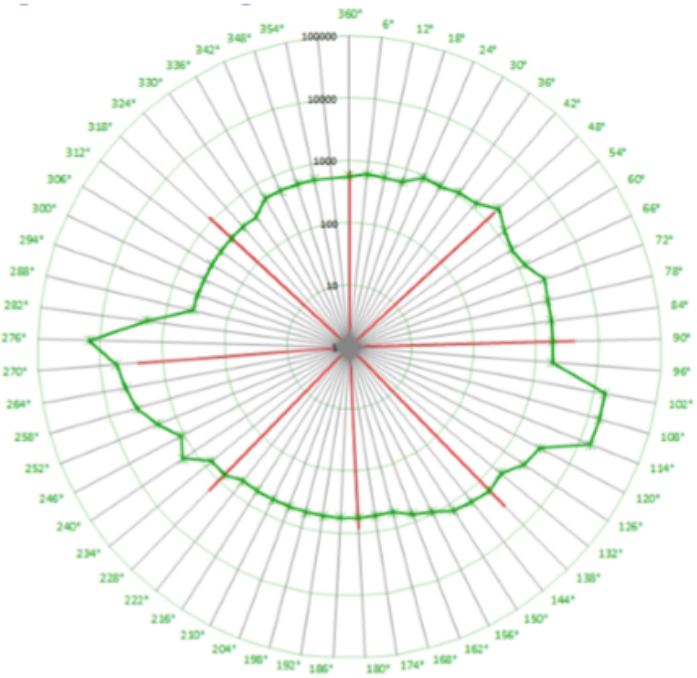

Figure 2.3.1: Fetch length analysis angle sectors (Noomas Sertifisering AS (2013)

The fetch length is referred to as the distance from the point where the wind-induced waves are to be determined, to the nearest land calculated in the wind direction. The effective fetch length is dependent on the width of the fetch and can therefore be calculated significantly less than measured. An example for this, according to Standard Norway (2010), can occur if the aquaculture site is located near narrow fjord arms.

SWAN

Another frequently used method to estimate the environmental conditions at a fish farm location is SWAN, which is a wave model developed at Delft University of Technology in the Netherlands. The model computes short-crested wind-generated waves in coastal regions and inland waters. It is the second most used method for determining wave conditions at Norwegian aquaculture sites, according to Stemsrud (2018).

Unlike the effective fetch length method, SWAN takes wave transformation effects into account, by having the local bathymetry as one of the inputs. In addition, SWAN utilizes a wave spectrum, like the JONSWAP spectrum and hindcast data of the local environmental conditions, to create short-crested wave spectra and the corresponding wave parameter estimations for the chosen area. According to the SWAN user manual by Delft University of Technology (2019), SWAN obtains realistic estimates of wave properties in coastal areas, making it a good fit for determining the wave conditions in relation to site surveys. However, it is pointed out that it is not a very efficient model to use at open ocean areas.

Shortcomings of NS 9415:2009

According to Kristiansen et al. (2017) there is some concern that NS 9415:2009 does not adequately describe how to obtain estimations of environmental loads. Only the fetch length analysis is described thoroughly in the standard, which is deemed unfit for estimating wave conditions for sites at open ocean areas, where the fetch lengths can grow too great for them to be applicable in the method. In addition, Stemsrud (2018) points out that fetch length analysis is not applicable for the determination of ocean swells, should they occur at an aquaculture site. NS 9415:2009 proposes three possible alternatives for determining wave height and wave period of swells:

- Diffraction and refraction analysis
- Measurements
- Other method which is deemed fit

The most common way to determine wave height and period is by doing calculations. If the parameters are decided based on measurements, they will be dependent on statistical models. According to Bore & Amdahl (2017), NS 9415:2009 does not mention any statistical treatment method of the measured values, leading to uncertainty in the calculated return periods due to the influences of seasonal variance and variance of measuring period.

NS9415:2009 requires documentation of waves, wind and current in at least 8 concurrent directions. This means that fetch length must be indicated in at least 8 directions when applying fetch length analysis to estimate wind-waves. Aquaculture sites features large variation in fetch length due to complex bathymetry and topography. This causes much larger directional dependency of sea state characteristics than what is typical at open ocean sites. Bore & Amdahl (2017) stated that a model including directional variation of waves describes extremes much better than one excluding directions for wave conditions at aquaculture sites.

However, there are reports that NYTEK and NS 9415 are currently (2019) under revision. The revision will include methods for extreme value analysis evaluated for current determination, wave calculation methods will be described more thoroughly, in addition to being more adjusted to the new types of aquaculture installations that will occur. The new revision of NS 9415 is reported to be finished towards the end of 2019/early 2020, according to Fiskeri-og havbruksnæringens forskningsfinansiering (2018) and Ministry of Trade, Industry and Fisheries (2018).

Chapter 3

Wave conditions in coastal areas and fish cage behaviour in waves

In this chapter, the relevant wave theories and equations used to estimate the wave conditions at Hosenøyan will be presented. The effects that occurs to waves propagating towards the coastline will be investigated. In addition, fish cages in general and the dynamics of fish cages in waves will be investigated.

3.1 Classifications of wave theories

Waves as a process are considered irregular and random in terms of both wave height, wave length and wave velocity. A consequence of this is according to DNV GL (2017) that a real sea state will be best described as a random stochastic model. Wave models are usually divided into linear and non-linear wave models:

- A linear wave model is a sum of linear wave components with different amplitude, frequency and direction.
- A non-linear wave model will allow sum and difference of frequency wave components caused by non-linear interactions between the different individual wave components.

To describe waves, several different wave parameters can be used. For this thesis, the main topic will be on the wave height H, the wave period T and the wave direction θ. From these parameters, other wave parameters such as the wave length λ, wave frequency $\omega = 2\pi f$, wave number $k = {}^{2\pi}/_{\lambda}$ and wave steepness s can be derived.

3.1.1 Linear wave theory

The simplest wave theory is obtained by assuming the wave height to be much smaller than both the wave length and the water depth. This theory is often referred to as linear wave theory or Airy theory. Using the recommended practice from (DNV GL (2017), the main resulting parameters assuming this theory can be assumed as described below.

For regular linear waves the wave crest height A_c is equal to the wave trough height A_t and is denoted the wave amplitude A, hence $H = 2A$. The surface elevation is given by:

$$\zeta(x, y, z) = \frac{H}{2} cos\Theta \tag{3.1.1}$$

where $\Theta = k(xcos\theta + ysin\theta) - \omega t$ is the phase and θ is the direction of propagation, measured from the positive x-axis.

The dispersion relationship gives the relationship between wave period T and wave length λ. For linear waves in finite water depth d, it is given according to Equation 3.1.2:

$$\lambda = \frac{g}{2\pi} T^2 \tanh(\frac{2\pi d}{\lambda}) \tag{3.1.2}$$

By implementing the angular frequency $\omega = \frac{2\pi}{T}$ and the wave number $k = \frac{2\pi}{\lambda}$ the dispersion relation can be written according to Equation 3.1.3:

$$\omega^2 = gk \tanh(kd) \tag{3.1.3}$$

For linear waves, the phase velocity c only depends on wave length λ, and is therefore independent of the wave amplitude A. The phase speed can be described according to Equation 3.1.4:

$$c = \frac{\lambda}{T} = \frac{\omega}{k} = \sqrt{\frac{g\lambda}{2\pi} \tanh(\frac{2\pi d}{\lambda})} \tag{3.1.4}$$

Shallow water assumptions

In shallow water, where $\frac{d}{\lambda} \leq 0.04$, the factor $\tanh kd$ in the dispersion relationship can be assumed to limit $\tanh kd \rightarrow kd$, resulting to the equations for the dispersion relation and the wave length being simplified into Equation 3.1.5:

$$\begin{aligned} \omega^2 &= gk^2 d \\ \lambda &= \sqrt{gT^2 d} \end{aligned} \tag{3.1.5}$$

Deep water assumptions

For deep water $d > \frac{\lambda}{2}$, $\tanh kd \rightarrow 1$, meaning that the equations for the dispersion relation, the wave length and phase speed can be simplified according to Equation 3.1.6:

$$\begin{aligned} \omega^2 &= kg \\ c &= \sqrt{\frac{g\lambda}{2\pi}} = \frac{g}{\omega} = \frac{gT}{2\pi} \\ \lambda &= \frac{gT^2}{2\pi} \end{aligned} \tag{3.1.6}$$

3.1.2 Stokes wave theory

The Stoke wave theory is a non-linear wave theory that can be seen as an expansion of the linear wave theory. A first order Stoke wave is identical to an Airy wave, but for a second order Stoke wave for instance, the wave elevation is multiplied with an additional factor as shown in Equation 3.1.7 :

$$\zeta = \frac{H}{2}\cos\Theta + \frac{\pi H^2}{8\lambda}\frac{\cosh kd}{\sinh^3 kd}[2 + \cosh 2kd]\cos 2\Theta \tag{3.1.7}$$

where $\theta = k(x\cos\beta + y\sin\beta) - \omega t$

Apart from the first order Stoke wave, the wave crest A_c is larger than the wave trough A_t. In addition, wave crests are steeper, and wave troughs are wider, compared with an Airy wave. According to DNV GL (2017) the the crests and troughs for a second order Stoke wave are given according to Equation 3.1.8:

$$\begin{aligned} A_c &= \eta(\Theta = 0) = \frac{H}{2}(1 + \frac{\pi H}{2\lambda}) \\ A_T &= \eta(\Theta = 0) = \frac{H}{2}(1 - \frac{\pi H}{2\lambda} \end{aligned} \tag{3.1.8}$$

DNV GL (2017) states that the linear dispersion relation holds for a Stoke wave as well, meaning that the wave length λ remain independent of the wave height.

3.1.3 Application limits

To determine which theory to apply on the measurements at Hosenøyan, three different dimensionless parameters can be combined to indicate the validity of the different theories. These dimensionless parameters are the the wave steepness parameter s, shallow water parameter μ and Ursell number U_r, which are calculated as shown in Equation 3.1.9 according to DNV GL (2017):

$$\begin{aligned} s &= 2\pi\frac{H}{gT^2} = \frac{H}{\lambda_0} \\ \mu &= 2\pi\frac{d}{gt^2} = \frac{d}{\lambda_0} \\ U_r &= \frac{H\lambda^2}{d^3} \end{aligned} \tag{3.1.9}$$

λ_0 refers to the wave length at deep waters.When the parameters are calculated, Figure 3.1.1 can be used to determine the validity of a theory:

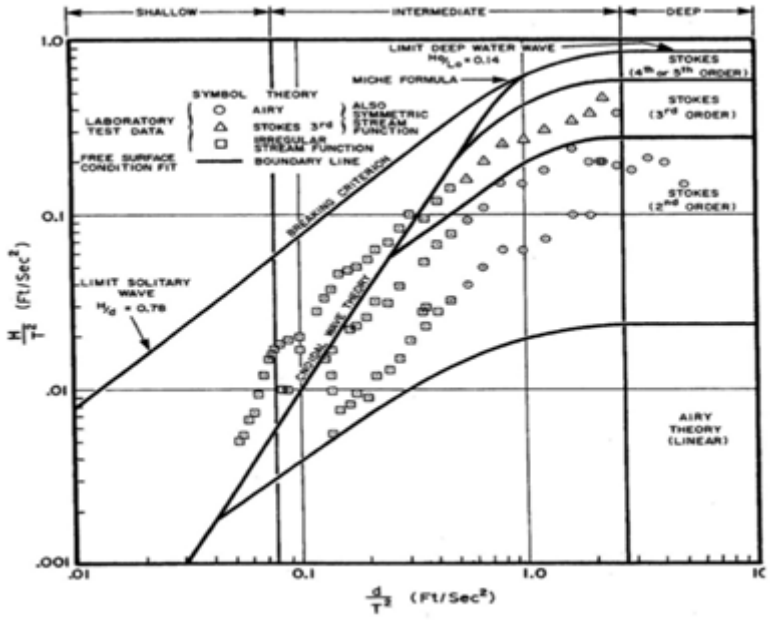

Figure 3.1.1: Ranges of validity for various wave theories. Source: DNV GL (2017)

According to Myrhaug (2006), the Stoke's theory works well in deep water cases. It is not very applicable in shallow waters ($U_R > 30$), where DNV GL (2017) recommends cnoidal wave theory or stream function wave theory. The fish cages at Hosenøyan is located at intermediate depth, bordering deep waters. At such depths, linear theory is assumed to be applicable. Therefore, in addition to being practical, the linear theory will be used in this thesis.

The estimation of the dimensionless parameters are presented in section 4.3

3.2 Wave transformations

With environmental conditions at and around a fish farm being the topic, it is important to underline the differences in behavior for waves at open oceans and near-shore waves. One of the main differences are that waves propagating towards a shoreline will be affected by a change in water depth, bathymetry, in addition to interactions with islands or marine structures on the surface. Waves in open oceans are assumed to have more constant conditions. According to Myrhaug (2006) is common to divide the change of water depth into two categories:

- Sudden change of water depth, for instance an underwater cliff. Causes a change of waves due to reflection.
- Slow change of water depth, typical phenomena of the water depth as it approaches the coast. Causes no significant reflection, but the waves will change slowly.

The change of water depth and sea-bed contours leads to wave transformation processes like reflection, refraction/diffraction and shoaling. In addition, if waves encounter larger structures on the surface, part of the wave energy will be deflected. The theories for the mentioned wave transformation processes will be described below:

Shoaling

According to DNV GL (2017) the wave height increases according to Equation 3.2.1 when travelling towards the coast line, assuming two-dimensional motion:

$$\frac{H}{H_0} = K_s = \sqrt{\frac{c_{g,0}}{c_g}} \tag{3.2.1}$$

Where K_s is the shoaling coefficient and c_g is the group velocity given by Equation 3.2.2:

$$c_g = \frac{1}{2}[1 + \frac{2kd}{\sinh(2kd)}]\sqrt{\frac{g}{k}\tanh(kd)} \tag{3.2.2}$$

Wave number k is related to the wave period T by the dispersion relation. The zero subscript refer to deep water values at water depth $d = d_0$.

Reflection

Reflection occurs when the waves encounter an abrupt change of water depth compared to the wave length. It can also be caused by a surface barrier like an island. When surface waves encounter a subsurface or surface piercing vertical barrier, part of the wave energy is reflected, as illustrated in Figure 3.2.1.

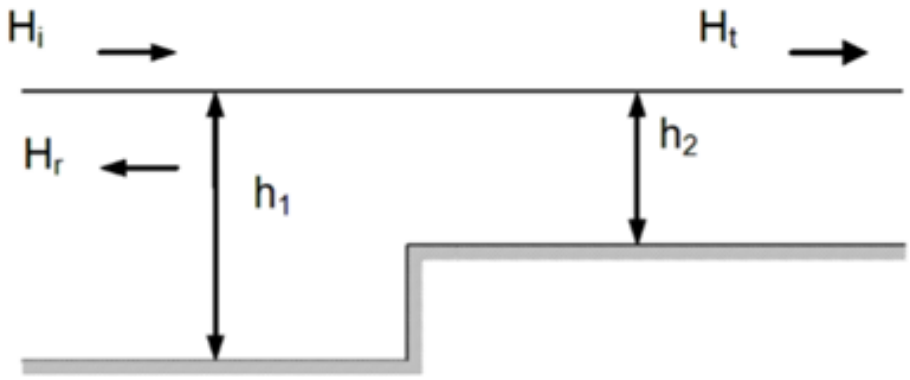

Figure 3.2.1: Waves passing over a subsurface barrier - water depth changes from h_1 to h_2. Source: (DNV GL (2017))

According to the recommended practice by DNV GL (2017) the free surface elevation for linear standing waves against a surface piercing vertical wall can be given as shown in Equation 3.2.3:

$$\zeta = H\cos(kx)\cos(\omega t) \tag{3.2.3}$$

The reflection coefficient $R = H_r/H_i$ is defined as the ratio of reflected wave height to incident wave height. For long waves with wave length much larger than the water depth, propagating in a direction θ relative to the normal to the subsurface barrier, the reflection coefficient is given by:

$$R = \frac{\alpha_1 h_1 - \alpha_2 h_2}{\alpha_1 h_1 + \alpha_2 h_2} \tag{3.2.4}$$

Where $\alpha_i = k_i \cos\theta_i, k_1 \sin\theta_1 = k_2 \sin\theta_2, k_i = \omega\sqrt{gh_i}$. ω is the wave frequency and the indices $1, 2$ correspond to values for depth 1 and 2 respectively. The transmission coefficient $T = H_t/H_i$ is defined as the ratio of transmitted wave height to incident wave height. For $h_1 < h_2$ total reflection ($R = 1$) occurs for a critical angle of incidence, which can be calculated according to Equation 3.2.5:

$$(\theta_1)_{cr} = \arctan\frac{k_2}{\sqrt{k_1^2 - k_2^2}} \tag{3.2.5}$$

Refraction and diffraction

According to Myrhaug (2006), refraction occurs when waves encounter a slow change of water depth compared to the water depth. The wave may change its direction, length and amplitude as a consequence of a change in the water depth.

The phase speed varies as a function of the water depth d. Therefore, for a wave approaching the depth contours at an angle other than the normal, the water depth will vary along the wave crest, and so will the phase speed. As a result, DNV GL (2017) states that the crest will tend to bend towards alignment with the depth contours and wave crests tend to become parallel with the shoreline.

For parallel sea bed contours, Snell's refraction law will apply, described in Equation 3.2.6:

$$\frac{\sin\alpha}{c(kd)} = constant \tag{3.2.6}$$

Where $c = c(kd)$ is the phase velocity and α is the angle between the wave ray and the normal to the bed contour. Refraction also has an effect on the wave amplitude, according to DNV GL (2017). For depth contours parallel with the shoreline, the change of wave height is given by Equation 3.2.7

$$\frac{H}{H_0} = K_s K_r \tag{3.2.7}$$

K_s is the shoaling coefficient given in Equation 3.2.1 and K_r is the refraction coefficient defined as in Equation 3.2.8:

$$K_r = [\frac{1 - \sin^2(\alpha_0)\tan^2(kd)}{\cos^2(\alpha_0)}]^{\frac{1}{4}} \tag{3.2.8}$$

Where α_0 is the angle between the wave crest and the depth contours at deep water.

Myrhaug (2006) writes that the conservation of three relationships will determine the change of waves moving over a slowly changing water depth. These are the conservation of the frequency dispersion relation, the conservation of wave crests and the conservation of wave action. The equations are presented in Equation 3.2.9:

$$\begin{gathered} \omega^2 = gk\tanh kh \\ \frac{\partial \vec{k}}{\partial t} + \nabla\omega = 0 \\ \frac{\partial}{\partial t}(\frac{E}{\omega}) + \nabla\cdot(\vec{c_g}\frac{E}{\omega}) = 0; E = \frac{1}{2}\rho g\zeta_A^2 \end{gathered} \tag{3.2.9}$$

Assuming a stationary wave field, the equations reduces to Equation 3.2.10.

$$\begin{aligned} \omega^2 &= gk \tanh kh = constant \\ \frac{\partial k_y}{\partial x} &- \frac{\partial k_x}{\partial y} = 0 \\ Ec_g b &= constant; E = \frac{1}{2}\rho g \zeta_A^2 \end{aligned} \tag{3.2.10}$$

Wave and current interaction

F. Cardia and A. Lovatelli (2015) states that the wave field can also be affected by currents, as winds against currents will generate shorter and steeper waves. Assuming that the current vector $\vec{U}$ does not vary significantly relative to the wave length and period, refraction from both the varying water depth and from the current will occur. Apart from the conservation of wave crests, this will alter the equations given in Equation 3.2.9 into Equation 3.2.11:

$$\begin{aligned} \omega &= \vec{k} \cdot \vec{U} + \sigma \\ \frac{\partial}{\partial t}(\frac{E}{\sigma}) &+ \nabla \cdot [(\vec{c_g} + \vec{U})\frac{E}{\sigma}] = 0 \end{aligned} \tag{3.2.11}$$

Here, $E = \frac{1}{2}\rho g \zeta_A^2$ as given above, and the component $\sigma = \sqrt{gk \tanh kh}$ is introduced, described as the wave frequency for a reference system moving with the current velocity $\vec{U}$. The group velocity is given as $c_g = \frac{1}{2}\frac{\sigma}{k}(1 + \frac{2kh}{\sinh 2kh})\frac{\vec{k}}{k}$

Assuming a stationary wave field, the equations reduce to Equation 3.2.12:

$$\begin{aligned} \omega &= \vec{k} \cdot \vec{U} + \sigma = constant \\ \nabla &\cdot [(\vec{c_g} + \vec{U})\frac{E}{\sigma}] = 0 \\ \frac{\partial k_y}{\partial x} &- \frac{\partial k_x}{\partial y} = 0 \end{aligned} \tag{3.2.12}$$

In general the combination of these equations can be used to determine the changes to a wave in a wave-current interaction, with Myrhaug (2006) pointing out the following general results:

- For a following current with velocity $\vec{U}$, the wave length λ will increase, and will keep increasing for increasing current velocity. The wave amplitude ζ_A will in this case decrease, and keep decreasing for increasing current velocity.
- If the wave and current have the opposite direction, the wave length λ will decrease with increasing current velocity until the point where the wave breakes. The wave

amplitude ζ_A will increase, and will keep increasing for increasing current velocity $\vec{U}$

Wave and current interaction may not always have a significant impact on the heave motion of a floating structure. An example of this can be found in Fredriksson et al. (2005), where the analysis showed that the current did not have a significant impact on the heave motion of the fish cage. It did however have rotational effects on the structure. Nevertheless, for the measurements done at Hosenøyan, no data of the current is measured during the period of measuring accelerations on the fish cages, leading to the estimation of the wave-current interactions to be difficult.

3.3 Irregular waves

The linear theories does not give a realistic model of a sea state, which is random by nature. However, according to Myrhaug & Lian (2009), by describing the sea state using statistics and the theory of random processes, irregular seas can be estimated.

According to Tupper (2013), an irregular sea state surface can be viewed as a sum of small waves with every small wave having its own length, height and direction. It is common to divide irregular waves into two different categories.

- Long crested waves:
  These are waves that travel in the same direction, leading to a constant irregular pattern across the breadth of the wave. Can be referred to as a one-dimensional irregular system, with wave frequency being the variable.
- Short crested waves:
  Short crested waves represent the sea states in general, where the components of a wave travel in different directions leading to the sea surface being a series of random short crests and troughs. Can be referred to as a two-dimensional irregular system, with wave frequency and wave direction being the variables.

For long crested waves with the frequency being the variable, the wave elevation for a particular location can be estimated according to Equation 3.3.1:

$$\zeta(x,t) = \sum_{(n=1)}^{N} \zeta_{An} \cos(\omega_n t + \epsilon_n) \tag{3.3.1}$$

Where the short crested waves, being dependent on both the frequency and the direction, can be estimated using Equation 3.3.2

$$\zeta(x,y,t) = \sum_{i=1}^{I} \sum_{j=1}^{J} \cos(\omega_i t - k_i x \cos\theta_j - k_i y \sin\theta_j + \epsilon_{ij}) \tag{3.3.2}$$

In irregular waves, the free surface elevation $\zeta(x,y,t)$ is a random process. Using the recommended practice by DNV GL (2017), the local wavelength of irregular waves can be defined as the distance between two consecutive zero up-crossings. The wave crest in irregular waves can be defined as the global maximum between a positive up-crossing through the mean elevation, and the following down-crossing through the same level. A similar definition will apply to the wave trough.

The wave conditions in a sea state in the near coast area can for the most part be divided into the types of short crested waves:

- Wind waves, generated by the local wind.
- Swells, which are waves that have travelled out of the areas where they were generated. Swells have no relationship with the local wind, and several swell components may be present at a given location.

Conventional fish farms are usually located in an area which is relatively well protected from ocean swells. According to NS 9415 by Standard Norway (2010), the wave height for incoming ocean swells are therefore significantly lower than for the sea outside. The wave period however, remain almost unchanged.

3.3.1 Statistical representation of irregular wave elevation – wave spectra

DNV GL (2017) states that short term stationary irregular sea states may be described by a wave spectrum, which is the power spectral density function of the vertical sea surface displacement. The most appropriate wave spectrum depends on the geographical area with local bathymetry and the severity of the sea state.

According to Myrhaug & Lian (2009), the spectrum for long crested waves $S(\omega)$ is defined as the area inside a small frequency interval $\Delta\omega$, and it is equal to the energy of all wave components within this interval:

$$\frac{E}{\rho g} = \sum_{n=1}^{N} \frac{1}{2}\zeta_{An}^2 = \sum_{n=1}^{N} S(\omega_n)\Delta\omega \tag{3.3.3}$$

Assuming $N \to \infty$ and $\delta\omega \to 0$, the sum can be converted into an integral:

$$\frac{E}{\rho g} = \sum_{n=1}^{N} \frac{1}{2}\zeta_{An}^2 = \int_0^{\infty} S(\omega)d\omega \tag{3.3.4}$$

Combining these two equations leads to an equation for the wave elevation ζ as a function of time:

$$\zeta(t) = \sum_{n=1}^{N} \sqrt{2S(\omega_n)\Delta\omega}\cos(\omega_n t + \epsilon) \tag{3.3.5}$$

For short crested waves the direction of the waves must also be taken into account, leading to the inclusion of a directional factor.

$$\frac{E}{\rho g} = \int_0^{2\pi} \int_0^{\infty} S(\omega, \theta) d\omega d\theta \tag{3.3.6}$$

and consequently the following expression for the wave elevation:

$$\zeta(x, y, t) = \sum_{i=1}^{I} \sum_{j=1}^{J} \sqrt{2S(\omega_i, \theta_j)\Delta\omega\Delta\theta} \cos(\omega_i t - k_i x \cos\theta_j - k_i y \sin\theta_j + \epsilon_{ij}) \tag{3.3.7}$$

$S(\omega, \theta)$ is referred to as a directional spectrum. The relationship between the spectra can be described with Equation 3.3.8.

$$S(\omega) = \int_0^{2\pi} S(\omega, \theta) d\theta \tag{3.3.8}$$

Obtaining wave parameters from spectra

According to DNV GL (2017), it is common to assume that the sea surface is stationary for a duration ranging from around 30 minutes to around 3 hours. A stationary sea state is often characterized by the following parameters:

- The significant wave height H_s, defined as the average height (trough to crest) of the highest one-third waves in the indicated period of time. Also denoted $H_{1/3}$. The significant wave height is perhaps the most applied parameter to describe a sea state.
- The peak period T_p, determined by the inverse of the frequency at which a wave energy spectrum has its maximum value. Alternatively, the zero-up-crossing period T_z can be used, which is the average time interval between two successive up-crossings of the mean sea level.

For this Master Thesis, two of the main parameters of interest obtainable from a spectrum is the significant wave height and the zero crossing period. From a spectrum the significant wave height is denoted H_{m0} and corresponds well to the definition of significant wave height as described above. To estimate the wave parameters it is common to use the moments of the spectra, defined in Equation 3.3.9:

$$m_n = \int_0^{\infty} \omega^n S(\omega) d\omega; n =, 0, 1, 2, ... \tag{3.3.9}$$

Where n represents the power of the moment. From the zero-th spectral moment m_0, which represents the variance of the wave elevations, the significant wave height H_{m0} can be estimated according to Equation 3.3.10:

$$H_{m0} = 4\sqrt{m_0} \tag{3.3.10}$$

The zero-crossing period, often denoted T_{m02} when estimated using a spectrum, can similarly be estimated using Equation 3.3.11:

$$T_{m02} = 2\pi\sqrt{\frac{m_0}{m_2}} \tag{3.3.11}$$

In addition, several standardized wave spectra have been made to describe a sea state. The most used standardized spectra are the JONSWAP spectrum, which is an extension of the Pierson-Moskowitz (PM) spectrum. Using standardized wave spectra may prove difficult at specified coastal areas, such as the fish farm at Hosenøyan. The reason for this is that they are often generalized from measured data for a location that does not necessarily have similar surrounding conditions, bathymetry and level of exposure. A description of the JONSWAP spectrum and the PM spectrum can be found in the Appendix, section A.2.

3.4 Floating fish farms

The first type of floating fish farms were named after and developed by Ove Grøntvedt and Sivert Grøntvedt. This represented a significant shift from keeping fish in a net with a system of sticks attached to the sea floor, to the use of moored floating collars, making it possible to use other areas than the limited space of shallow water. The Grøntvedt cage as it is commonly known as, was made of wooden beams with expanded polyester as floats, a purse seine as net and was kept in place with ropes and anchors. Fredheim & Langan (2009) states that it represents the start of the technical and operational development of the industry of aquaculture as we know it in Norway today.

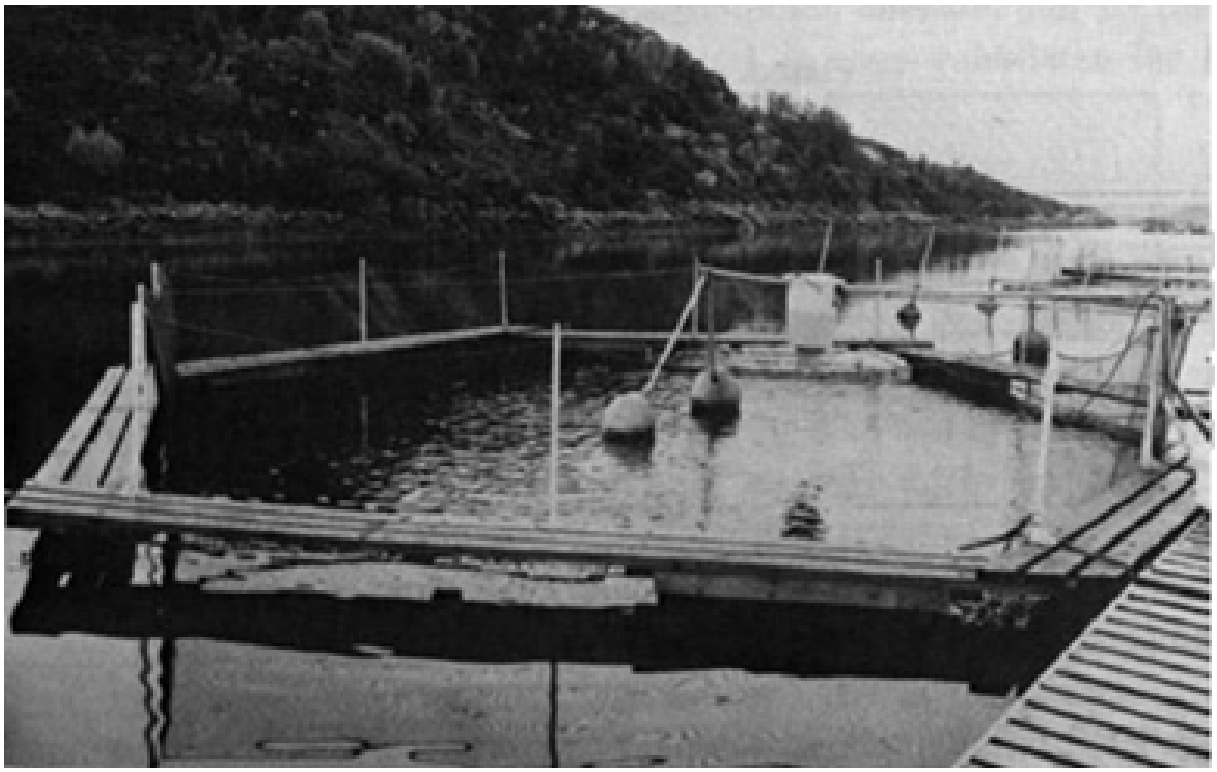

Figure 3.4.1: The Grøntvedt fish farm. Source: Fredheim & Langan (2009)

The Grøntvedt cages were later altered into the HDPE (High-Density polyethylene) circular fish farms that are most commonly used today. The first version of this type of fish cage was called the Polarcirkel. In the beginning these fish cages were small, with a circumference of about 30 m to 40 m. Today, the size of the fish cages has increased to a standard circumference of around 156 m. According to Fredheim & Langan (2009), one of the great benefits of a circular HDPE collar is the flexible nature of HDPE, making the floating collar very durable and resistant against harsh environmental conditions.

To create a sturdier fish cage in order to improve work conditions, in addition to gaining the ability to attach heavy equipment to the fish cage, steel cages have also been developed.

According to Fredheim & Langan (2009), there are several different designs of the steel based cage, from a cage with steel hulls connected by hinged bridges (i.e. Catamaran fish farms) to floating collars made of steel. In sheltered locations, steel fish farms are often preferred over circular HDPE fish cages due to the improved working conditions.

Types of fish cages

Today, several different types of fish farms exists. One way to categorize them is according to Fredheim & Langan (2009), the following:

- Gravity fish farms, where the shape of the net is maintained using different kinds of weight such as a sinker tube and traditional point weights.
- Anchor tension farms, where both the shape of the net and the fish farm itself is maintained by a special mooring system
- Semi-rigid fish farms, where a combination of both ropes and rigid steel maintains the shape of the net
- Rigid fish farms, where a fully rigid structure ensures the integrity of the fish farm. Usually made of steel, but not exclusively.
- Other types

For this thesis however, it is more practical to differentiate the types of fish farms in terms of structural properties and behaviour in waves:

- Flexible fish farms
- Hinged fish farmes
- Rigid fish farms

Figure 3.4.2: A circular HDPE floating fish farm. Source: The Norwegian Seafood Federation (2011)

Figure 3.4.3: An example of a steel hinged fish farm. Source: AKVA Group

Regardless of the system of categories which is applied, it is nevertheless practical to also separate between submersible, partially submersible and surface fish farms.

3.4.1 Circular HDPE fish farms

The most used fish farm type is flexible fish farms with HDPE circular floating collars. This is also the fish farm type that the measurements made by Stemsrud (2018) was conducted on, and therefore its main components will described in the following chapter.

HDPE floating collar

Fredheim & Langan (2009) states that the HDPE pipes are a relatively low-tech product which means it can easily produced everywhere. The range of the circumference can vary from around 70 m to 190 m. A typical size is a diameter of 50 m, and therefore a circumference of 157 m. The thickness of the pipes typically vary from 315 mm to 500 mm, depending on the circumference. The pipes can be installed alone, but there is also systems providing two or three pipes, connected with clamps made of steel or HDPE. As an example, the fish cages at Hosenøyan consists of two pipes. Many HDPE fish farms, especially the larges ones, have walkways and railings installed on them to improve work conditions.

Mooring

The main objective of the mooring system is to keep the fish farm where it is intended to be by resisting the forces of the environmental conditions. The mooring equipment are determined based on the size of the fish farm, bathymetry of the area and the expected environmental conditions at the site. An illustration of a grid mooring is shown in Figure 3.4.4.

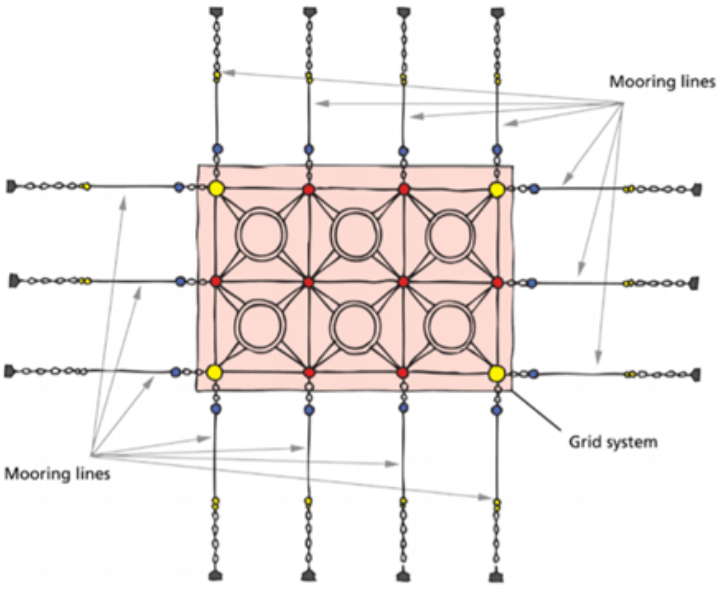

Figure 3.4.4: An example of a grid system and mooring lines in a frame module of six cages. Source: F. Cardia and A. Lovatelli (2015)

According to Fredheim & Langan (2009), grid mooring is the most commonly applied mooring system for a circular HDPE fish farm. This is due to the low horizontal stiffness in the HDPE floating collar. Bridles are used to connect the HDPE collar to the grid system, which is usually located 5-10 m below the fish farm to avoid being destroyed by propellers of service vessels at the site. The mooring system for a conventional circular HDPE fish farm usually consists of a system of ropes, chains, floats and anchors. Several smaller components like shackles, connection plates etc. are also used to connect the mooring system.

Net cage

The net cage connected to the floating collar contains the fish within the fish farm. It is usually made of a synthetic material like nylon, with a frame of ropes and underlying sinkers and/or sinker tubes designed according to the size of the fish cage to help preserve its shape and volume. According to Fredheim & Langan (2009) the material should be flexible enough to withstand environmental forces yet rigid enough to help retain its shape. This is important to ensure that the biomass in the fish cage retains the legally required minimum fish density of 25 $^{kg}/_{m^3}$ among other factors.

Advantages and disadvantages

As mentioned, the main advantage with the HDPE circular fish cage is the flexibility of the material, giving the ability to withstand wave loads well. This means that these types of fish farms can be used at moderately exposed locations. According to Fredheim & Langan (2009), the investment costs are low compared to the other alternatives a well. The distance between each fish cage in the fish farm is also quite large, leading to good water flow and oxygen flow for the fish. The HDPE fish farm have been customary for a long time due to these advantages, and is a known system for fish farmers, leading to efficiency of production.

However, the main disadvantage compared to other types of fish farms are the work conditions. Fredheim & Langan (2009) states that this is partially due to the flexibility of the material, leading to potentially large movements of the floating collar in waves. There is also less space, both for the workers and for equipment, compared to for instance steel hinged fish farms. This makes it necessary to use service vessels for operations such net change etc.

3.5 Dynamics of a floating fish cage in waves

3.5.1 Loads on a floating fish cage

According to Faltinsen (1990), linear theory can approximately describe the wave-induced motions on a semi-submersible structure like a floating fish cage, given that the sea state is not to severe. Linear theory is used with the assumption of a steady state condition, with the consequence of the assumption being that that the motions of the fish cage are assumed to oscillate with the same frequency as the wave loads on the structure. Furthermore, the waves are assumed to have a low steepness. If regular waves are considered, the dynamics of a semi-submersible structure like a fish cage can be divided into experiencing two different types of wave loads:

- Wave excitation loads, described as the loads on the fish cage when it is restrained from oscillating as a result of the incident waves
- Added mass, damping and restoring loads, which describes the loads on a structure without the loads of incident waves, and only the loads that occur when the fish cage is oscillating with the excitation frequency of the waves.

If linearity is assumed, the two types of loads can be added together according to the superposition principle. If irregular waves are considered, the response of the fish cage can be estimated by adding together regular waves of different amplitudes, wave lengths and wave directions.

For this Master Thesis, the focus is to investigate the fish cage response in heave, written as η_3. According to Faltinsen (1990), the linear vertical force due to added mass and dampening can be estimated according to Equation 3.5.1. Here, the linearized pressure is integrated over the mean position of the fish cage, and hydrostatic pressure is excluded:

$$F_3 = -A_{33}\frac{d^2\eta_3}{dt^2} - B_{33}\frac{d\eta_3}{dt} \tag{3.5.1}$$

where A_{33} is the added mass in heave and B_{33} is the dampening coefficient in heave. Faltinsen (1990) writes that these coefficients may be hard to determine, and are therefore often estimated empirically.

For a floating structure, the restoring coefficient C_{kj} is used to estimate the restoring force. Assuming a symmetric submerged plane, it can be estimated according to Equation 3.5.2:

$$F_3 = -C_{3j}\eta_j \tag{3.5.2}$$

For moored structures like the fish cages are, the restoring coefficients can be very hard to find as well, as the mooring will have a varying influence. According to Faltinsen (1990), this is especially the case for waves with long wavelengths compared to the radius of the fish cage.

The wave excitation forces can be explained as forces occurring as a result of unsteady pressure of the fluid, which is a result of incident waves. Wave excitation forces are usually divided into two categories, with the assumption of regular waves:

- Froude-Kriloff forces, occurs due to the unsteady pressure field of the fluid
- Diffraction forces, occurs as a result of the changes in the pressure field caused by the fish cage itself

Equation 3.5.3 is a generalized equation described by Faltinsen (1990). The equation is used to estimate the wave excitation forces on a structure which has a characteristic cross-section diameter significantly smaller than the incident wave length, often referred to as a small-volume structure.

$$\begin{gathered} \vec{F} = \vec{i}F_1 + \vec{j}F_2 + \vec{k}F_3 \\ where: F_i = -\int\int_S pn_i ds + A_{i1}a_1 + A_{i2}a_2 + A_{i3}a_3 \end{gathered} \tag{3.5.3}$$

where the integration of the pressure p is done over the wet surface S, and a_1, a_2 and a_3 represents acceleration components in x, y, and z-direction of the undisturbed wave field.

Faltinsen (1990) further states that the equations for added mass loads and excitation loads can be added together using the superposition principle and Newton's second law, assuming steady state sinusoidal motions. This will result into the equation of motion in heave, shown in Equation 3.5.4:

$$\sum_{n=1}^{6}[(M_{k3} + A_{k3})\ddot{\eta}_k + B_{k3}\dot{\eta}_k + C_{k3}\eta_k] = F_3 \exp^{i\omega_e t} \tag{3.5.4}$$

The right hand side describes the complex amplitudes of the wave excitation force with frequency ω_e, and the left side represents the added mass, dampening and restoring loads.

Newman (1977) investigates the motion of a slender floating torus, combining slender body theory with the complex nature of free-surface waves. The paper have the following assumptions regarding the wavelength λ of the incident waves in relation to the geometry of the torus in question:

- $\frac{\lambda}{a} = O(1)$, meaning that the wavelenght and the cross-section radius of the torus (small radius) are comparable in size
- $\frac{\lambda}{c} \leq 1$, meaning that the torus' large radius is significantly larger than the incident wavelength.
- In addition, the small radius a is assumed much smaller than the larger radius c of the torus.

For the measurements at Hosenøyan, these assumptions will not always hold. Another assumption made by Newman (1977) is a freely floating torus, i.e the effects of mooring of the structure are being neglected. Nevertheless, Equation 3.5.5 can be used to describe the motion in heave using the complex amplitude $\eta_3 = i\omega\zeta_3 e^{i\omega t}$. It is based on the linear equation of motion as stated in Equation 3.5.4, assuming no coupling effects between the surge, heave and pitch motions. Figure 3.5.1 illustrates the motions of a torus for different values of ka.

$$[-\omega^2(m_{33} + m) + i\omega b_{33} + 4\pi\rho gac]\zeta_3 = X_3 \tag{3.5.5}$$

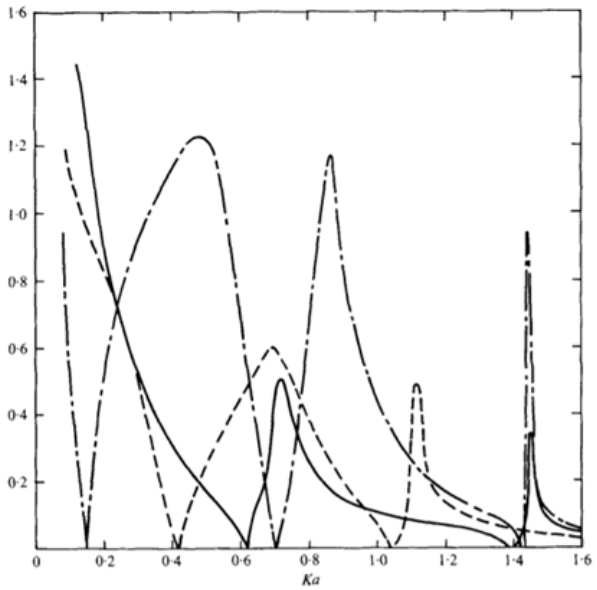

FIGURE 4. Amplitudes of body oscillations in surge (ξ_1), heave (ξ_3) and pitch (ξ_5) for torus with $a/c = 0{\cdot}2$ in incident waves of amplitude A. ——, $|\xi_1|/A$; – – –, $|\xi_3|/A$; —·—, $|\xi_5|c/A$.

Figure 3.5.1: Torus motion amplitudes for surge, heave and pitch for torus with $a/c = 0.2$. Not valid for low frequencies. Source: Newland (2005)

3.5.2 Natural period of a floating fish cage

To further understand the motion of a fish cage in waves, the natural period of the structure should be investigated to determine if the motion is affected by resonance. According to Faltinsen (1990) the natural period in heave for a floating fish cage can be described as shown in Equation 3.5.6:

$$T_{n3} = 2\pi(\frac{M + A_{33}}{\rho g A_w})^{\frac{1}{2}} \tag{3.5.6}$$

where A_w represents the water plane area.

Stemsrud (2018) investigated the natural frequency of the fish cages at Hosenøyan both numerically and through experiments. To calculate the natural frequency numerically, Equation 3.5.7 was used to find the natural period:

$$T_{n3} = 2\pi(\frac{\frac{1}{2}a^2\pi\rho + A_{33}}{\rho g 4\pi c a})^{\frac{1}{2}} \tag{3.5.7}$$

The natural period was determined neglecting the influences of the mooring system and the weights and bottom ring, due to practical reasons. This lead to the estimation of M and A_w to be $M = \frac{1}{2}a^2\pi\rho$ and $A_w = 4\pi ca$. The results of the numerical estimation were $\omega_{n3} = 22.63^{rad}/_{sec}$ indicating a natural period of $T_{n3} = 0.28s$ for mode $n = 0$ to $\omega_{n3} = 29.11^{rad}/_{sec}$ indicating a natural period of $T_{n3} = 0.22s$ for mode $n = 10$.

Experimentally however, using a MATLAB script, the natural period of the fish cages were found to be $T_{n3} = 1.7288s$. The reason for the deviance in results are not specified, but one can argue that the influence of mooring and the weights could be a part of the explanation.

3.5.3 Transfer function for a floating fish cage

The additional topic of this thesis was to investigate the validity of using the fish cages as wave buoys to estimate the local wave conditions at an aquaculture site, as described in section 1.2. To do this, the relation between the incident waves on the fish cages and the motion of the structures were investigated. If linearity is assumed, the term Response Amplitude Operator (RAO) may be applied, as defined in Equation 3.5.8 according to Faltinsen (1990):

$$RAO_3(\omega) = |\frac{\eta}{\zeta_a}| \tag{3.5.8}$$

Among other topics, Li (2017) investigated in his phD-thesis the transfer function of absolute value of the vertical motion using low-frequency slender body theory, and Equation 3.5.9:

$$|\frac{w_a(\beta,\omega)}{\zeta_a}| = \sum_{n=0}^{\infty} |\frac{a_{n,a}(\omega)}{\zeta_a} \cos n\beta| \tag{3.5.9}$$

where $w_a(\beta,\omega)$ is the amplitude of absolute value of the vertical motion, β represents the position on the torus, and $a_{n,a}(\omega)$ are complex values of amplitude of mode n where the phase angle between the incident wave and the torus response is included.

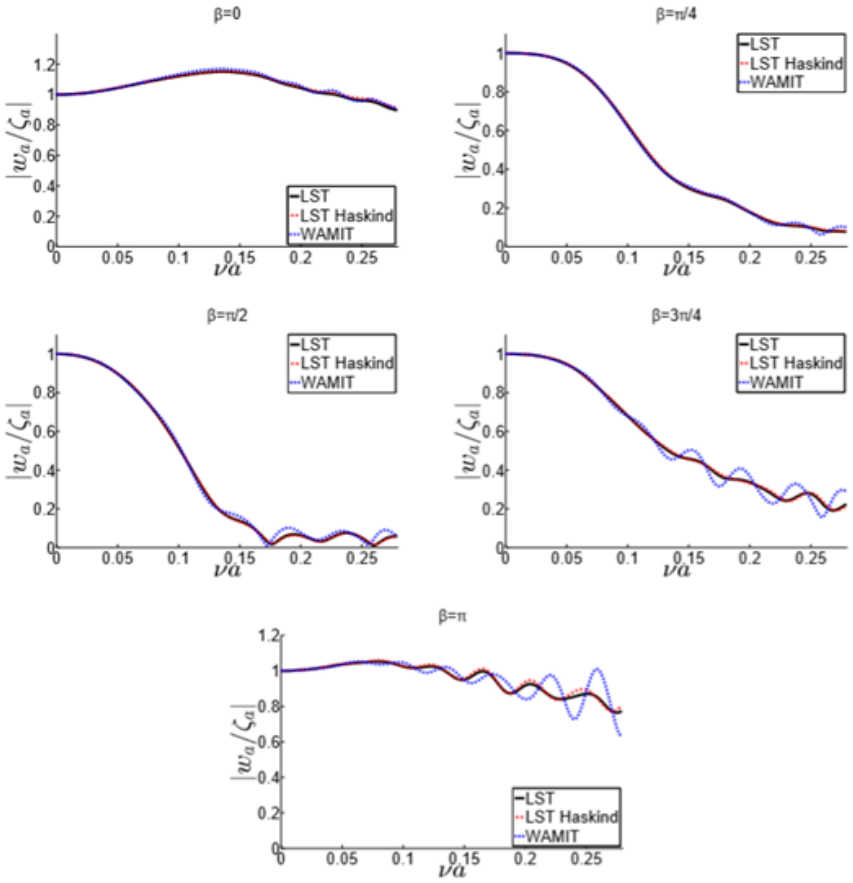

Figure 3.5.2: Transfer functions of absolute vertical motion at five positions of a torus with $\frac{a}{c} = 0.0253$. Source: Li (2017)

In Figure 3.5.2, $\nu = k = \frac{2\pi}{\lambda}$ is the wave number. Deep water assumption is applied, hence $\nu = k = \frac{\omega^2}{g}$. It is also worth mentioning that the relation between the cross-section radius of the floating collar a and the radius of the torus c is given as $\frac{a}{c} = 0.0253$ in Figure 3.5.2, whereas for Hosenøyan there are two floating collars with $\frac{a}{c} = \frac{0.25}{25} = 0.01$. In addition, the effects of net, weights and mooring are neglected.

For $\beta = 0$ and $\beta = \pi$, corresponding to the aft and front side of the torus relative to the incident wave, it can be seen that the transfer function is around 1 for all νa investigated, meaning that the structure corresponded to the incident waves to a high degree. While for $\beta = \pi/2$, the transfer function deteriorates as νa grows larger. For the measurements at Hosenøyan, this would indicate that the wave direction may play an important role in the resulting transfer function estimates.

In experiments done by Fredriksson et al. (2005), the fish cage investigated did not follow the waves in a one-to-one relationship. They estimated the significant heave motion of the structure to be 3,0 m in waves with a significant wave height of 8,27 m. It is worth mentioning that the research by Fredriksson et al. (2005) is done under much harsher environment than the Hosenøyan fish farm endured, in addition to the fish cage structure being of semi-submersible, anchor tension type. Nevertheless, this indicates that the motion of a fish cage does not necessarily correspond to the wave elevation.

Another thing worth mentioning is the simplification of neglecting the effects of the net, bottom weights and mooring of the fish farm, which may contribute to unsatisfactory results. To properly measure the effects of spatial variations within an aquaculture site, one could easily argue that these factors should be included before any definite conclusion could be made. In addition, according to Endresen (2011), it is not certain that the assumption of linearity holds for frequencies higher than the first natural frequency of the floating structure. Nevertheless, due to lack of data regarding the effects of the mooring system, linear transfer functions are estimated for the measurements at Hosenøyan.

Chapter 4

Measurements at Hosenøyan

In Chapter 4 the aquaculture site itself and the practical measuring method of the measurements at Hosenøyan will be described. The chapter is largely based on the Master Thesis by Stemsrud (2018). It is the main source of information available regarding the practical aspect of the measurements, as they were done for her Master Thesis in 2018.

4.1 Description of the site

4.1.1 Hosenøyan

Hosenøyan is located in Flesafjorden, north east of Frohavet outside Stokkøya in Trøndelag. The fish farm is well sheltered from waves coming from the open ocean in the West and North West direction. However, except for a small island, it is relatively unprotected to waves coming in from the South West direction, which are waves coming from the open and somewhat harsh environment of Frohavet. Waves coming from the North East direction also has the potential to be of significant size. The location of the fish farm is pointed out in Figure 4.1.1, Figure 4.1.2 and Figure 4.1.3.

Figure 4.1.1: Image of the location of Hosenøyan. Source: Google Maps

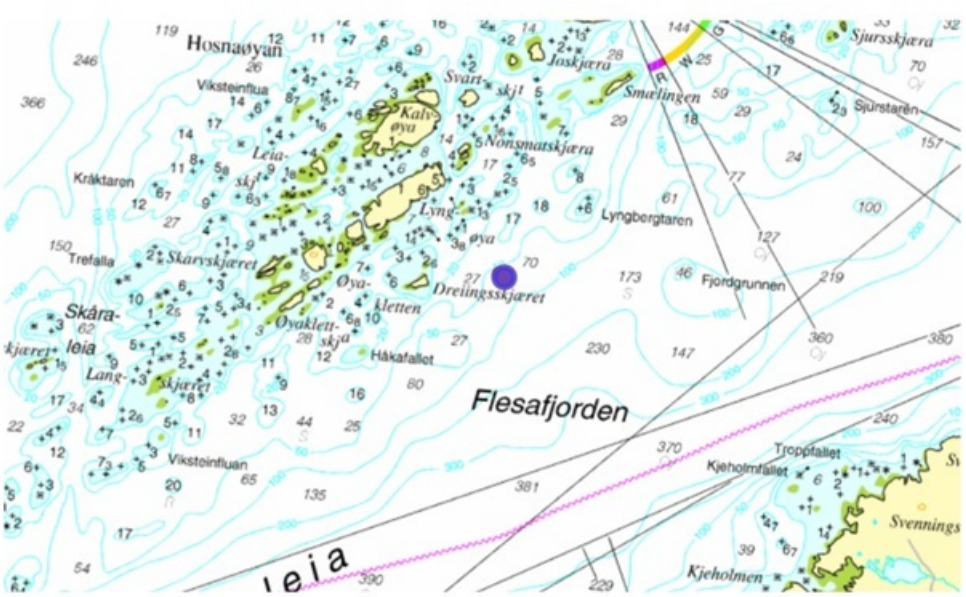

Figure 4.1.2: Detailed image of the location of Hosenøyan, as shown in master thesis by Stemsrud (2018)

Figure 4.1.3: Satellite image of the location of Hosenøyan. Source: Google Maps

Structure of the aquaculture farm

As Figure 4.1.4 indicates, the longitudinal direction of the fish farm is across the strait, from North West to South East. It contains a standard mooring system for a circular HDPE fish farm, with capacity to hold 12 fish cages. When the measurements were done, the fish farm had eight cages in use according to Stemsrud (2018). The feed barge is located north west, where the protection from waves were assumed to be the highest.

The floating collars are delivered by Aqualine with the following dimensions and technical description, according to Stemsrud (2018):

- Two HDPE 80/100 tubes
- Mean torus radius of 25 m (Circumference 157 m)
- Pipe radius of 0.25 m
- Sinker tube of 80 kg/m at depth of 17.5 m outside the fish cage on each cage
- Sinker of 1000 kg at the bottom of each cage.

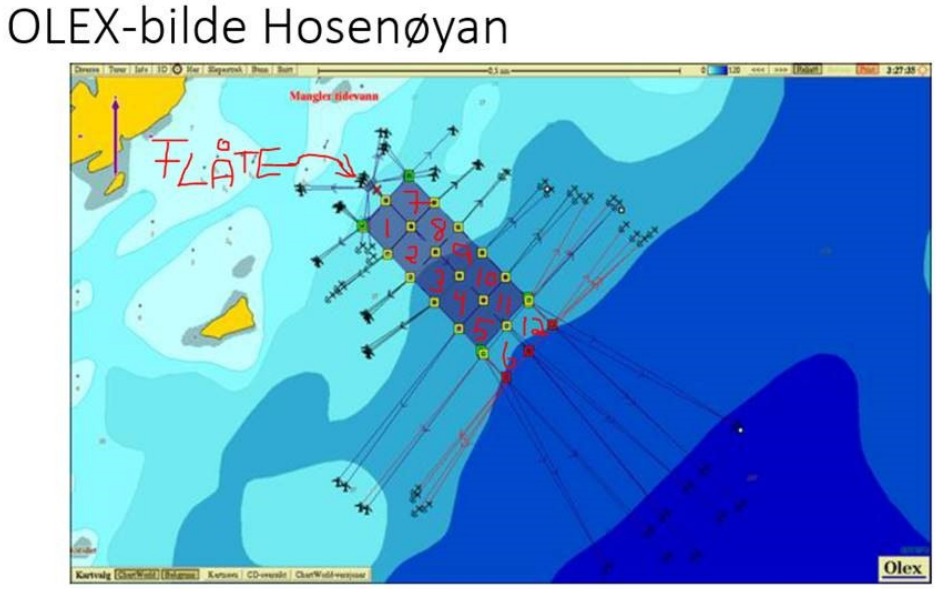

Figure 4.1.4: OLEX image of the structure at Hosenøyan. Source: Stemsrud (2018)

Stemsrud (2018) also includes the level of wave exposure of the fish farm, using data from NYTEK schemes obtained from the Norwegian Directorate of Fisheries, presented in Table 4.1.1. This indicates that the fish farm at Hosenøyan can be categorized to have high to extreme degree of wave exposure

$H_{s_{wind,10yrs}}[m]$	$T_{p_{wind,10yrs}}[s]$	$H_{s_{wind,50yrs}}[m]$	$T_{p_{wind,50yrs}}[s]$	$H_{s_{comb,10yrs}}[m]$
2.9	7.7	3.3	8.6	1
$H_{s_{swell,10yrs}}[m]$	$T_{p_{swell,10yrs}}[s]$	$H_{s_{swell,50yrs}}[m]$	$T_{p_{swell,50yrs}}[s]$	$H_{s_{comb,50yrs}}[m]$
3.2	16.3	3.6	16.3	1

Table 4.1.1: NYTEK data from Hosenøyan fish farm. Source: Stemsrud (2018)

The fish cages used in this Master Thesis are fish cages 8 and 9, as shown in Figure 4.1.4. Using the website `norgeskart.no` the approximate coordinates and depths of the position of the measuring instruments on fish cage 8 and 9 at Hosenøyan could be estimated to the following:

- Cage 8: 64.086485 N, 9.882223 E
- Estimated depth by interpolation: 39 m.
- Cage 9: 64.085926 N, 9,883494 E
- Estimated depth by interpolation: 49 m.

The fish cages that the measurements are done on has a water depth of roughly 40-50 meters, leading to the assumption of deep water linear theory being acceptable for wave lengths shorter than 80-100 meters. This assumption proved valid for most of the period of measurements..

4.2 Data aquisition

4.2.1 Equipment description

To measure the accelerations of the fish cages at Hosenøyan, inertial measurement units (IMU) were used. The IMU's used by Stemsrud (2018) were the Yost Labs 3-space dataloggers, funded by SINTEF through EXPOSED Aquaculture. Additional information about the IMU can be found in the following URL: `https://yostlabs.com/product/3-space-data-logger/`

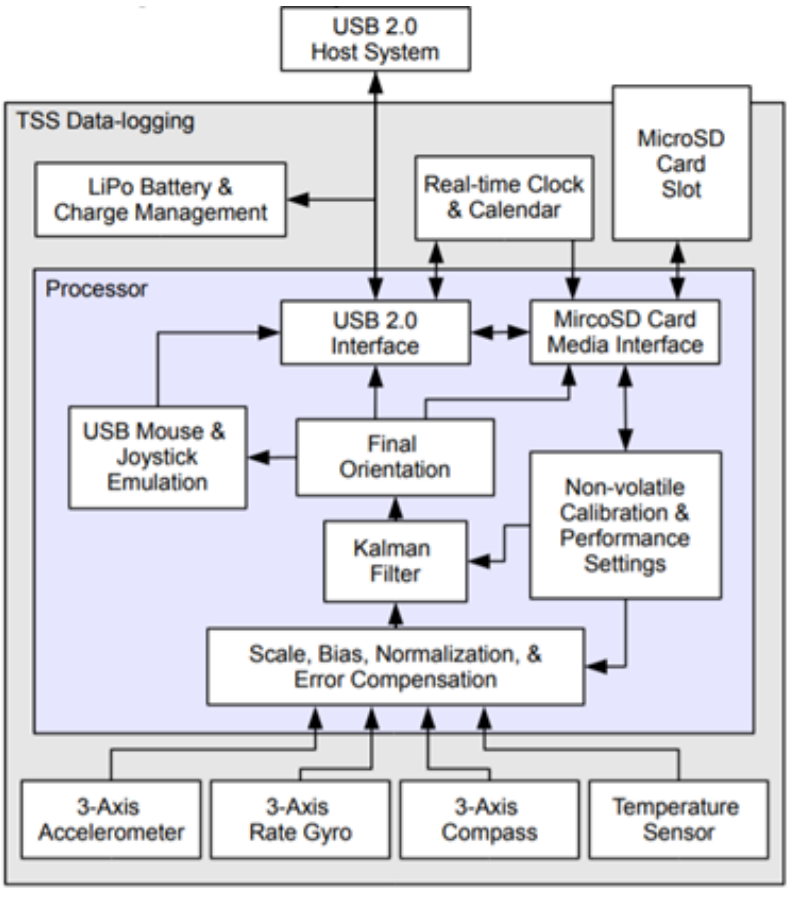

Figure 4.2.1: A block diagram of the sensor operation of the IMU:
Source: `https://yostlabs.com/wp/wp-content/uploads/pdf/3-Space-Sensor-Users-Manual-Data-Logging-1.pdf`

Figure 4.2.2: Example of the format of the raw IMU data

The output from the IMU's included among other the time, raw and linear acceleration, gyro measurements (angular motion), and compass measurements (magnetic directions). The focus of this Master Thesis is the use of the linear vertical acceleration parameter, which are given in units of g by the IMU. According to the user manual, the linear acceleration is the raw acceleration adjusted for the rotations measured by the IMU. This leads to the estimation of the acceleration in the "true" or global z-direction being obtainable directly from the IMU.

Figure 4.2.3 show the description of the linear acceleration command according to the user manual. The user manual is available at the following URL: `https://yostlabs.com/wp/wp-content/uploads/pdf/3-Space-Sensor-Users-Manual-Data-Logging-1.pdf`.

41(0x29)	Get corrected linear acceleration in global space	Returns the linear acceleration of the device, which is the overall acceleration which has been orientation compensated and had the component of acceleration due to gravity removed. Uses the tared orientation.	12	Acceleration Vector in units of G (float x3)	0	

Figure 4.2.3: Description of the linear acceleration command in Yost Labs 3-space dataloggers

Six IMU's were originally set up in 2018, calibrated in cooperation with researchers from SINTEF Ocean, Eirik Svendsen and Gunnar Senneset. For this thesis however, data from only two IMU's were obtainable. The other four data sets have been lost, either destroyed by sea water exposure or lost in the archives.

4.2.2 Practical measuring method

The idea of the set-up by Stemsrud (2018) was mainly to analyse and compare the spatial variations of linear acceleration in the fish farm. Therefore, the IMU's were aligned in pairs across the south-west, where the wave exposure was assumed to be the highest. The IMU positions which provided the data for this thesis are marked with purple in Figure 4.2.4.

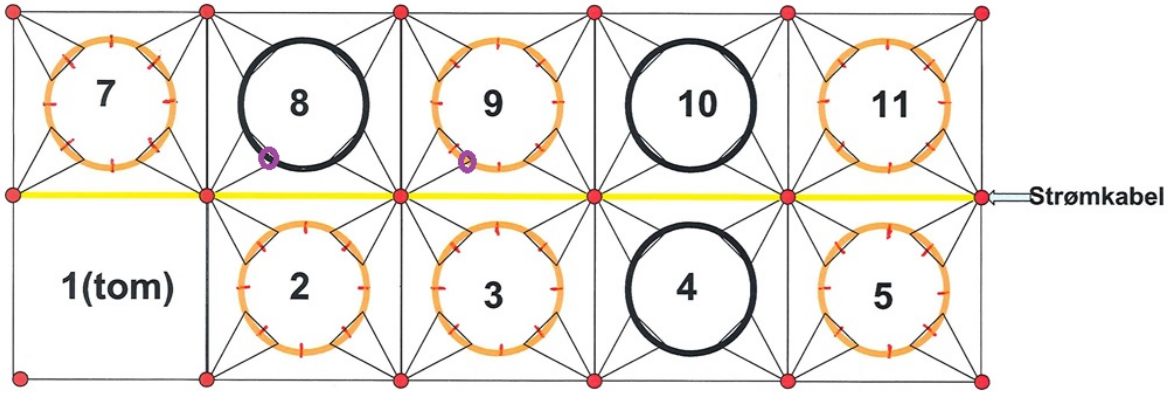

Figure 4.2.4: Placement of the IMU's at the fish farm, marked with purple

The IMU's were placed in the power cabinets of each fish cage, about 1,25 m above sea level as shown in Figure 4.2.5. All IMU's were aligned in the same direction.

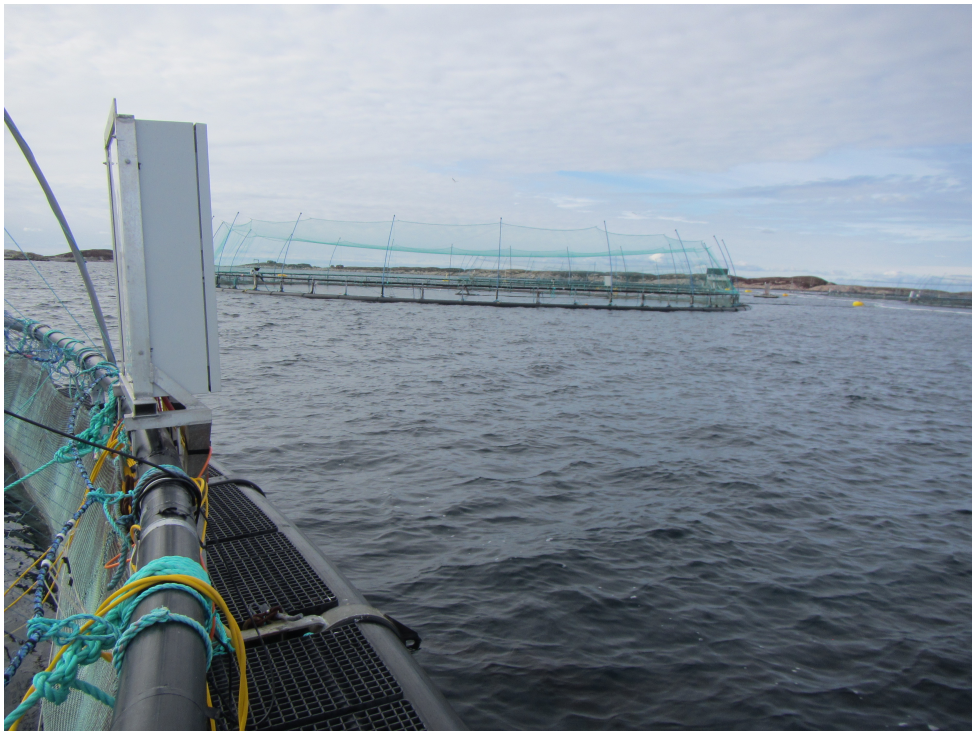

Figure 4.2.5: Image of the power cabinets the IMU's were placed in, 1,25 m above sea level. Source: Stemsrud (2018)

Figure 4.2.6: Image of the alignment of the IMU's inside the power cabinet. Source: Stemsrud (2018)

Sampling method

When conducting wave measurements, there are factors that might influence the results of the measurements and therefore lead to errors. Some most important factors are:

- Sampling frequency
- Duration of the recording
- Type of device used in the measurements

The sampling frequency will influence what kind of wave periods that will be detected and will define the resolution of the sample. The relationship between sampling frequency and sampled wave periods is given by the Nyquist theorem, described in Equation 4.2.1:

$$f_{Nyq} = \frac{1}{2\Delta t} = 2f_0 \leq f_s \tag{4.2.1}$$

This theorem indicates that the sampling frequency f_s must be at a minimum twice the target frequency f_0 of the sample, like the natural frequency of an object. If $2f_0 \geq f_s$, under-sampling could happen due to the sampling not fulfilling the Nyquist theorem. As a consequence, aliasing could occur, which can lead to a misidentified fish cage elevation response with much lower frequency than the actual response

Stemsrud (2018) used a sampling frequency of 10 Hz, for a continuous measurement of 645 hours. The recordings were split into 645 data files, each containing measured data for a period of one hour. The sampling frequency of 10 Hz came as a result of a calculation of one of the fish cage's natural frequency using dynamics of a semi-submerged torus. The natural frequency of the fish cages were found to be 1.7288 s, as described in subsection 3.5.2. In addition, since according to Figure 4.2.7 the main part of wind waves typically have the frequency of around 0.04 Hz to 2 Hz (i.e. wave period of 0.5 s and 25 s), this was seen as a fitting sampling frequency to record the fish cage motions.

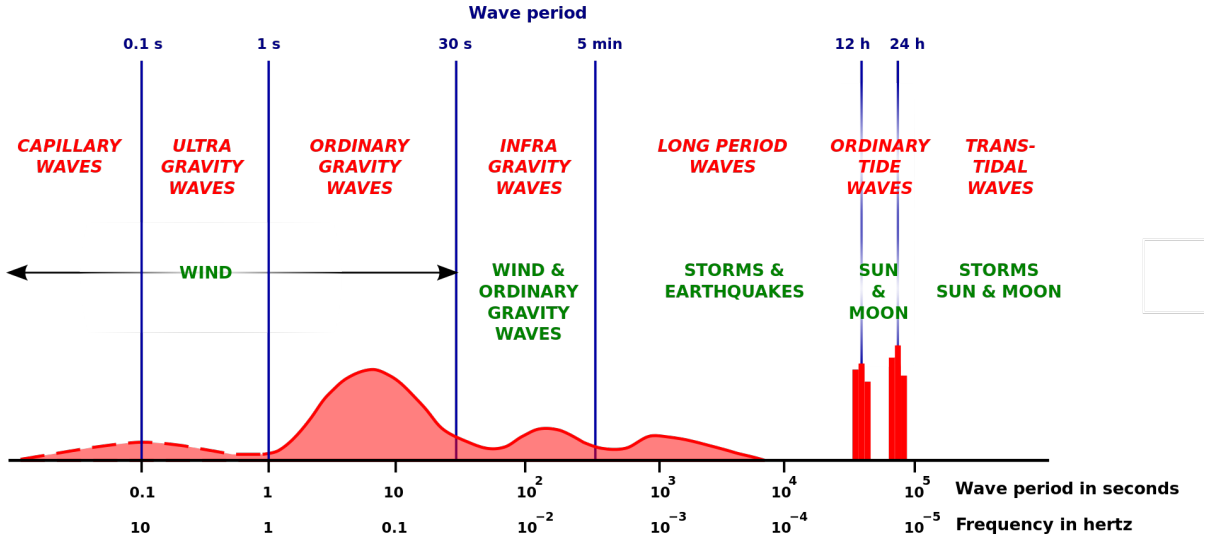

Figure 4.2.7: Diagram of the ocurrence of ocean waves as a function of wave period of wave frequency. Source: Walter H. Munck, (1950)

4.2.3 Wave buoy measurements

To compare with the results obtained by the acceleration measurements, wave buoy data in the close vicinity of Hosenøyan were obtained. The wave buoy data were given in the form of an Excel-document, and contained information and estimations of wave parameters describing the sea state. For the case of this thesis, the parameters of interest from the wave buoy data was primarily the significant wave height H_{m0}, the zero-crossing period T_{m02} and the wave direction θ. The assumption is that the wave buoy provides reliable estimates of these parameters, and would prove useful to verify the estimations of the acceleration measurements of the fish cages at Hosenøyan. In addition, the wave buoy data would be useful to give an estimate of the transfer function of the fish cage elevation responses due to incident waves.

Using the wave buoy as a reference point has some issues. One of them, as seen in Figure 4.2.8, is that the wave buoy is located about 350 m South East of the fish farm,

and about 500 m from the fish cages that the accelerations are measured on. The location indicates that the wave buoy has no particular sheltering from waves, as opposed to the fish cages. In addition, the depth at the location of the wave buoy is estimated to be over twice as large, according to `norgeskart.no`:

- Coordinates: 64.082111 N, 9.886194 E
- Estimated depth by interpolation: 113.5 m

This could mean that the assumption of identical wave conditions at the wave buoy and the fish farm may be incorrect. Another factor that could prove important for the results is that the sampling method and the measuring device is different. The sampling method of the wave buoy is as listed below:

- Measuring device: FOAS Wavesense instrument
- Sampling frequency: 2 Hz
- Sampling duration: 1024 s, providing 2048 samples per hour

This means that the wave buoy samples for 17 minutes and rests for the remaining 43 minutes of the hour. As mentioned, the measurements on the fish cages at Hosenøyan are continuous, meaning that the amount of samples are much higher at 36000 samples per hour. In addition, the sampling rate of 2 Hz indicate that some of the high frequency waves might not be detected. However, the main part of wind waves will still be detected by the wave buoy. Due to lack of other wave data closer to the fish farm, the wave buoy data will be used in this thesis.

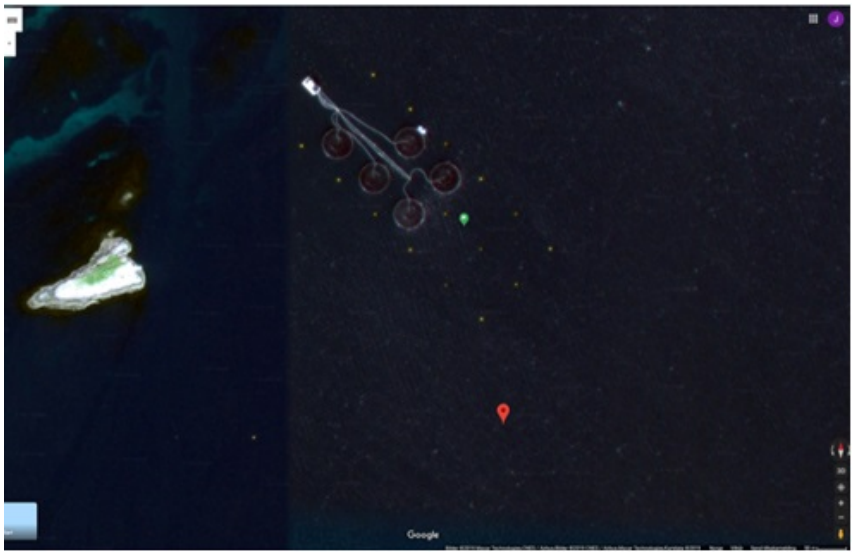

Figure 4.2.8: Satellite image of the location of the wave buoy at Hosenøyan. The red marker represents the wave buoy. Source: Google Maps

4.3 Theory assumptions at Hosenøyan

Linear wave theory validity

To estimate the validity of using linear theory to describe the waves, the application limits shown in Figure 3.1.1 was used. The parameters were estimated based on the data from the wave buoy described in subsection 4.2.3 and the equations described in subsection 3.1.3, yielding the results shown in Table 4.3.1, Table 4.3.2 and Table 4.3.3.

	H_{m0} [m]	T_{m02} [s]	k	λ [m]	ω [rad/s]
Min	0.0391	2.8320	0.0195	12.5115	0.4375
Max	1.6797	14.355	0.5013	321.4854	2.2175
Mean	0.3665	4.8524	0.2207	41.4256	1.4215
Std. dev.	0.3240	1.7361	0.1058	35.4233	0.3807

Table 4.3.1: Estimations of wave parameters based on wave buoy data and linear deep water theory

	H/λ	H/T^2 [$\frac{ft}{s^2}$]	U_r
Min	0.0010	0.0050	0.0004
Max	0.0511	0.2619	132.1981
Mean	0.0127	0.0652	0.7551
Std. dev.	0.6750	0.0625	0.0625

Table 4.3.2: Estimation of wave steepness and Ursell number based on wave buoy data

	d/λ, cage 8	d/λ, cage 9	d/T^2 [$\frac{ft}{s^2}$], cage 8	d/T^2 [$\frac{ft}{s^2}$], cage 9
Min	0.1244	0.1555	0.6375	0.7969
Max	3.1970	3.9963	16.3807	20.4759
Mean	1.4078	1.7597	7.2129	9.0161
Std. dev.	0.6750	0.8437	3.4584	4.3231

Table 4.3.3: Estimation of shallow water parameter based on wave buoy data. Depth at fish cage 8: $d = 40m$. Depth at fish cage 9: $d = 50m$

Using the mean value of the wave parameters from the wave buoy, linear theory in the form of Stoke second order was valid to use at the wave buoy depth of 100 m. Since the fish farm is at a location with smaller depth, it was decided that linear theory would be used to give an approximation of the wave parameters, as mentioned in subsection 3.1.3.

Statistical assumptions

According to Newland (2005), a large number of random stochastic realizations will approach a Gaussian distribution. This is the result obtained by the use of the central limit theorem. Waves are random by nature, and by assuming infinite water depth, the sea surface can then be assumed to be a random, Gaussian distributed process. Gaussian description can be further extended to include shallow water, under the assumption that no severe wave conditions such as storms occur, where statistical independence is questionable. If the recordings of the IMU are evaluated within approximately 30 minutes to three hours as mentioned in subsection 3.3.1, it will lead to the possibility that the wave elevation can be assumed a stochastic Gaussian process. To simplify the estimation, the sea state will also be assumed ergodic. This will make the statistical properties estimated for one realization of a sea state representative for the whole stochastic process itself. These assumptions will in turn lead to describing wave conditions with probabilistic models being a viable option.

Chapter 5

Method

The following chapter describes the method used to evaluate the acceleration measurements at Hosenøyan. Firstly, a literature study on double integration of acceleration measurements will be described. Following the literature study will be a description of the method, including a description of the MATLAB scripts written for this purpose.

5.1 Double integration of acceleration measurements - literature study

Due to limited prior knowledge of evaluating measured acceleration data, a literature study was done on the topic to ensure that the method was as good as possible.

The objective of determining position using acceleration data from IMU measurements by integrating them twice can prove to be difficult, according to Kowalczuk & Merta (2015). The results may easily contain significant errors, especially for a long sampling time such as the with the measurements done at Hosenøyan. The integration of the data will be heavily affected by drift and noise due to the characteristics of the MEMS (microelectromechanical system) sensors in the IMU.

In general, the integration of the IMU data can be done in the time domain by integrating the acceleration signals directly using for instance the trapezoid rule. It can also be done in the frequency domain by taking the inverse Fourier transform (IFT) of the Fourier transformed acceleration signal, by division with a scale of $-\omega^2$ per integration. Han (2010), who did research on the use of accelerometers, states that the Nyquist frequency of the digital sampling of the acceleration signal should be much higher than the highest frequency component of the signal if the position is to be estimated in the time domain. He mentions that a predetermined resolution in both time and frequency domain will lead

to biased errors. Double integrating high-frequency signals will lead to errors in the time domain, and double integrating low-frequency signals will produce errors in the frequency domain. Han (2010) also provides the following equation for estimating the errors per numerical integration for a pure sinusoidal type of acceleration signal:

$$E_2 = \frac{(\Delta t)^3}{12}\ddot{a}(t); 0 < t < \Delta t \tag{5.1.1}$$

with $\ddot{a}(t)$ having the relationship with the velocity $v(t)$ as described in Equation 5.1.2:

$$\ddot{a}(t) = -(2\pi f_0)^3 v(t) \tag{5.1.2}$$

giving the following expression for the relative error:

$$\epsilon_v = \frac{\pi^3}{12}(\frac{f_0}{f_{Ny}})^3 \tag{5.1.3}$$

Equation 5.1.3 can be rearranged to describe the relationship between the frequency of the signal, the Nyquist frequency ($f_{Ny} = \frac{1}{2\Delta t}$) and the maximum desired error, as shown in Equation 5.1.4:

$$f_0 = \sqrt[3]{\frac{12\epsilon_v}{\pi^3}} f_{Ny} \tag{5.1.4}$$

Using these equations, Han (2010) states that if a velocity signal shall be directly integrated in the time domain within a 5 % error margin, the highest frequency component to be reconstructed is $0.2685 f_{Ny}$. Within 1 % error, the highest frequency component to be reliably reconstructed is $0.1570 f_{Ny}$. In the case of the measurements at Hosenøyan, this means that the highest frequency component to be reconstructed within 5 % error is 1.34 Hz, and within 1 % error it is 0.785 Hz. According to the wave buoy data, the mean of the wave period is 4.85 s, giving a mean frequency of $= {}^1/_{4.85} = 0.21 Hz$. This indicates that the sampling frequency at Hosenøyan should hold for most of the measurements. However, Han (2010) adds that since the integration will be performed again to estimate position, the highest frequency component to be reliably reconstructed will be even lower.

A second source of error is due to not having information about the initial conditions in each integration process. This will according to Han (2010) produce a DC component which will influence the data. However, Han (2010) concludes by recommending to use the direct time domain method to measure structural responses with the IMU. As long as the resolution of the time sampling is well above the highest frequency component recorded it will yield acceptable results, but this is also heavily dependent on the unknown initial conditions of the integration. If the highest recorded frequencies are relatively high com-

pared to the Nyquist frequency, the frequency domain is preferable.

In an article by Brandt & Brincker (2014), the errors that occur in direct integration in the time domain are also pointed out, with the exception of low frequencies compared to the Nyquist frequency as described above by Han (2010). However, Brandt & Brincker (2014) could not recommend a "best" method for integrating IMU measurements, but points out that the integration in the frequency domain using long DFT (Discrete Fourier Transformation) integration is in general the best method they checked.

Seifert & Camacho (2007) mentions in their article on the topic that low pass filtering of the data is a good way to remove both mechanical and electrical noise of the IMU, a critical action to reliably estimate the position. Kowalczuk & Merta (2015) published an article containing an analysis of the sensor features, noise and drift, sensor angular position, dynamics of object movements and the efficiency or inefficiency of filtration of acceleration signals. Two main types of noise are described, which are thermo-mechanical noise and flicker noise. The thermo-mechanical noise will fluctuate much more rapidly than the sampling rate, leading to a Gaussian white noise at high frequencies. The flicker noise however will provide disturbances at low frequencies. The bias that occurs by the flicker noise will according to the article grow quadratically over time if the acceleration data is double integrated.

Kowalczuk & Merta (2015) points out that the angular errors due to gravity changes, which will affect the sensor rotations, causes the largest error of the integrated data for low-cost digital IMU's. For the IMU's at Hosenøyan, this is an issue which the IMU is handling internally, according to the instruction manual. The integration as a process however will in addition boost the low frequencies (i.e. drift) of the IMU data, meaning that the drift should be removed prior to integration to obtain reliable results. However, the problem of band filtration of the IMU data can be very difficult, to the point of being ineffective, as the acceleration data is extremely sensitive to the effects of filtration.

Bender III et al. (2010) published an article discussing the different methods of determining significant wave height on a discus buoy, where they mainly described five different types of accelerometer methods. The accelerometer of the IMU used at Hosenøyan will in this categorization be a type 5 accelerometer. This is a type of accelerometer that computes the true earth-referenced acceleration by using accelerations from all three axes and the corresponding rotation data. This method provided the most accurate data in their research.

Even though the true earth-referenced accelerations are estimated automatically by the IMU at Hosenøyan, the method by Bender III et al. (2010) will be described through a series of equations below, starting with the acceleration data X_S, Y_S, Z_S measured by the IMU:

$$\begin{aligned} X_S &= \frac{-a_x + g_x}{g} \\ Y_S &= \frac{-a_y + g_y}{g} \\ Z_S &= \frac{-a_z + g_z}{g} \end{aligned} \tag{5.1.5}$$

The next step is to use the recorded Euler angles to obtain the earth-referenced accelerations, which for the measurements at Hosenøyan are done with the linear acceleration command as described in Chapter 4:

$$\begin{bmatrix} X_E \\ Y_E \\ Z_E \end{bmatrix} \begin{bmatrix} a_1 & b_1 & c_1 \\ a_2 & b_2 & c_2 \\ a_3 & b_3 & c_3 \end{bmatrix} \begin{bmatrix} X_S \\ Y_S \\ Z_S \end{bmatrix} \tag{5.1.6}$$

If the measured values for pitch (θ), roll (ϕ) and yaw (ψ) are inserted, the matrix can be written as the following series of equations:

$$\begin{aligned} a_1 &= \cos\theta \cos\psi \\ b_1 &= \sin\phi \sin\theta \cos\psi - \cos\phi \sin\psi \\ c_1 &= \cos\phi \sin\theta \cos\psi + \sin\phi \sin\psi \\ a_2 &= \cos\theta \sin\psi \\ b_2 &= \sin\psi \sin\theta \sin\psi + \cos\phi \cos\psi \\ c_2 &= \cos\phi \sin\theta \sin\psi - \sin\phi \cos\psi \\ a_3 &= -\sin\theta \\ b_3 &= \sin\phi \cos\theta \\ c_3 &= \cos\phi \cos\theta \end{aligned} \tag{5.1.7}$$

Now the true earth-referenced accelerations can be estimated as given in Equation 5.1.8:

$$\begin{aligned} A_x &= -gX_e \\ A_y &= -gY_e \\ A_z &= g(1 - Z_e) \end{aligned} \tag{5.1.8}$$

Result of the litterature study

Through the results of the literature study done on the topic of double integration of acceleration data, the following method was decided to use to evaluate the acceleration measurements from Hosenøyan:

- Direct time domain integration, using the trapezoid rule.
- Try to find the best possible band pass filter, and empirically determine the best fitting cut-off frequencies. The mean of the data will also be removed prior to the estimations.
- Include a window function to prevent initial effects and end effects to affect the resulting position data.

5.2 Data evaluation

For the analysis of the acceleration measurements, the idea is to integrate the accelerations numerically twice into position using the trapezoid rule. This will be done using MATLAB and the internal function "trapz". Furthermore, the idea is to evaluate the position estimates both in frequency domain by calculating the zero-th moment using Parseval's theorem described in Equation 5.3.1, in addition to evaluating them directly in the time domain by calculating the mean of the one third highest waves, as described in section 3.3.1

The reason for this method is to showcase that the method of evaluating the acceleration data may have influence on the end results, especially when the raw data first must be integrated twice. During this process, drift and noise effects have a huge effect on the resulting position data, and the raw estimated positions can be as unreasonable as several kilometers high if not filtered, detrended and otherwise sufficiently treated. This will again lead to a potential large source of error regarding the accuracy of the estimated fish cage elevation responses. However, given that the IMU data from the two fish cages are treated identical, potential differences and therefore spatial variations may still be valid as long as the assumption that the two fish cages are identical holds.

The IMU data consists of 645 txt-files for each fish cage, each consisting of one hour of measurements at sampling speed 10 Hz, giving about 23,22 million measurement values per fish cage. Since each txt-file consist of one hour data, it is practical to estimate the statistical properties from each txt-file, which is an interval that can be assumed a Gaussian stochastic process as mentioned in section 4.3.

MATLAB scripts

The following list are a description of the main MATLAB scripts that have been written to evaluate the txt-files from the IMU measurements in MATLAB. ImportFilesFromHosenøyan.m, FileToMatrixFromHosenøyan.m and CalculateMoment.m are based on work done by Stemsrud (2018). The scripts can be found in Appendix B.

- ImportFilesFromHosenoyan.m: Imports the txt-files from the IMU to MATLAB.
- FileToMatrixFromHosenoyan.m: Converts numeric data from txt-files to a matrix in MATLAB.
- TrapzintegrationOfAcceleration.m: Numerically integrates the data twice using the built in function "trapz", which applies the trapezoid rule.
- CalculateMoment.m: Calculates and plots the zero-th moment of the fish cage elevation responses for every hour. In addition, it calculates and plots $\eta_{3,m0}$ using the calculated zero-th moment for each hour. Band pass filter and window function are included.
- CalculateHsandTz.m: Calculates and plots $\eta_{3,s}$ and T_z directly by using the mean of the 1/3 highest fish cage elevation responses recorded per hour for $\eta_{3,s}$, and the mean of the zero-crossing periods for T_z. Band pass filter and window function are included in the script.
- Comparedirectionalwaves.m: Sorts the calculated fish cage elevation response data and wave buoy data into eight directions (N, NE, E etc.), using wave direction data from the wave buoy.
- transferfunctionVSwaveDirection.m: Sorts the calculated transfer function into eight directions (N, NE, E etc.) using wave direction data from the wave buoy.

In addition to the MATLAB scripts, several scatter plots of both H_s, T_z and the transfer functions shown in Chapter 6 have been made in Excel.

5.2.1 Numerical integration methods

To double integrate the acceleration data into elevation response estimates for such a high number of discrete measurements, a numerical integration approach was chosen. The trapezoid rule is a two-point numerical integration method, meaning that it approximates the integral using only the end points a and b, as seen in the Equation 5.2.1

$$\int_a^b f(x)dx \approx [\frac{f(a)+f(b)}{2}](b-a) \tag{5.2.1}$$

whereas the Simpson's rule is a three point numerical integration method, described in Equation 5.2.2:

$$\int_{x_0}^{x_2} f(x)dx \approx \frac{1}{3}[f_0 + 4f_1 + f_2](x_2 - x_0) \tag{5.2.2}$$

The Simpson's rule assumes the three point being equally distant from one another, which is ensured given the constant sampling speed of 10 Hz of the IMU. For that reason $x_2 - x_0 = b - a = \Delta t = 0.1s$

The idea was at first to use both the trapezoid rule and the Simpson's rule in the integration process for comparison, and for that reason scripts in MATLAB for both methods were written. For the trapezoid rule, MATLAB has a built in function called "trapz", and a similar script were used for the Simpson's rule where the integration algorithm were altered into the Simpson's rule. However, since the end result of these two numerical integration methods showed little to no difference, only the results from the trapezoid rule are used in further analysis. The reason for the small differences, even though the Simpson's rule is assumed to yield a better approximation than the trapezoid rule, seems to be that the effects of filtering the data are much more significant than the type of integration method that is used.

As described in section 5.1, integration of the acceleration measurements will induce drift that will heavily influence the results. For that reason, the unfiltered integrated data will also be shown in the results in Chapter 6, to indicate the significant effect filtering of the data has on the estimated fish cage elevation responses.

Removing offsets and trends

After integrating the acceleration measurements twice, the MATLAB function "detrend" is used to remove unwanted trend lines/offsets that might have occurred due to the errors generated by the integration process. The MATLAB function "detrend" removes polynomial trends of the chosen degree n. According to Beck & Wannick (2017), if an offset O_1 occur in the first function, it will lead to a linear offset after the first integration and further to a quadratic offset after the second integration, as described in Equation 5.2.3:

$$\begin{aligned} \int (f(t) + O_1)dt &= \int f(t)dt + O_1 \cdot t + O_2 \\ \int \int (f(t) + O_1)dtdt &= \int \int f(t)dtdt + O_1 \cdot t^2 + O_2 \cdot t + O_3 \end{aligned} \tag{5.2.3}$$

Therefore, the "detrend" function with degree $n = 2$ is implemented to the integrated values after the integration. In addition, the mean value of the data is removed prior to integration in order to remove disturbances of the measured data.

5.2.2 Filter and window functions – treatment of the measured data

Due to the assumption that the IMU will record noise which will affect the estimated fish cage elevation responses, an appropriately designed filter is necessary to make sense of the results. The idea with the use of the filter is to remove unwanted noise signals, in order to ensure that the values of the estimations are representative and give realistic values of the actual motions of the fish cages. However, according to the literature study done in section 5.1, this task is not simple. As a result, some noise of the signal will be expected.

It is customary to differentiate between high pass, low pass and band pass filters:

- High pass filters: Lower frequencies than the chosen cut off frequency are attenuated
- Low pass filters: Higher frequencies than the chosen cut off frequency are attenuated
- Band pass filters: Both high and low frequencies are attenuated, and only frequencies between the cut-off frequencies are allowed to pass.

Which filter type to use should depend on where in the frequency realm the noise from the measuring instrument is located, or assumed to be located.

Butterworth band pass filter

As showed in Figure 4.2.7, wind waves typically have wave periods in the range of 0.5 s to 25 s, corresponding to a frequency band from 0.04 Hz to 2 Hz. The main part of the waves usually have a frequency around 1 Hz. Due to the sampling speed of the IMU being 10 Hz, this means that the waves within this interval should be detected according to both the Nyquist theorem and the equations by Han (2010) as described in section 5.1.

Using the result from the literature study and by empirically comparing the resulting fish cage elevation responses with the data from the wave buoy, it was determined to use a 5. order Butterworth band-pass filter to attenuate both noise and drift. The Butterworth filter is characterized with having a flat frequency respond, but a slow roll of. As stated by Beck & Wannick (2017), the slow roll of would only be a problem if a perfect cut-off frequency could be found, which is not the case due to the noise frequencies and the elevation frequencies potentially fading into each other.

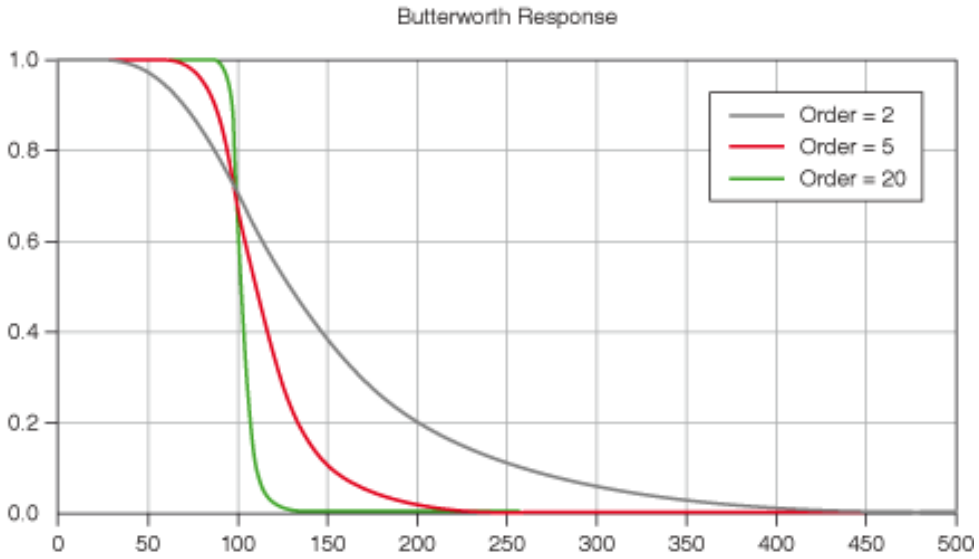

Figure 5.2.1: Illustration of the Butterworth filter for different orders. Source: National Instruments retrieved from: `https://zone.ni.com/reference/en-XX/help/371361R-01/lvanlsconcepts/lvac_butterworth_filters/`

For evaluation directly in time domain, three different low cut-off frequencies are empirically chosen for comparison. These were set to 0.1, 0.125 and 0.15 Hz and the high cut-off frequency was set to 3 Hz. For evaluation in the frequency domain, two different low cut-off frequencies were chosen empirically. They were set to 0.25 and 0.275 Hz, while the high cut-off frequency remained at 3 Hz. MATLAB has a built in function of the Butterworth filter called "butter", where the input are normalized cut-off frequencies. This means that the chosen cut-off frequencies were divided with the Nyquist frequency $f_{Ny} = \frac{f_s}{2} = \frac{10}{2} = 5[Hz]$. In Table 5.2.1 the cut-off frequencies yielding the assumed best results are listed, which are a low cut-off frequency of 0.125 Hz for evaluation in the time domain, and low cut-off frequency of 0.275 Hz in the frequency domain.

	Time domain evaluation	Spectral evaluation
Normalized low cut-off freq.	0.025	0.055
Normalized high cut-off freq.	0.6	0.6

Table 5.2.1: Cut-off frequencies for the 5. order Butterworth filter used in the analysis

It was seen through the empirical testing of different cut-off frequencies that the low cut-off frequency had the most impact on the results. Overall, the filtering of the data had the most significant effect on the results out of all treatment of the data, as expected from the literature study in section 5.1.

Bingham window

Lastly, a window function was applied to the position estimates to avoid spectral leakage and the other frequency ranges that spectral leakage might produce. In addition, applying a window function on the data would help reducing potential initial effects and end effects that might contribute to unsatisfactory results. The window function chosen was the Bingham window as written in Newland (2005):

$$\omega(n) = 0.5 + 0.5 \cos \frac{2n}{N}\pi, n = -\frac{N}{2}, ..., -1, 0, 1, ..., \frac{N}{2} - 1 \tag{5.2.4}$$

The Bingham window function is set to gradually attenuate the first and last 10 % of the data in every txt-file, shown in Figure 5.2.2.

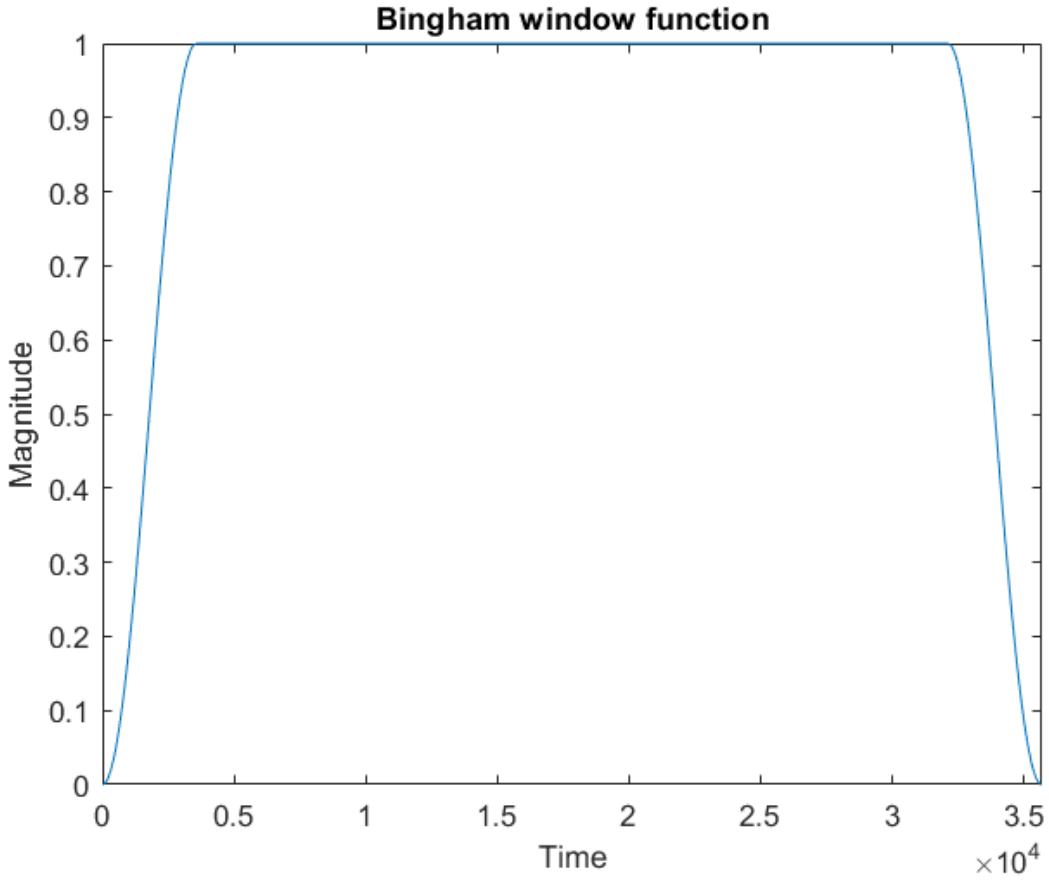

Figure 5.2.2: Illustration of the Bingham window function.

5.3 Estimating wave parameters and fish cage motion parameters

5.3.1 $\eta_{3,s}$, $\eta_{3,m0}$ and T_z

As stated in the introduction, the parameters of interest to estimate from the measured data is H_s and T_z. The significant fish cage elevation response will be denoted $\eta_{3,s}$ for fish cage elevation responses estimated in the time domain, and $\eta_{3,m0}$ for fish cage elevation responses estimated using spectral moments. The following section will give an explanation to how those parameters are estimated.

Estimating $\eta_{3,s}$ and T_z directly in time domain

To estimate $\eta_{3,s}$ directly, the script "calculateHsandTz" was written in MATLAB to localize the position of the zero up-crossing of the samples. The script will also count every zero up-crossing period that occurs for all of the 645 txt-files. Further the maximum of the samples within that interval were found, meaning that the maximum fish cage elevation response for that particular interval is determined. When all of the maximums have been found, the mean of the $1/3$ highest fish cage elevation responses was calculated. This provides an estimation of $\eta_{3,s}$ for every txt-file, which as mentioned represents one hour of samples.

A similar approach was then done to estimate the zero up-crossing period T_z. Since the MATLAB script calculated the position of every zero up-crossing point in the data, and the samples were measured with a constant sampling speed of 10 Hz, or in other words every 0.1 s, T_z was found by multiplying the difference in position for the zero-crossing with $\Delta t = 0.1s$. For instance, if a zero up-crossing was detected at sample 71 and 112, the zero up-crossing period would be $(112 - 71) \cdot \Delta t = 4.1s$. The script can be found in the Appendix, section B.6.

Estimating $\eta_{3,m0}$ using zero-th spectral moment

As written in section 3.3.1, it is possible to estimate statistical wave parameters using spectral moments, with the significant wave height being estimated as $H_s \approx H_{m0} = 4 \cdot \sqrt{m_0}$.

To establish a power spectrum to calculate the zero-th spectral moment of the calculated fish cage elevation response data, Parseval's theorem has been used. According to Vogel et al. (n.d.) the use of Parseval's theorem can be used to calculate the zero-th moment m_0 directly in the time domain, by combining Equation 3.3.9 and Equation 5.3.1:

$$\sum_{n=0}^{N-1} x[n]^2 = \frac{1}{N} \sum_{k=0}^{N-1} X[k]^2 = m_0 \tag{5.3.1}$$

where x[n] is a sequence with N points, and X[k] is the Fast Fourier Transformation (FFT) of the signal, defined according Equation 5.3.2:

$$F(\omega) = \int_{\infty}^{\infty} f(t) e^{-i\omega t} \tag{5.3.2}$$

In MATLAB, the Discrete Fourier Transform (DFT) can be calculated using a built in function called "fft". The DFT can be described according to Equation 5.3.3:

$$X_k = \sum_{n=0}^{N-1} x_n \cdot e^{-\frac{i2\pi}{N} kn} \tag{5.3.3}$$

The spectral moments for every txt-file is calculated, giving an estimate for m_0 for every hour of the measurements. This is done using the script CalculateMoment, which can be found in the Appendix, section B.5

5.3.2 Wave parameters

Other wave parameters such as wave length λ, wave number k and wave frequency ω were estimated in Excel based on the wave buoy estimates of T_{m02}. The estimations were done for each hour of data as with the estimations of the fish cage elevation responses. The parameters were estimated according to deep water linear theory. Further, the various wave parameters were analysed by estimating the minimum value, maximum value, the mean of the parameter and the standard variation of the parameter.

Linear transfer functions

The linear transfer functions were also estimated in Excel according to Equation 3.5.8, using H_{m0} from the wave buoy. As discussed in subsection 4.2.3, the wave buoy is located around 500 m South/South East of the fish cages that are evaluated, at a location having approximately twice the depth. This would mean that the waves that induces the fish cage motions could for many cases be different than the waves measured by the wave buoy, which could possibly lead to a significant error when estimating the linear transfer functions. Nevertheless, due to the lack of data regarding the wave conditions at closer proximity of the cages, the wave buoy data will be used for for the results presented in Chapter 6.

The linear transfer functions will be evaluated with regards of the incident wave direction θ, the wave period T_z, the wave length λ and similar to Figure 3.5.2 by Li (2017), with regards to $k \cdot a$. The wave number k is estimated according to deep water linear theory as described in subsection 3.1.1, i.e. using $k = \frac{2\pi}{\lambda}$ and $\lambda = \frac{gT^2}{2\pi}$.

Chapter 6

Results and discussion

In this chapter, the results of the evaluation of the acceleration measurements at Hosenøyan will be presented. Both the evaluation done directly in time domain and the evaluation done by calculating the spectral moment will be shown. Comparisons with the wave buoy data for $\eta_{3,s}$, $\eta_{3,m0}$ and T_z will be presented. The differences of the period and the elevation response of the two fish cages will be investigated. Furthermore, the estimated fish cage elevation responses will be analysed with respect to the wave directions measured by the wave buoy. The linear transfer function between H_{m0} from the wave buoy and the fish cage elevation responses will be presented and discussed. Lastly, a discussion of the potential factors leading to error and bias will be listed and discussed.

6.1 Fish cage elevation response

6.1.1 Evaluation of $\eta_{3,s}$

Figure 6.1.1 shows the estimated fish cage elevation responses for fish cage 8 and fish cage 9, arranged according to Figure 4.2.4. The top plot shows the fish cage elevation responses that are evaluated with the Butterworth band pass filter and Bingham window, while the bottom plot represents the elevation response data without any treatment. As expected, without treatment of the data, the fish cage elevation responses are very unreasonably estimated to be as high as a peak 35000 meters, displaying the huge effect filtering of the data has on the end results. Additional results, showcasing the effects of the chosen cut-off frequencies can be seen in the Appendix, subsection A.1.1.

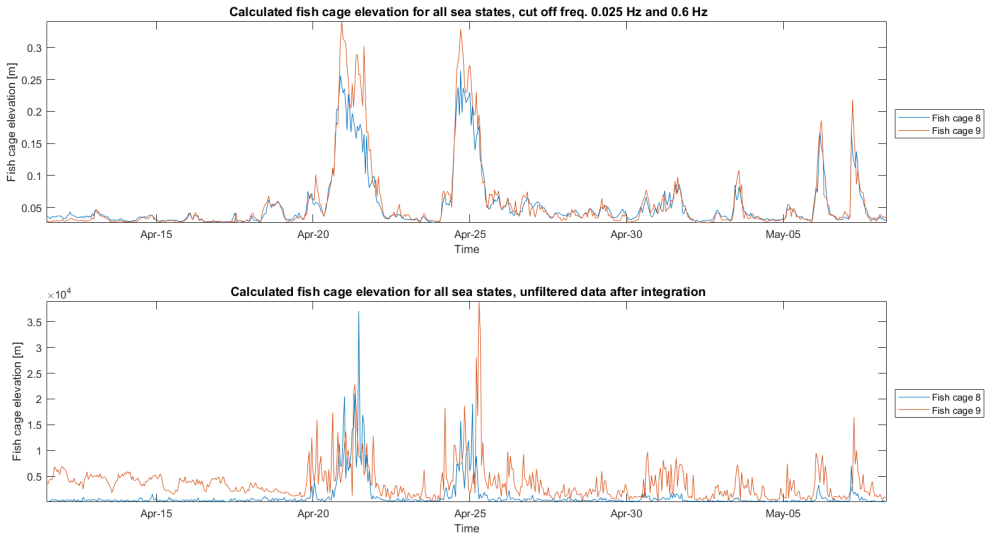

Figure 6.1.1: Estimated elevation responses with normalized low cut-off freq. 0.025 and high cut-off freq. 0.6

The results show differences of the estimated fish cage elevation responses in several different periods of time. Most notably, the differences seem to grow larger when exposed to larger waves, as can be seen in the peak elevation responses in Figure 6.1.1.

Fish cage elevation response in comparison with wave buoy data

The main challenge was to design the cut-off frequencies of Butterworth filter such that the resulting fish cage elevation responses corresponded as well as possible with the incoming waves estimated by the wave buoy data. The hypothesis prior to estimation was that the fish cage motions would correspond well with the incoming waves for the most part, and especially for wave lengths longer than the diameter of the fish cages of 50 m. However, as shown in Figure 6.1.2, it proved to be a difficult task. The main issue were to ensure that the estimated fish cage elevation responses were not significantly larger than the incoming waves, while simultaneously make the fish cage elevation responses correspond to the incoming peak waves as well as possible. This proved to be a problem during the periods of low wave height according to the wave buoy data, which often occurred during the first third of the measurements as seen in Figure 6.1.2.

It turned out to be very difficult that both of the criteria mentioned was met, and the end results display that. From Figure 6.1.2 it is clear that the fish cage elevation responses did not correspond to the incoming waves measured by the wave buoy as well as one could assume prior to the analysis. The peak elevation responses of the fish cages are below half of the peak wave elevations, and still some of the fish cage elevation responses are larger

than the incoming waves at other periods of time. This will be presented in section 6.4. In Figure 6.1.2, the wave buoy estimation of H_{m0} is divided by two to represent the wave crest height ζ_{m0} using linear theory.

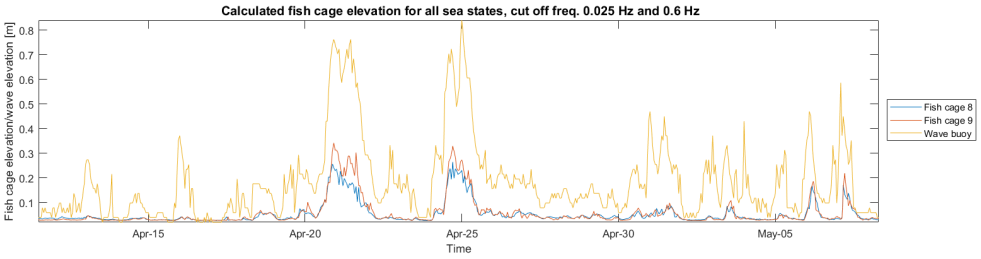

Figure 6.1.2: Estimated elevation response in comparison with data from the wave buoy with normalized low cut-off freq. 0.025 and high cut-off freq. 0.6

Table 6.1.1 presents the minimum value, maximum value, the mean of the data and the standard deviance of the data, indicating the differences of the motions of the two fish cages themselves and the differences between the fish cages and the wave buoy measurements. Most notably is the low mean of the elevation responses in comparison to the wave buoy data. This is a consequence of preventing the fish cage elevation responses from being larger than the incoming waves, and this issue can be demonstrated by the low standard deviance of the data.

	$\eta_{3,s}$ [m], fish cage 8	$\eta_{3,s}$ [m], fish cage 9	ζ_{m0}, wave buoy [m]
Min	0.0261	0.0259	0.0196
Max	0.2638	0.3414	0.8399
Mean	0.0537	0.0578	0.1833
Std. dev.	0.0437	0.0577	0.1620

Table 6.1.1: Estimation of fish cage elevation responses using normalized low cut-off freq. 0.025 and high cut-off freq. 0.6.

6.1.2 Evaluation of $\eta_{3,m0}$

Similar results were achieved by calculating the zero-th spectral moment to evaluate the position data, presented in Figure 6.1.3. Just as with the direct estimation method, the main issue was the large effect of the band pass filter. This lead again to the issue of not overestimating the fish cage elevation response when the wave buoy measures low wave heights, while also ensuring that the fish cage elevation responses corresponded well to the peak waves. This required a change of cut-off frequencies in comparison to the direct evaluation, with the normalized low cut-off frequencies being slightly higher at 0.055.

The results of the fish cage elevation responses by calculating the spectral moment can be seen in Figure 6.1.4. The minimum value, maximum value, mean of the data and standard deviation of the data are shown in Table 6.1.2. Additional results can be seen in the Appendix, subsection A.1.1.

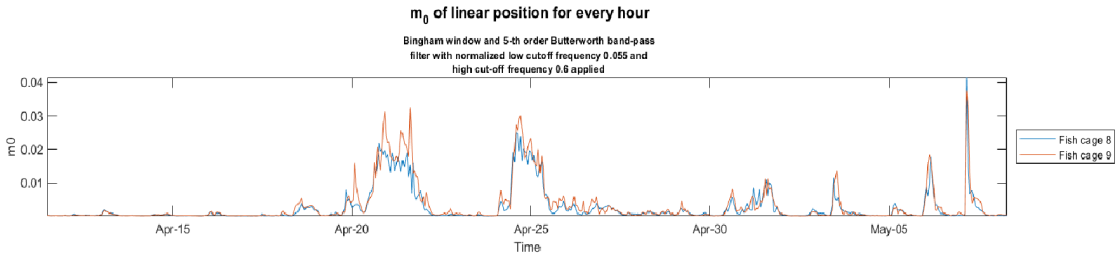

Figure 6.1.3: m_0 of the resulting fish cage elevation response data, filtered with normalized low cut-off freq. 0.055 and high cut-off freq. 0.6

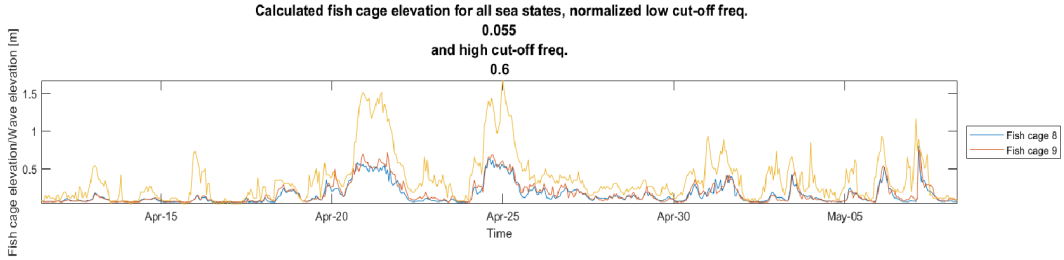

Figure 6.1.4: Resulting fish cage elevation response using m_0, filtered with normalized low cut-off freq. 0.055 and high cut-off freq. 0.6

	$\eta_{3,m0}$ [m], fish cage 8	$\eta_{3,m0}$ [m] fish cage 9	H_{m0}, wave buoy [m]
Min	0.0574	0.0584	0.0391
Max	0.8143	0.7747	1.6797
Mean	0.1629	0.1771	0.3665
Std. dev.	0.1312	0.1466	0.3240

Table 6.1.2: Estimation of fish cage elevation responses using the zero-th spectral moment. Normalized low cut-off freq. 0.055 and high cut-off freq. 0.6.

Comparing the two methods for estimating the fish cage elevation responses, it seems like the spectral analysis provided slightly better results. It seems to correspond to the incident waves slightly better, especially towards the end of the measuring period. Looking at Table 6.1.2, all of the values are higher and closer to the data from the wave buoy. Note that the values of Table 6.1.2 are scaled with a factor of two, compared to Figure 6.1.2 and Table 6.1.1. However, both methods have large deviance with the data from the wave buoy. The reason for the deviance will be further discussed in section 6.5.

6.1.3 Fish cage elevation responses for every wave direction

Figure 6.1.5, Figure 6.1.6 and Figure 6.1.7 show the estimated fish cage elevation responses ($\eta_{3,m0}$) for incoming waves of eight directions (North, North East, East etc). The fish cage response estimates used here are estimated using the zero-th spectral moment. The x-axis describe the number of times a wave were recorded from that particular direction. The directions are defined according to the compass directions, identical to Figure 2.3.1. For example, East is defined as 45 $\pm$ 22.5 degrees. The wave directions available from the wave buoy data are used.

A surprising result is that the highest estimated values of fish cage elevation response seem to be as the result of incoming waves from West, North West and North, even though these are areas well protected by islands and skerries. The wave directions assumed to have the harshest waves, South/South West and North East, displays some of the lowest results of fish cage elevation responses.

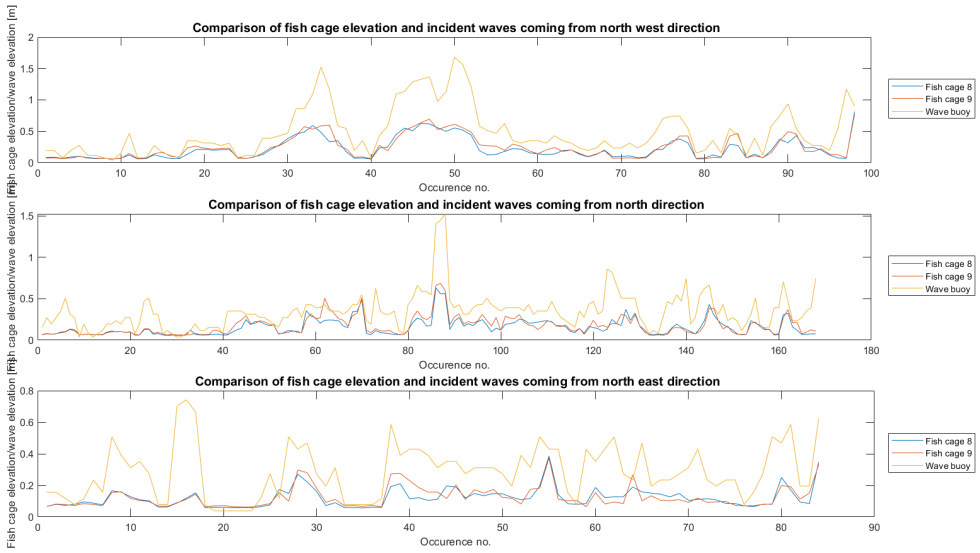

Figure 6.1.5: Estimated fish cage elevation responses from spectrum analysis for waves coming from North west, North and North East.

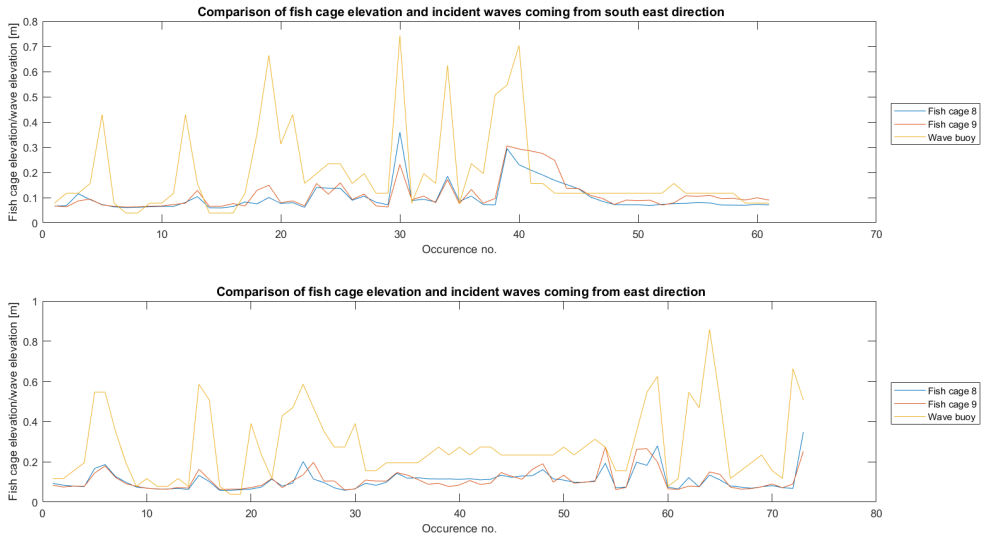

Figure 6.1.6: Estimated fish cage elevation responses from spectrum analysis for waves coming from South East and East.

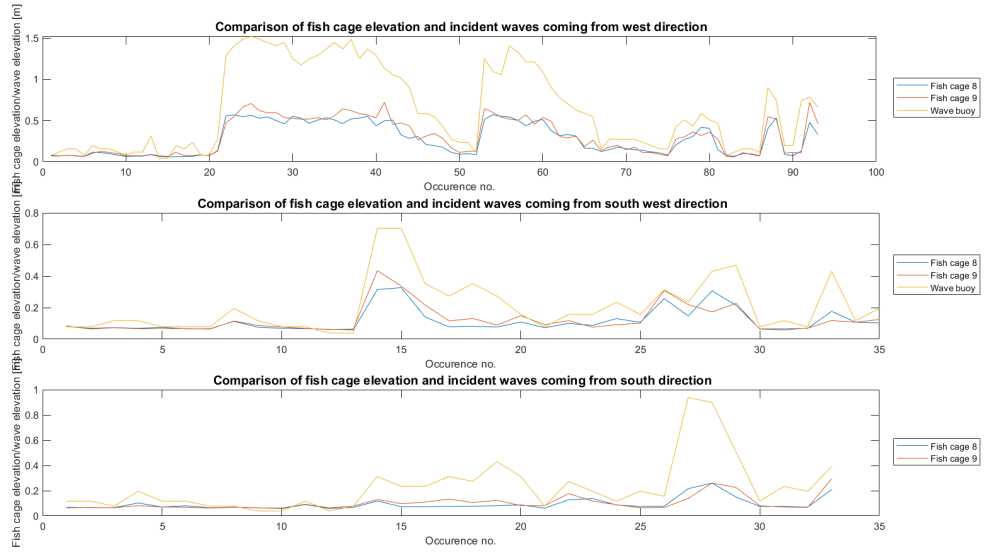

Figure 6.1.7: Estimated fish cage elevation responses from spectrum analysis for waves coming from West, South West and South.

However, since the wave directions are estimated from the wave buoy, which is located about 500 m South/South East of the fish cages in question as described in subsection 4.2.3, this result increases the probability of the wave conditions at the fish farm being different than measured by the wave buoy. It seems that the direction the fish farm is set, from North West to South East as seen in Figure 4.1.4, may be an important factor on the end results. According to Figure 1.1.1, fish cages 1 and 7 were absent at the time of the recording. This would indicate that the waves coming from the North West and West directions would propagate towards the IMU's at fish cage 8 and

9 with the least obstacles compared to waves coming from any other direction. Since the IMU's were placed towards the center of the fish farms as shown in Figure 4.2.4, it seems that waves coming from other wave directions are significantly dampened by the floating collars and corresponding nets before reaching the IMU's of fish cage 8 and 9. It may also be reasonable to assume that part of the wave energy is reflected due to the obstacles.

Figure 6.1.8 show a scatter plot of the fish cage elevation responses estimated using the zero-th moment. The x-axis represents the direction of the waves recorded by the wave buoy. The scatter plot indicates the low mean and variations of the fish cage elevation responses compared with the wave data from the wave buoy, in addition to indicate the high-value results from North, North West and West directions.

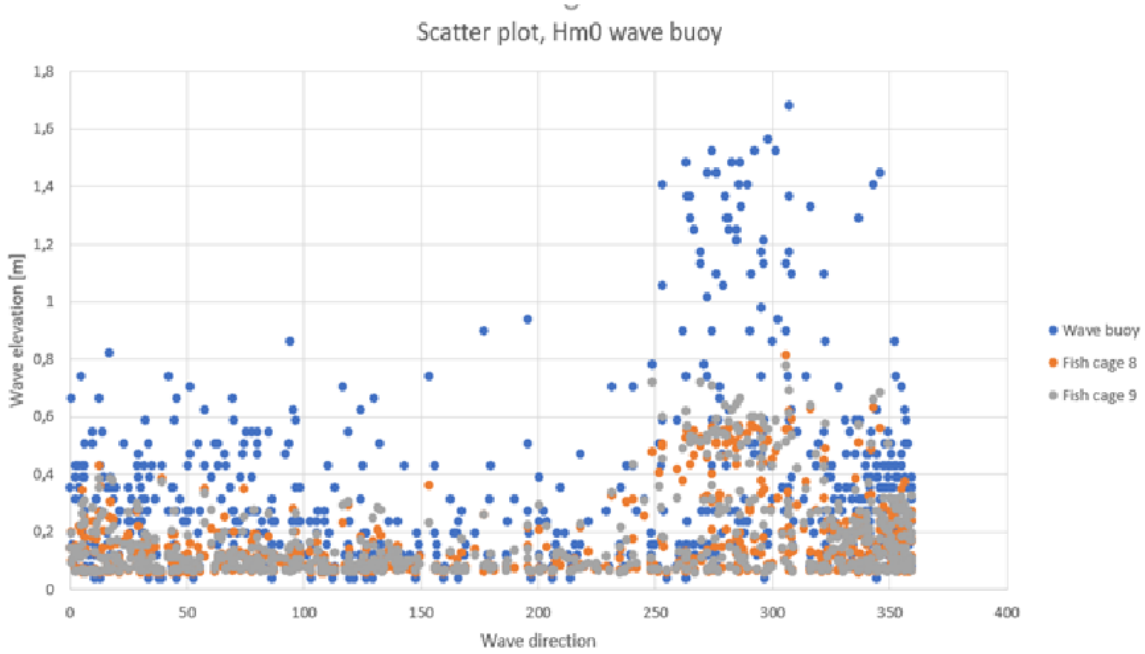

Figure 6.1.8: Scatter plot of fish cage elevation responses and wave buoy elevation data.

The same plots are made with the fish cage elevation responses obtained with the direct estimation method. The results had similar trends, if anything the trends were even more apparent in these plots. The plots can be found in the Appendix, subsection A.1.2.

6.2 Fish cage elevation period

6.2.1 Evaluation of T_z

As described in section 5.3, the zero up-crossing period T_z were estimated directly from the fish cage elevation response data. The estimated zero up-crossing periods are shown in Figure 6.2.1. As with the estimation of $\eta_{3,s}$, the integration of the acceleration data will result in very bad estimations of the resulting elevation periods if not treated sufficiently, showed in the bottom plot in Figure 6.2.1. The top half of Figure 6.2.1 represents the data after it is filtered with the Butterworth band pass filter, and the Bingham window function is applied.

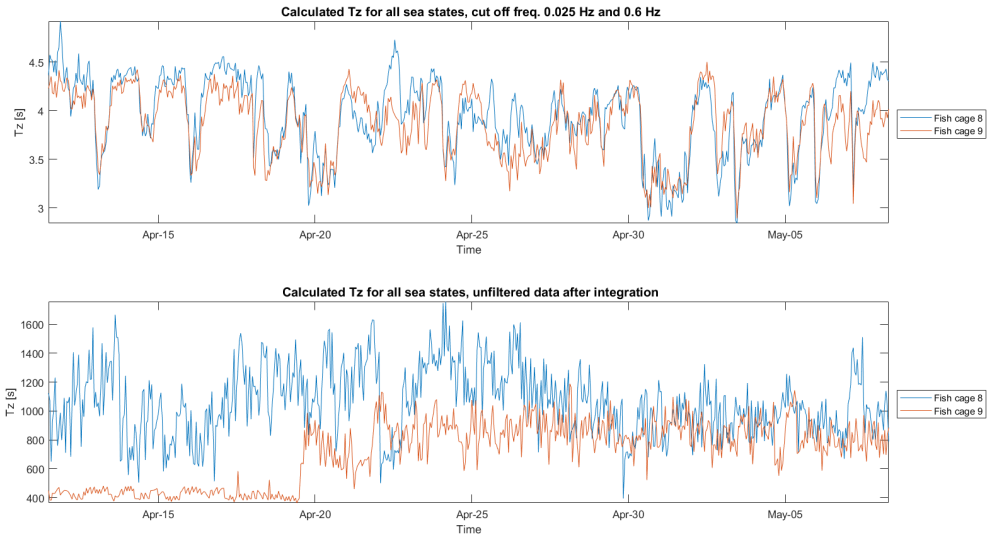

Figure 6.2.1: Estimated fish cage elevation period with normalized low cut-off freq. 0.025 and high cut-off freq. 0.6

From Figure 6.2.1 it is clear that the deviance of the elevation period between the two fish cages are for the most part small. Another observation is that T_z only ranges from around 3 s to around 4.5 s. This is a very small range of elevation period, that most likely is a result of the filtering of the data. However, the effects of the mooring, bottom weights and the net of the fish cages might also have an effect on the short range of the elevation period.

Fish cage elevation period comparison with wave buoy data

Figure 6.2.2 shows the estimated elevation periods with the estimated incident wave period T_{m02} from the wave buoy data. Here, the short range of the elevation period of the fish cages compared to the wave buoy data is evident. The short range of elevation periods due to the filtering might have played a significant role in the estimation of the fish cage elevation responses, as it could imply that not all of the different incoming waves were evaluated after the filtering. This could lead to smaller estimated elevation responses than the fish cages originally had.

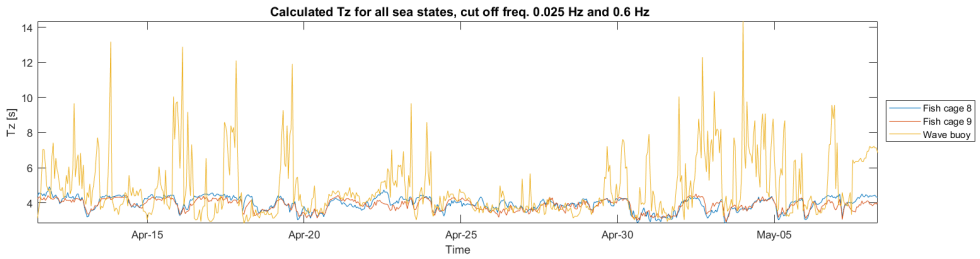

Figure 6.2.2: Estimated fish cage elevation period in comparison with wave buoy data with normalized low cut-off freq. 0.025 and high cut-off freq. 0.6

As with the estimation of the fish cage elevation responses, the minimum value, maximum value, the mean of the data and the standard deviation of the fish cage elevation periods were calculated, as shown in Table 6.2.1. Here it is easy to observe the range of the period, which can be represented by the difference between the maximum value and the minimum value, is very different. It is also indicated by the large difference of the standard deviation. However, the mean of the data is still quite similar, indicating that the resulting estimations of the periods are relatively acceptable.

	T_z [s], fish cage 8	T_z [s], fish cage 9	T_{2m0}, wave buoy [s]
Min	2.8423	2.8923	2.8320
Max	4.9217	4.5014	14.3555
Mean	3.9506	3.8638	4.8524
Std. dev.	0.3960	0.3422	1.7361

Table 6.2.1: Estimation of fish cage elevation periods using normalized low cut-off freq. 0.025 and high cut-off freq. 0.6. (8) represents fish cage 8, (9) represents fish cage 9

Figure 6.2.3 show a scatter plot of the estimated fish cage elevation periods, with the x-axis being the wave directions recorded by the wave buoy. The low range of the fish cage elevation period compared to the period of the incident waves are very clear. In addition, the estimated period of the fish cage elevation responses seem to be independent of the wave direction judging by this scatter plot.

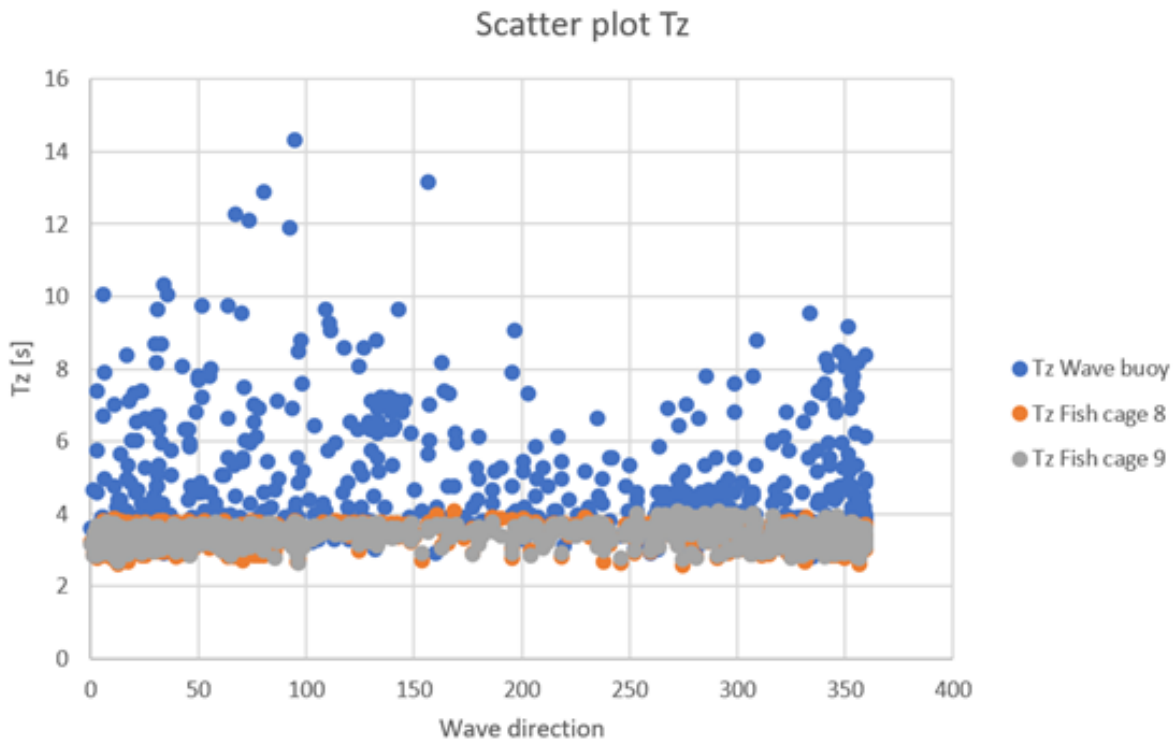

Figure 6.2.3: Scatter plot of fish cage elevation period and wave buoy elevation period.

Additional results for different cut-off frequencies of the Butterworth filter can be seen in the Appendix, subsection A.1.3. The additional results show the same trend of a low range in the period, where the main difference of the results are a shift in values of the mean of the elevation periods.

6.3 Spatial variations – discussion

Judging by the results presented in this chapter, there are some indications of spatial variations of the fish cage elevation responses. For both of the methods used to estimate the fish cage elevation responses, fish cage 9 contained in general the maximum value of the data, as seen in Table 6.1.1 and Table 6.1.2. Looking at Figure 6.1.1 and Figure 6.1.4, there is a general trend that fish cage 9 had the highest fish cage response of the two cages, in particular during the peak values which represents the elevation responses of the fish cages during the harshest wave conditions of the measurement period. This is surprising considering that fish cage 9 is located in the middle of the fish farm, and fish cage 8 is presumed to be more exposed to waves coming from North and North West, which are the directions of the waves leading to the highest fish cage motions according to Figure 6.1.8. However, the difference of the maximum values are only about 4 cm for the spectral evaluation, and about 8 cm for the direct estimation method. In addition, since the trend seems to be that fish cage 9 in general have higher fish cage response, there is reason to believe that measuring errors and the treatment of the data might have affected the results, and therefore result in unreliable data.

From the perspective of spatial variations of wave conditions having an impact on the reliability of site surveys, the result indicates only minor differences of the motions of the fish cages. However, there seem to be a trend that the differences grow larger as the wave conditions gets harsher, which can prove to be important if the fish farm in question is located at more exposed areas. This is in particular observed from the direct estimations presented in Figure 6.1.1, but the same trend is also present in Figure 6.1.4.

In terms of elevation period, the difference of the two fish cages seem to be very small, judging by Figure 6.2.2. Table 6.2.1 shows that there is a slight difference in the maximum value of the data, but that the mean value of the data is very similar. The estimated elevation periods for both fish cages have a very short range compared to the period of the incident waves, and does not vary with the direction of the waves, as seen in Figure 6.2.3. This would indicate that the effects of filtering could be significant, but the effects of mooring, bottom weights and the net of the fish cage might have also played a role of the resulting elevation period. Nevertheless, it is reasonable to assume that the short range of frequencies could affect the estimated fish cage elevation responses.

6.4 Linear transfer functions

6.4.1 Transfer function comparison for every wave direction

Figure 6.4.1, Figure 6.4.2 and Figure 6.4.3 presents the estimated transfer functions, sorted by the direction of the incident waves using data from the wave buoy. For the most part of the measurement period, the transfer function is less than 1, but there are several peaks where the transfer function is well over 1. The highest transfer function estimated is around 2, which is a result that can be assumed to be plain wrong.

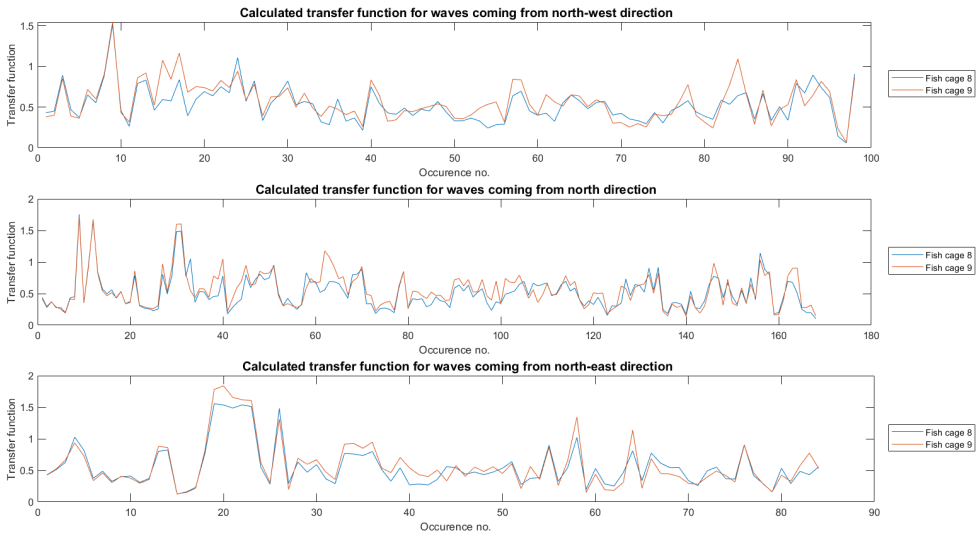

Figure 6.4.1: Estimated transfer functions from spectrum analysis for waves coming from North West, North and North East

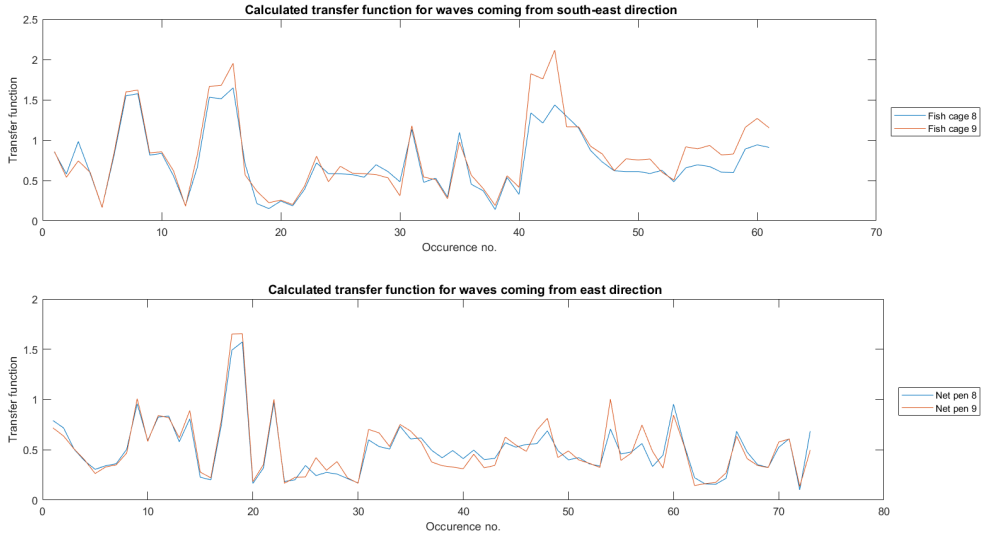

Figure 6.4.2: Estimated transfer functions from spectrum analysis for waves coming from South East and East.

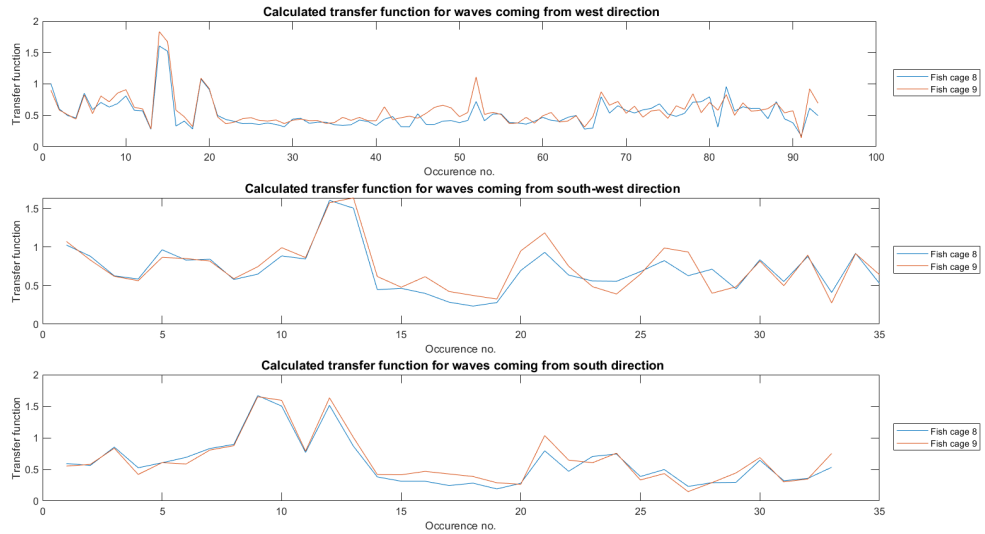

Figure 6.4.3: Estimated transfer functions from spectrum analysis for waves coming from West, South West and South.

Table 6.4.1 describes the minimum value, maximum value, the mean of the data and the standard deviation of the estimated transfer functions. The table displays some curious results such as the maximum values of the transfer function being unreasonably high. According to Figure 3.5.2, the transfer functions should rarely be larger one, leading to the fact that the peaks of the results must be disregarded. Most likely, the error is a result of the noise in the measurement, or the integration and filtering of the data. However, it can also be explained by the different sampling methods of the wave buoy and the IMU's at Hosenøyan. Since the wave buoy only records for 17 minutes of every hour, and the

IMU's measures continuously, there is a possibility that the IMU's could have endured harsher conditions for the remaining minutes of the hour. In that case, the assumption that one hour of measurements can be assumed a stationary process is wrong. This could explain the standout, single peaks of the figures, where the value of the transfer function is well over 1. In addition, the assumption of the wave buoy representing the wave conditions at the fish farm may not hold, as discussed in subsection 4.2.3.

	$RAO_{3,m0}$, fish cage 8	$RAO_{3,m0}$, fish cage 9
Min	0.0578	0.0676
Max	1.7543	2.1135
Mean	0.5591	0.6009
Std. dev.	0.2937	0.3259

Table 6.4.1: Estimation of linear transfer function $RAO = \frac{\eta_3}{\zeta_3}$, using ζ_3 from wave buoy data and normalized low cut-off frequency of 0.055 on the fish cage elevation response $\eta_{3,m0}$

Figure 6.4.4 show a scatter plot of the transfer function as a function of the wave direction. No observation of trends can be seen from the figure. Both the values below 1 and the error values at around 1.5 and above are to some extent evenly distributed for all wave directions.

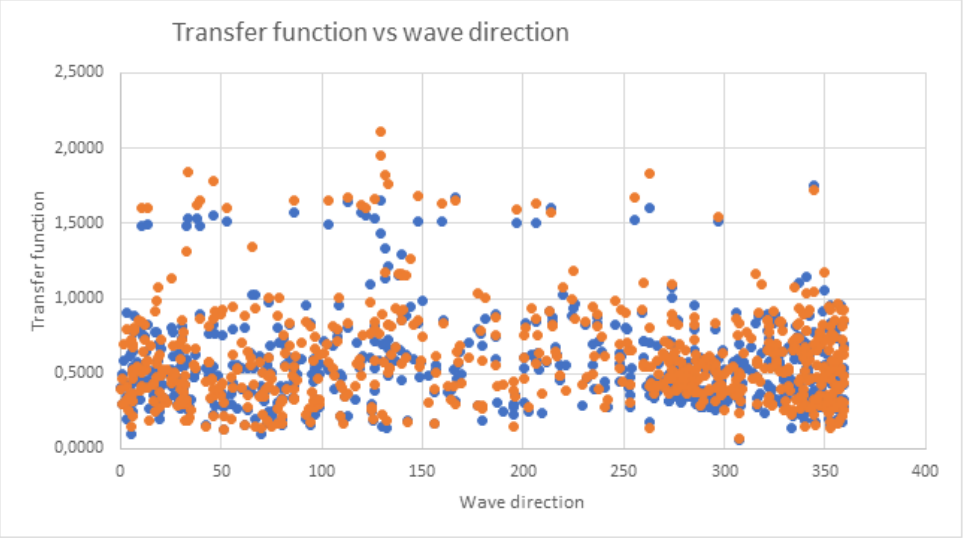

Figure 6.4.4: Scatter plot of estimated transfer functions from spectrum analysis for every wave direction

6.4.2 Transfer functions as a function of T_{m02}, λ and ka

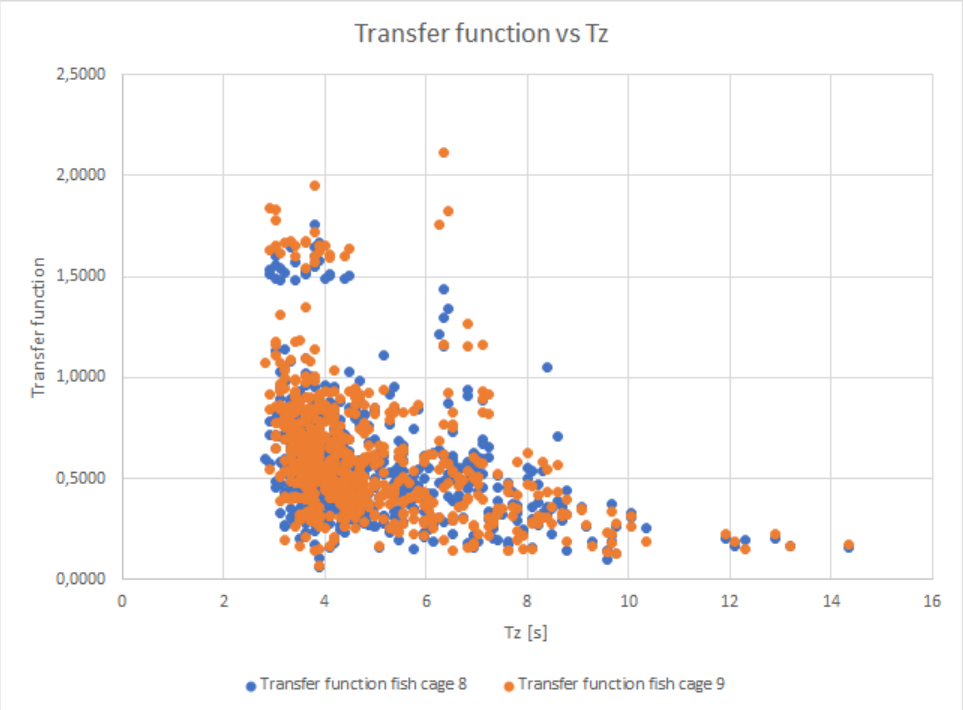

Figure 6.4.5: Scatter plot of estimated transfer functions from spectrum analysis as a function of T_{m02} from the wave buoy data

Figure 6.4.5 displays the transfer functions as a function of the zero-crossing wave elevation period T_{m02} from the wave buoy data. Once again the scatter plot does not display any clear trend of the transfer functions, other than that the unreasonably high transfer functions only occurs at the periods from around 3 s to 6 s. Figure 6.4.6 shows the transfer functions with regards of the wave length λ. Since wave period and wave length are related, where high values of T_{m02} lead to long wavelengths λ, the same lack of trends are apparent in Figure 6.4.6 as in Figure 6.4.5. Surprisingly the transfer function seem to be lower for long wavelengths, even though the assumption was the fish cage would correspond well with waves with long wave lengths. However, the degree that the fish cage motions corresponds to the incident waves is according to Li (2017) dependent on the angle the incident waves are interacting with the fish cage relative to the position of the IMU's, as seen in Figure 3.5.2.

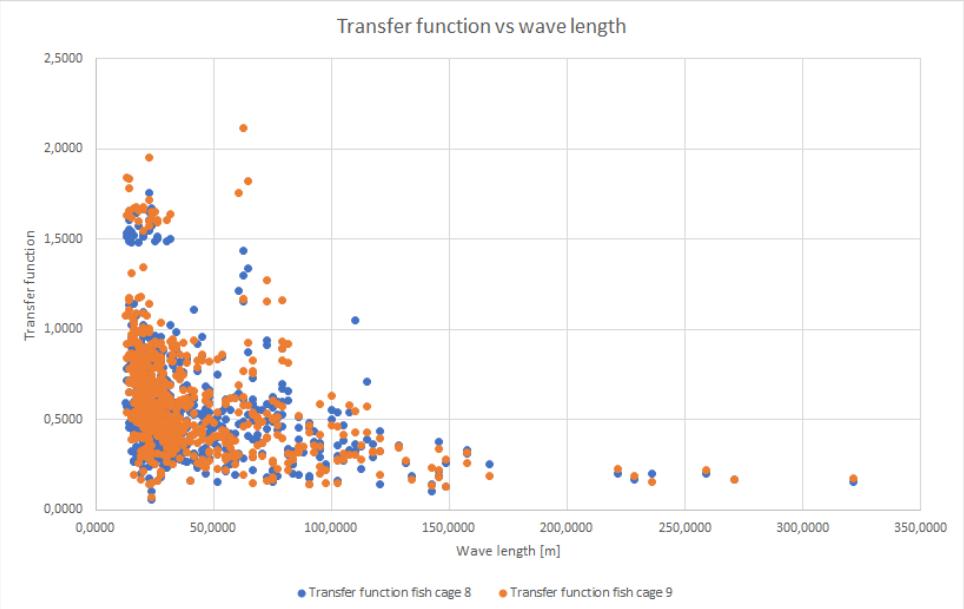

Figure 6.4.6: Scatter plot of estimated transfer functions from spectrum analysis as a function of the estimated wave length λ

Figure 6.4.7 presents the estimated transfer functions, with the wave number k multiplied with the cross-section radius of the floating collar a representing the x-axis. This is the same two axis used in Figure 3.5.2. However, no apparent trend could be observed by this result either, as the estimated transfer functions seem independent of the wave number. Figure 3.5.2 presents different results for the different positions of the torus, but since the estimated transfer function show no apparent dependency on the wave direction either, it stands to reason that including positions of the floating collar would also lead to unsatisfactory results.

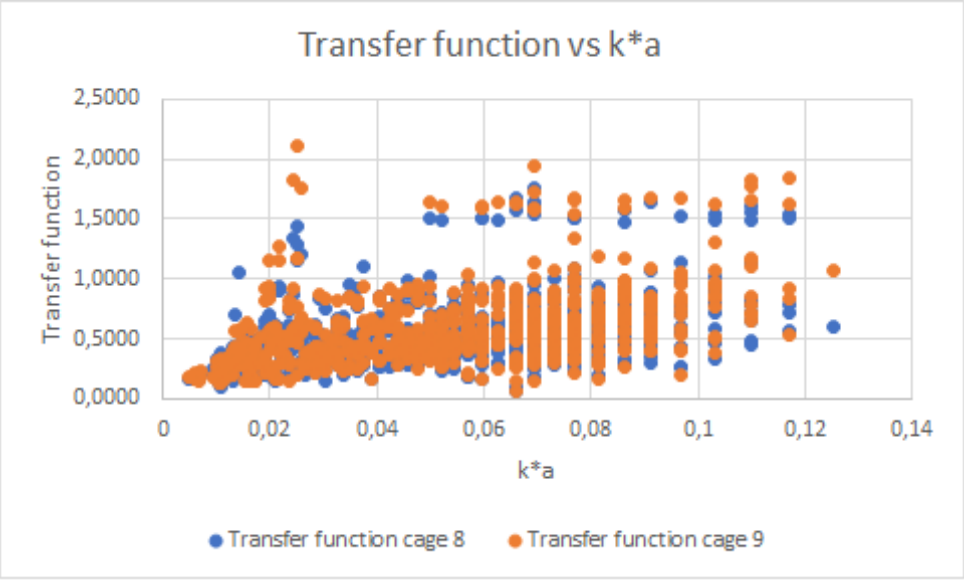

Figure 6.4.7: Scatter plot of estimated transfer functions from spectrum analysis as a function of $k \cdot a$

The results presented in this chapter indicates that the linear transfer function did not apply well for the integrated acceleration measurements of the fish cages. The reasons for this could be a combination of a lot of factors mentioned in this thesis. One could however argue that the linear assumption, the errors in estimating the fish cage elevation responses and the error of assuming the wave buoy data to be representative of the wave conditions at Hosenøyan are the main factors contributing to errors of the transfer functions. In addition, the placement of the IMU's towards the center of the fish farm may lead to even higher uncertainty in assuming the wave buoy representative for the wave conditions at the position of the IMU's. This is because the waves might be influenced by dampening effects and reflection of the wave energy before the fish cage motions caused by the incident waves are recorded by the IMU.

Still, it is worth mentioning that the effects of mooring, weights and bottom ring, and the net of the fish cage are not accounted for by Li (2017) in Figure 3.5.2. This leads to difficulties when compared with the estimated transfer functions, where those effects were presents. In addition, the study by Li (2017) focuses on a single HDPE floating collar with $a/c = 0.0253$, whereas the fish cages at Hosenøyan consists of two HDPE floating collars with $a/c = 0.01$, as described in subsection 3.5.3. These differences could also be contributing factors of the deviance of the resulting transfer functions.

6.5 Sources of error

The results shown in this chapter may have been influenced by several different sources of error. This section will attempt to make a description of them and how they might have affected the results.

Prior to the treatment of the acceleration measurements were done, there were already multiple factors that could lead to error. Most of the factors are mentioned in Chapter 4 and Chapter 5, and will be summarized below.

- Uncertainty in measurements from the IMU itself. According to the user manual of the IMU, the IMU should be used with care in moving objects, as the disturbances may give inaccurate readings. In addition, the IMU's malfunction if they are exposed to sea water.
- There were no available data of possible disturbances of the measurements on the fish farm, such as service operations with service vessels etc.
- The comparison method with the data from the wave buoy may lead to incorrect results regarding the actual wave conditions of the site, as described in subsection 4.2.3. This is due to the difference in both distance and water depth of the two locations, leading to wave transformations as described in section 3.2, and the difference of the sampling methods. In addition, the placement of the IMU's towards the center of the fish farm might also affect the recorded accelerations, as the waves might be dampened and some of the wave energy could be reflected.
- The effects of weights, net and mooring are not accounted for, leading to uncertainty in how the fish cage motions theoretically should be expected to look like.

As described in section 5.1, both the integration and the filtration of the data have dramatic effects on the recorded accelerations. If noise and drift are present in the measurements, it is almost impossible to reconstruct a fully reliable elevation response estimate from the acceleration measurements. In particular, the short range of the elevation period might be a direct consequence of the filtration of the measurements. When calculating the spectral moments, the assumptions of a stationary process within each hour may not always hold, which will affect the results. In addition, the results of the direct estimation method and the results by calculating the zero-th spectral moments required two different low cut-off frequencies to be reasonable when compared to the wave buoy data, indicating the difficulties of creating the perfect band pass filter as described in section 5.1.

Chapter 7

Conclusion

In Norway, a site survey is required before any fish farm can be installed at a location. The site surveys are to be done according to the NYTEK regulations and NS 9415, and the wave conditions at a site are usually determined with calculations rather than measurements. If wave measurements are done, they are usually done at one single point of the site. If the aquaculture industry shall continue to expand as expected, the more environmentally exposed areas of the Norwegian continental shelf may have to be exploited. In order to ensure safe working conditions and reduce the risk of fish escape, the standards used to set the requirements for the fish farms must be adapted to apply to exposed areas as well as the more sheltered areas.

The results of this thesis indicates that spatial variations could be present at an aquaculture farm, even though the results only suggest that the differences are minor for the fish farm at Hosenøyan. However, the results indicates that the differences of the estimated elevation responses grow larger as the surrounding waves grow larger. This could possibly be an important element of future site survey's done at areas where the wave conditions are harsher. As for the idea of using the fish cages of a fish farm as a wave buoy in order to determine the local wave conditions at an aquaculture site, the results from this thesis showed no indication that this can be done reliably, assuming linear transfer functions.

However, for both the estimation of the two fish cage elevation responses and the linear transfer function analysis, it was clear that errors affected the results heavily. The main errors for the estimations in this Master Thesis included errors of the measurements of the IMU itself, errors that occurred as a result of integrating and filtering the data, and the assumption of making the data from the wave buoy representative for the wave conditions at the fish farm. If the factors of error were minimized, the result would prove to be more reliable than the results presented in this thesis.

Nevertheless, since the acceleration data from the two fish cages were integrated and filtered identically, the indication of spatial variations of the fish cage motions can to some degree be assumed reliable. At the very least, the increased deviance of the fish cage elevations for larger incident waves should be noted for site survey's at exposed locations. For relatively sheltered areas however, the results of this thesis does not indicate that spatial variations are significant for the reliability of a site survey done according to NS 9415:2009.

Chapter 8

Further Work

Validity of transfer functions.

Using the fish cages response in heave to estimate the wave conditions at a fish farm should be investigated more thoroughly. Only a linear relation is studied in this thesis, and the question remains whether using non-linear transfer functions would lead to better results.

Effects of mooring, weights and fish cage net.

To properly understand the motion of the fish cages in incident waves, the effects of mooring, bottom rings, weights and the net should be mapped, as it might influence the results.

Type and position of the measuring device.

The measuring device used in this thesis may not be as reliable as it should be if used for the purpose of this thesis. To ensure reliable results, the best possible measuring device should be used. In addition, to minimize the effects of obstacles and other interference of the incident waves, the position of the measuring device should be considered.

Integration and treatment of acceleration data.

The task of integrating and filtering the acceleration data should be investigated more. The measured data is very sensitive to the effects of both integration and filtration, which in turn makes a huge impact on the end results. Perhaps with a good enough measuring device, the noise and drift of the acceleration signals will be reduced, simplifying the treatment of the data.

Validity of using linear theory at coastal areas.

The effects due to wave transformation that occurs for waves propagating towards a shoreline should be thoroughly mapped to ensure that the results are as good

as possible. Alternatively, a reliable wave buoy in close vicinity of the measuring devices at the fish cages could be effective as well.

Including motions in sway and surge

In this thesis, only the linear acceleration in heave is investigated. To properly estimate the motion of the fish cages, the motions in sway and surge should also be included.

Spatial variations at exposed locations

The results of this thesis indicate a trend that the spatial variations of the fish cage elevation responses seem to grow larger as the incident waves grow larger. Therefore a similar experiment done at an open ocean environment could lead to interesting results.

Bibliography

Barbariol, F., Benetazzo, A., Carniel, S. & Sclavo, M. (2015), 'Space-time wave extremes: The role of metocean forcings', Journal of Physical Oceanography **45**(7).
URL: *https://journals.ametsoc.org/doi/10.1175/JPO-D-14-0232.1*

Beck, J. & Wannick, O. (2017), 'Wave measuring buoy', Wissenschaftliche artikel .

Bender III, L., Jr., N. G., Walpert, J. & Howden, S. (2010), 'A comparison of methods for determining signicant wave heights—applied to a 3-m discus buoy during hurricane katrina', Journal of Atmospheric and Oceanic Technology **27**, 1012–1028.

Bore, P. & Amdahl, J. (2017), 'Determination of environmental conditions relevant for the ultimate limit state at an exposed aquaculture location', 36th international conference on ocean, offshore and arctic engineering (OMAE2017-61413) **36**.
URL: *https://proceedings.asmedigitalcollection.asme.org/proceeding.aspx?articleid=2655488*

Brandt, A. & Brincker, R. (2014), 'Integrating time signals in frequency domain - comparison with time domain integration', Measurement **58**, 511–519.

Bruserud, K. & Haver, S. (2017), 'Uncertainties in current measurements in the northern north sea', Journal of Atmospheric and Oceanic Technology .
URL: *https://journals.ametsoc.org/doi/full/10.1175/JTECH-D-16-0192.1*

Delft University of Technology (2019), 'Swan user manual'.

DNV GL (2017), 'Environmental conditions and environmental loads, recommended practice'.
URL: *https://rules.dnvgl.com/docs/pdf/DNVGL/RP/2017-08/DNVGL-RP-C205.pdf*

Endresen, P. (2011), 'Vertical wave loads and response of a floating fish farm with circular collar'.

F. Cardia and A. Lovatelli (2015), 'Aquaculture operations in floating hdpe cages'.

Faltinsen, O. (1990), Sea loads on ships and offshore structures, Cambridge University Press.

Faltinsen, O. & Shen, Y. (2017), 'Wave and current effects on floating fish farms'.
URL: *https://ntnuopen.ntnu.no/ntnu-xmlui/bitstream/handle/11250/2592745/aquacultureharbin$_F$ir*
4

Fiskeri-og havbruksnæringens forskningsfinansiering (2018), 'Revisjon av norsk standard ns 9415 for flytende oppdrettsanlegg: Ekstremverdianalyse av strøm basert på korte tidsserier'.
URL: *https://www.fhf.no/prosjekter/prosjektbasen/901506/*

Forristal, G. (2011), 'Maximum crest hights under a model tlp. deck', International conference on offshore mechanics and arctic engineering (OMAE2011) **2**, 571–577.

Fredheim, A. & Langan, R. (2009), Advances in technology for off-shore and open ocean finfish aquaculture, pp. 914–944.

Fredriksson, D. W., Swift, M. R., Eroshkin, O., Tsukrov, I., Irish, J. D. & Celikkol, B. (2005), 'Moored fish cage dynamics in waves and currents', Journal of Oceanic Engineering **30**(1).

Hagen, (2019), 'Stubholt mener utviklingskonsesjoner har vært et blindspor'.
URL: *https://fiskeribladet.no/tekfisk/nyheter/?artikkel=67023*

Han, S. (2010), 'Measuring displacement signal with an accelerometer', Journal of Mechanical Science and Technology **24**(6), 1329–1335.

Kowalczuk, Z. & Merta, T. (2015), 'Evaluation of position estimation based on accelerometer data', Proceedings of the 10th International Workshop on Robot Motion and Control **10**.

Kristiansen, D., Aksnes, V., Su, B., Lader, P. & Bjelland, H. (2017), 'Environmental description in the design of fish farms at exposed locations', International conference on offshore mechanics and arctic engineering (OMAE2017) **36**.

Li, P. (2017), A Theoretical and Experimental Study of Wave-induced Hydroelastic Response of a Circular Floating Collar, PhD thesis.

Ministry of Trade, Industry and Fisheries (2018), 'Havbruk til havs'.
URL: *https://www.regjeringen.no/no/dokumenter/havbruk-til-havs/id2625352/*

Myrhaug, D. (2006), TMR4230 Oceanography - Wind Waves, Akademika Forlag.

Myrhaug, D. & Lian, W. (2009), TMR4182 Marine Dynamics - Irregular waves, Akademika Forlag.

Newland, D. (2005), An introduction to random vibrations, spectral wavelet analysis.

Newman, J. (1977), 'The motions of a floating slender torus', Journal of Fluid Mechanics **83**(4), 721–735.

Noomas Sertifisering AS (2013), 'Lokalitetsrapport kråkøya regnr. 12652'.
URL: *https://docplayer.me/14186545-Lokalitetsrapport-krakoya-regnr-12652.html*

Norwegian Directorate of Fisheries (2016), 'Retningslinjer for behandling av søknader om utviklingstillatelse til oppdrett av laks, ørret og regnbueørret'.
URL: *https://www.fiskeridir.no/Akvakultur/Tildeling-og-tillatelser/Saertillatelser/Utviklingstillatelser*

Norwegian Ministry of Trade, Industry and Fisheries (2005a), 'The aquaculture act'.
URL: *https://www.regjeringen.no/globalassets/upload/kilde/fkd/reg/2005/0001/ddd/pdfv/255327-l-0525$_a$kvakulturloveneng.pdf*

Norwegian Ministry of Trade, Industry and Fisheries (2005b), 'Technical requirements for fish farming installations'.
URL: *https://www.regjeringen.no/globalassets/upload/kilde/fkd/bro/2005/0013/ddd/pdfv/255320-technical$_r$equirements.pdf*

Olafsen, T., Winther, U., Olsen, Y. & Skjermo, J. (2012), 'Verdiskaping basert på produktive hav i 2050'.

Sakshaug, S. (2018), 'Communication through e-mail'.

Seifert, K. & Camacho, O. (2007), 'Implementing positioning algorithms using accelerometers. application note. freescale semiconductor. an3397'.
URL: *https://www.nxp.com/docs/en/application-note/AN3397.pdf*

SINTEF EXPOSED (2018), 'Annual report 2018'.
URL: *https://exposedaquaculture.no/wp-content/uploads/EXPOSED-Annual-report-2018-web.pdf*

Standard Norway (2010), 'Ns 9415.e:2009 - marine fish farms - requirements for site survey, risk analyses, design, dimensioning, production, installation and operation'.
URL: *http://www.standard.no/no/Nettbutikk/produktkatalogen/Produktpresentasjon/?ProductID=4*

Statistics Norway (2019), '03024: Eksport av fersk og frosen oppalen laks 2000u01 - 2019u46'.
URL: *https://www.ssb.no/statbank/table/03024*

Stemsrud, S. (2018), 'Site surveys at norwegian aquaculture sites'.
URL: *https://ntnuopen.ntnu.no/ntnu-xmlui/handle/11250/2564517*

The Norwegian Seafood Federation (2011), 'Norsk havbruk'.
URL: *https://sjomatnorge.no/wp-content/uploads/2014/04/eff$_f$hl$_k$omplett$_l$owres.pdf*

Tupper, E. C. (2013), Introduction to Naval Architecture, 5 edn.

Vogel, F., Holm, S. & Lindgjære, O. (n.d.), 'Spectral moments and time domain representation of photoacoustic signals for detection of crude oil in produced water'.
URL: *https://pdfs.semanticscholar.org/2bc4/8e298768035e4748b84dbc1c08838a61b28a.pdf*

Appendix A

Additional material

A.1 Additional results

A.1.1 Additional results of the estimated fish cage elevation responses

Estimation of $\eta_{3,s}$

In Figure A.1.1 and Figure 6.1.1, the same type of plots are shown, where the only difference of the plots are a slight change of the low cut-off frequencies of the Butterworth band pass filter. They are included to showcase the effect of changing the filters cut-off frequencies, even though the increment is only +− 0.05.

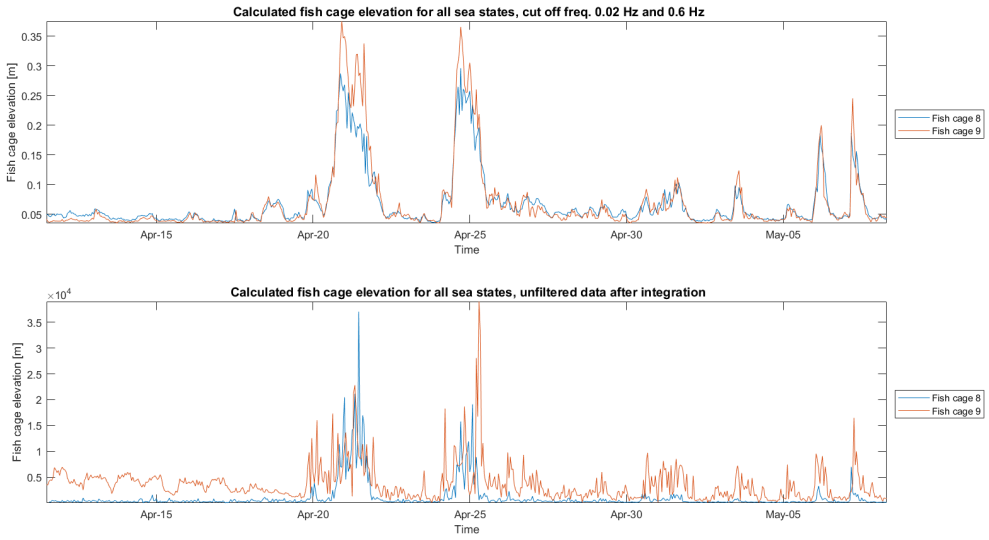

Figure A.1.1: Estimated elevation response with normalized low cut-off freq. 0.02 and and high cut-off freq. 0.6

	$\eta_{3,s}$ [m], fish cage 8	$\eta_{3,s}$ [m], fish cage 9	ζ_{m0}, wave buoy [m]
Min	0.0358	0.0348	0.0196
Max	0.2955	0.3751	0.8399
Mean	0.0674	0.0696	0.1833
Std. dev.	0.0470	0.0624	0.1620

Table A.1.1: Estimation of fish cage elevation response using normalized low cut-off freq. 0.02 and high cut-off freq. 0.6.

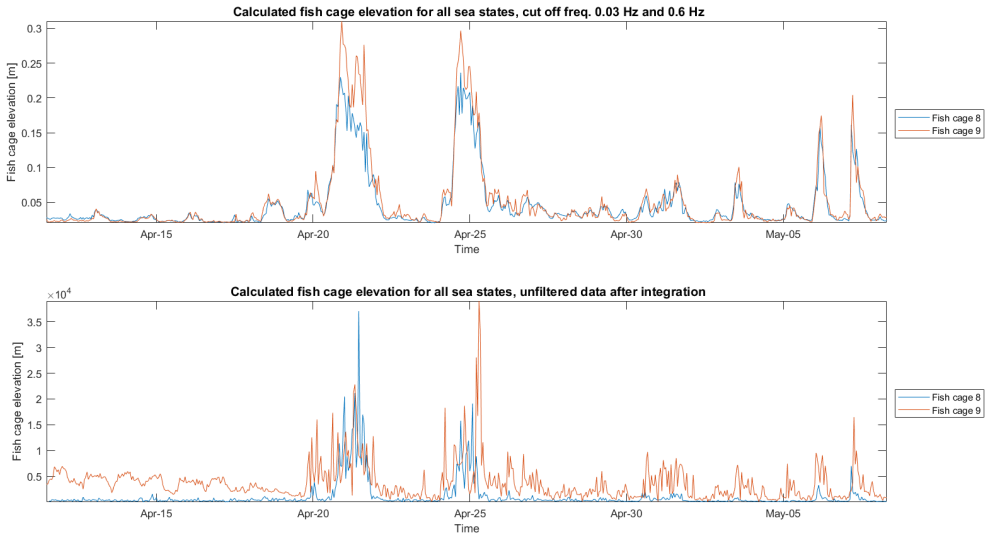

Figure A.1.2: Estimated elevation response with normalized low cut-off freq. 0.03 and high cut-off freq. 0.6

	$\eta_{3,s}$ [m], fish cage 8	$\eta_{3,s}$ [m], fish cage 9	ζ_{m0}, wave buoy [m]
Min	0.0206	0.0206	0.0196
Max	0.2365	0.3104	0.8399
Mean	0.0917	0.1010	0.1833
Std. dev.	0.0820	0.1064	0.1620

Table A.1.2: Estimation of fish cage elevation response using normalized low cut-off freq. 0.03 and high cut-off freq. 0.6.

Estimation of $\eta_{3,m0}$

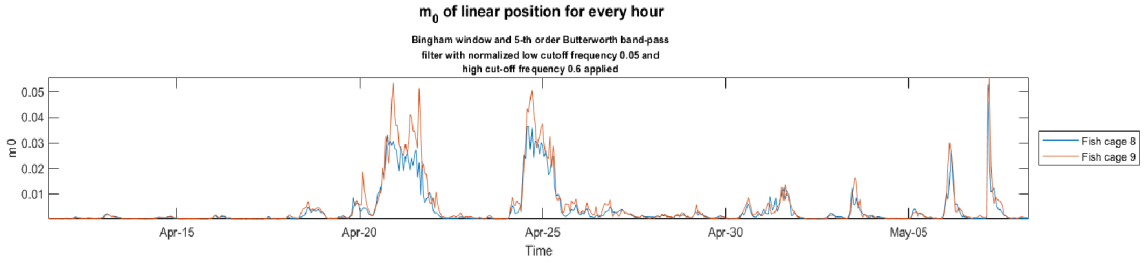

Figure A.1.3: m_0 of the resulting fish cage elevation response, filtered with normalized low cut-off freq. 0.05 and high cut-off freq. 0.6

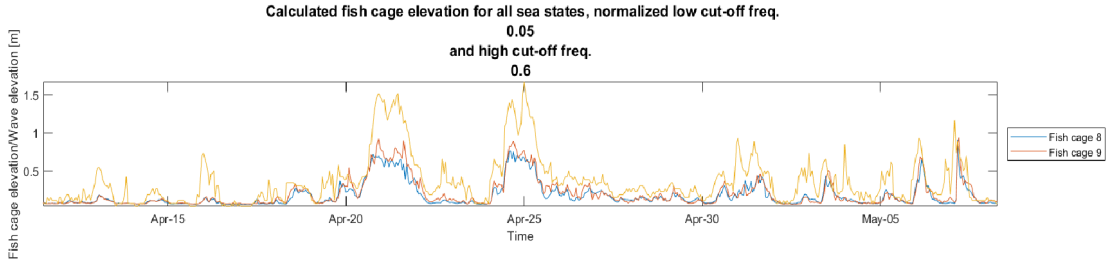

Figure A.1.4: Resulting fish cage elevation responses using m_0, filtered with normalized low cut-off freq. 0.05 and high cut-off freq. 0.6

	$\eta_{3,m0}$ [m], fish cage 8	$\eta_{3,m0}$ [m], fish cage 9	H_{m0}, wave buoy [m]
Min	0.0659	0.0666	0.0391
Max	0.9187	0.9436	1.6797
Mean	0.1852	0.2042	0.3665
Std. dev.	0.1585	0.1839	0.3240

Table A.1.3: Estimation of fish cage elevation response using the zero-th spectral moment. Normalized low cut-off freq. 0.05 and high cut-off freq. 0.6.

A.1.2 Additional results for directional fish cage elevation responses

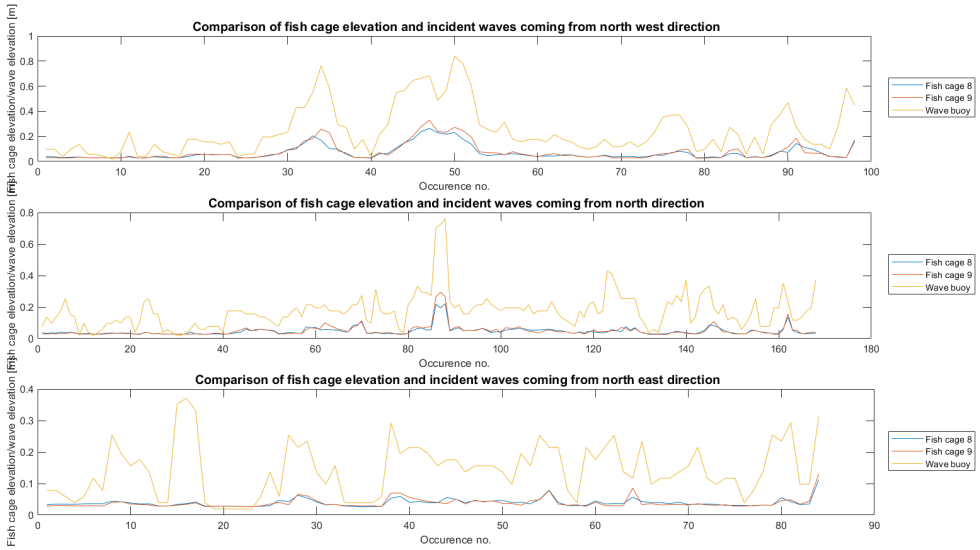

Figure A.1.5: Estimated fish cage elevation responses for waves coming from North west, North and North East.

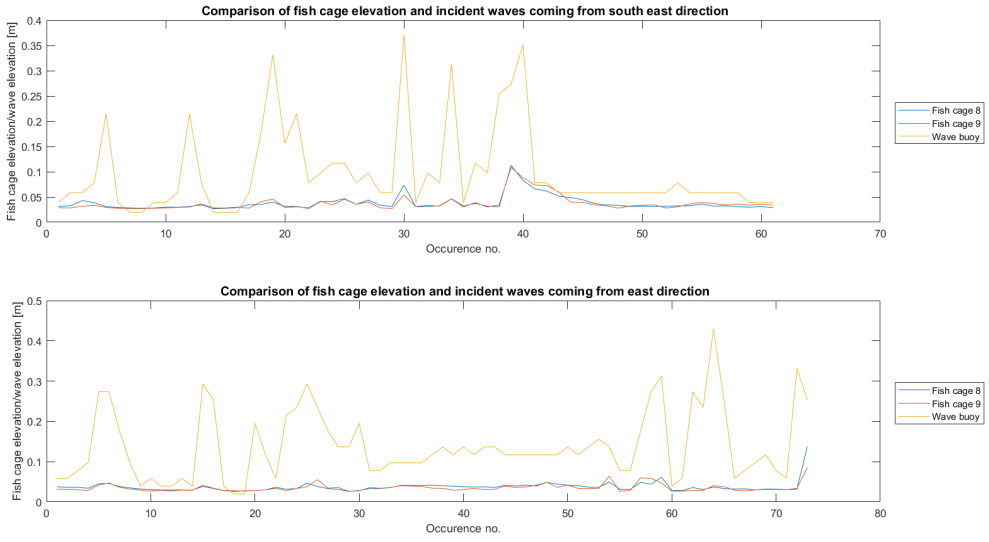

Figure A.1.6: Estimated fish cage elevation responses for waves coming from South East and East.

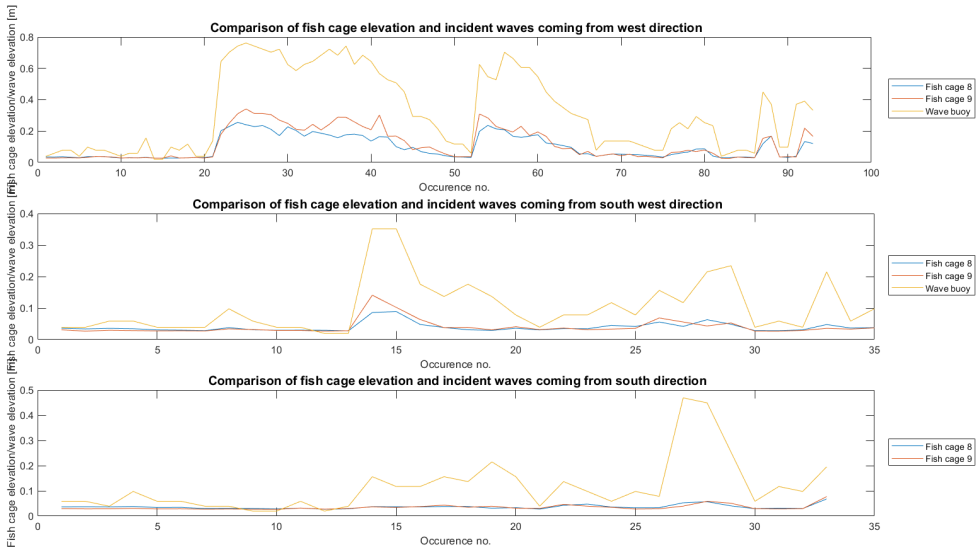

Figure A.1.7: Estimated fish cage elevation responses for waves coming from West, South West and South.

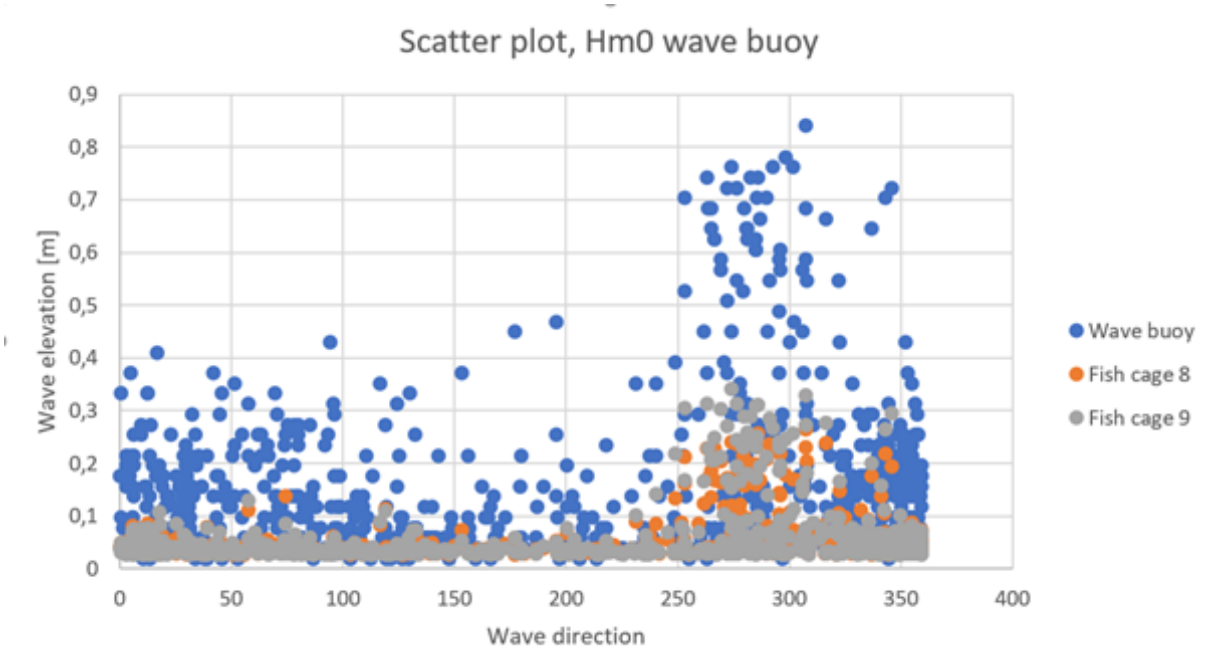

Figure A.1.8: Scatter plot of fish cage elevation responses and wave buoy elevations.

A.1.3 Additional results of estimated T_z

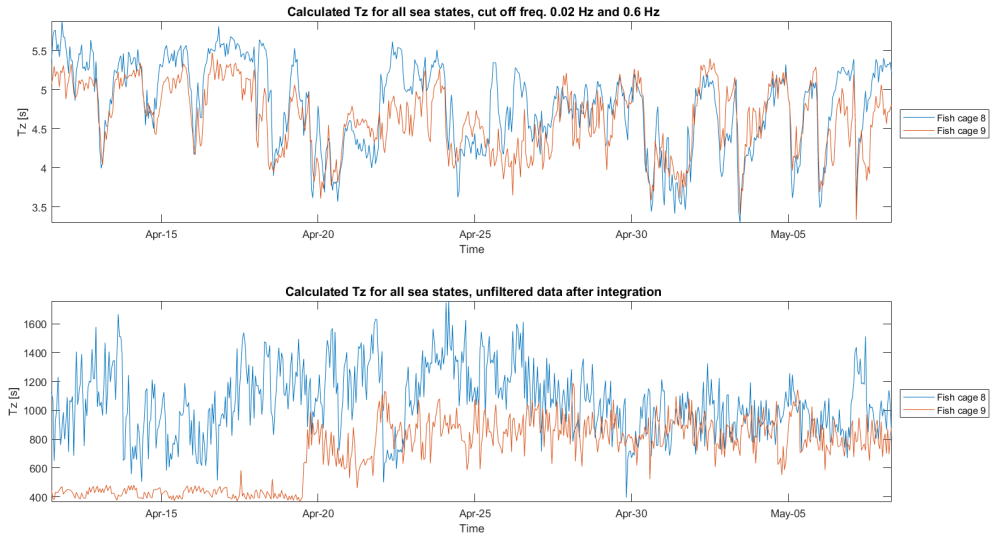

Figure A.1.9: Estimated fish cage elevation period with normalized low cut-off freq. 0.02 and high cut-off freq. 0.6

	T_z [s], fish cage 8	T_z [s], fish cage 9	T_{2m0}, wave buoy [s]
Min	3.2951	3.3330	2.8320
Max	5.8786	5.4749	14.3555
Mean	4.8008	4.6331	4.8524
Std. dev.	0.5490	0.4417	1.7361

Table A.1.4: Estimation of fish cage elevation period using normalized low cut-off freq. 0.02 and high cut-off freq. 0.6.

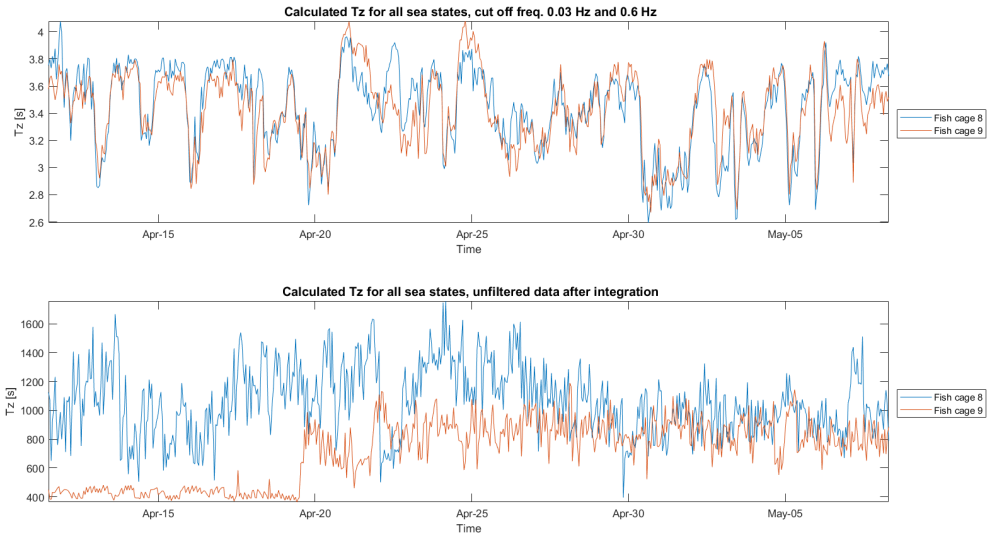

Figure A.1.10: Estimated fish cage elevation period with normalized low cut-off freq. 0.03 and high cut-off freq. 0.6

	T_z [s], fish cage 8	T_z [s], fish cage 9	T_{2m0}, wave buoy [s]
Min	2.5931	2.6699	2.8320
Max	4.0757	4.0781	14.3555
Mean	3.4378	3.4162	4.8524
Std. dev.	0.3002	0.2804	1.7361

Table A.1.5: Estimated of fish cage elevation period using normalized low cut-off freq. 0.03 and high cut-off freq. 0.6.

A.1.4 Additional results for estimated transfer functions

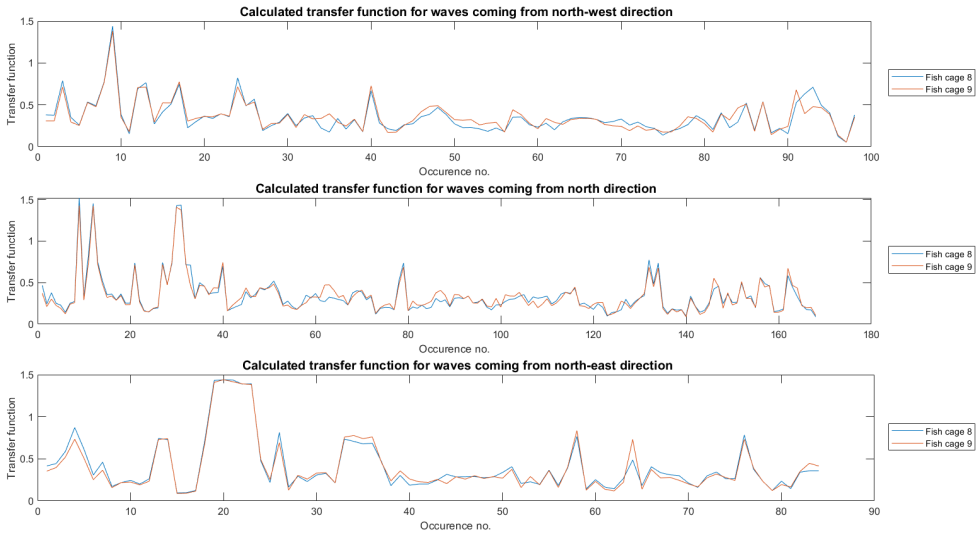

Figure A.1.11: Estimated transfer functions for waves coming from North West, North and North East.

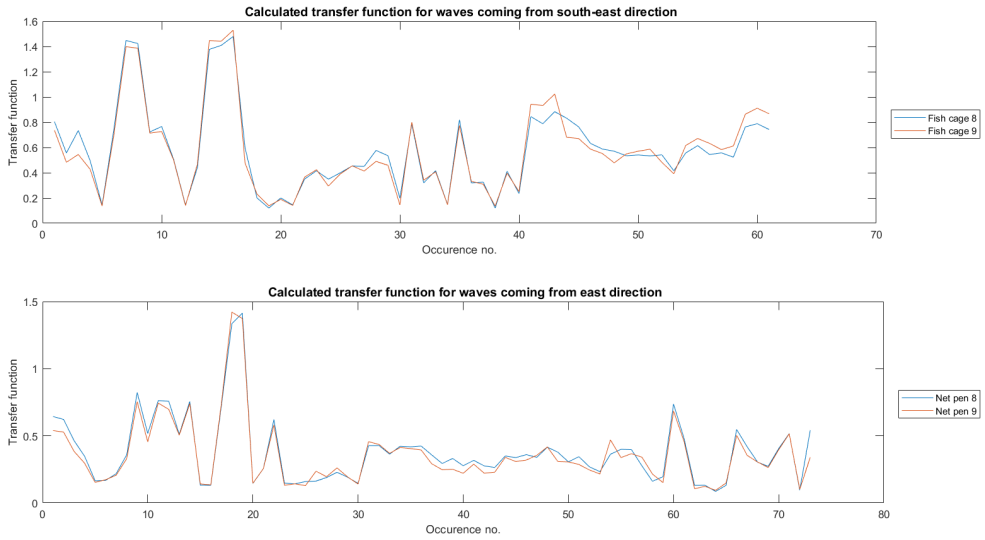

Figure A.1.12: Estimated transfer functions for waves coming from South East and East.

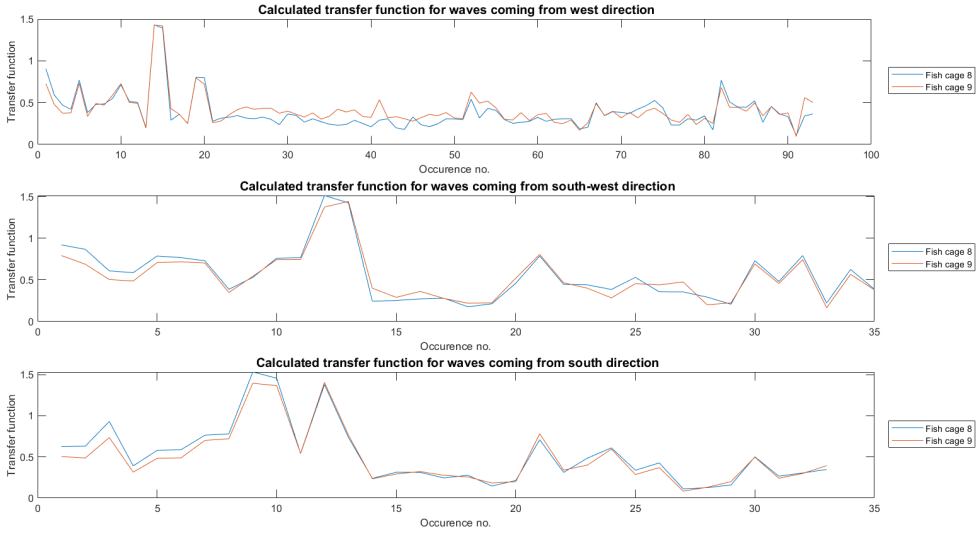

Figure A.1.13: Estimated transfer functions for waves coming from West, South West and South.

	$RAO_{3,s}$, cage 8	$RAO_{3,s}$, cage 9
Min	0.0533	0.0544
Max	1.5310	1.5285
Mean	0.4086	0.4074
Std. dev.	0.2728	0.2642

Table A.1.6: Estimation of linear transfer function $RAO = \frac{\eta_3}{\zeta_3}$, using ζ_3 from wave buoy data and normalized low cut-off frequency 0.025 on the fish cage elevation response $\eta_{3,s}$

A.2 Standardized wave spectra - PM spectrum and JONSWAP spectrum

Two of the spectra mentioned in NS 9415:2009 are JONSWAP spectrum and Pierson-Moskowitz spectrum, both commonly applied for analyzing wind sea. The JONSWAP spectrum extends the Pierson-Moskowitz by including fetch limited sea and can therefore be utilized to describe developing sea stated. The Pierson-Moskowitz spectrum however was originally designed for analysis of fully developed sea states.
According to DNV GL (2017), the Pierson-Moskowitz (PM) spectrum $S_{PM}(\omega)$ is given by:

$$S_{PM} = \frac{5}{16} H_s^2 \omega_p^4 \omega^{-5} \exp(-\frac{5}{4}(\frac{\omega}{\omega_p})^{-4}) \tag{A.2.1}$$

Where $\omega_p = \frac{2\pi}{T_p}$ is the angular spectral peak frequency.

As mentioned, The JONSWAP spectrum $S_J(\omega)$ is formulated as a modification of the Pierson-Moskovitz spectrum for a developing sea state in fetch limited sea.

$$S_J = A_Y S_{PM}(\omega) \gamma^{\exp(-0.5(\frac{\omega-\omega_p}{\sigma\omega_p})^2))} \tag{A.2.2}$$

Where:

- $S_{PM}(\omega)$ = Pierson-Moskovitz spectrum
- γ = non-dimensional peak shape parameter
- σ = Spectral width parameter
- $\sigma = \sigma_a$ for $\omega \leq \omega_p$
- $\sigma = \sigma_a$ for $\omega > \omega_p$
- $A_Y = 1 - 0.297 \ln(\gamma)$

It is worth noticing that for $\gamma = 1$ the JONSWAP spectrum reduces to the Pierson-Moskowitz spectrum.

According to DNV GL (2017) the average values for the JONSWAP experiment data are:

- $\gamma = 3.3$
- $\sigma_a = 0.07$

- $\sigma_b = 0.09$

While in NS 9415:2009, the following parameters are required to be applied for wind sea and ocean swell analysis:

- $\gamma = 2.5$ for wind sea
- $\gamma = 6.0$ for ocean swells

The JONSWAP spectrum is expected to be a reasonable model for $3.6 < \frac{T_p}{\sqrt{H_s}} < 5$. Outside of this interval, the JONSWAP spectrum does not provide reliable estimations of the wind sea conditions. (DNV GL (2017))

The effect of the shape parameter γ is shown in the following figure from DNV GL (2017):

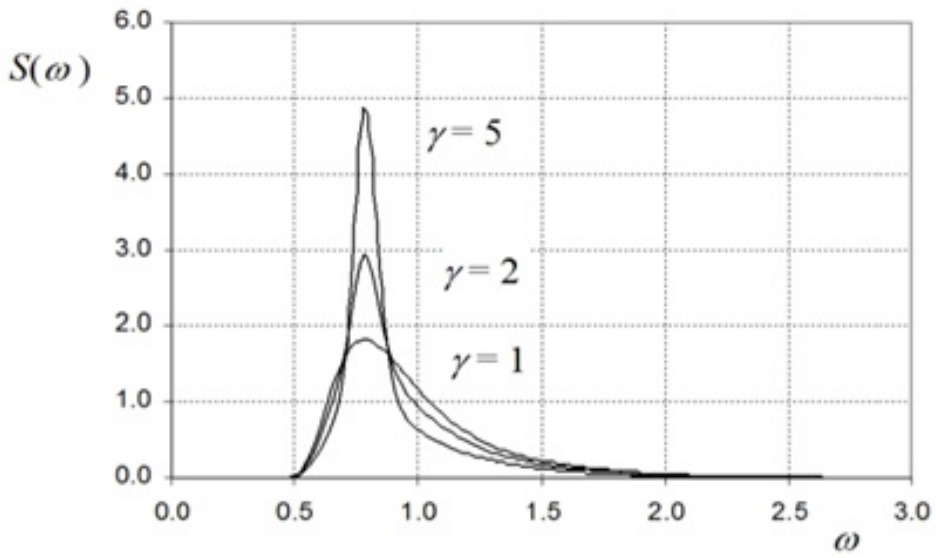

Figure A.2.1: JONSWAP spectrum for $H_s = 4.0m, T_p = 8.0s$ for $\gamma = 1, \gamma = 2$ and $\gamma = 5$ Source: DNV GL (2017)

Appendix B

MATLAB scripts

B.1 Import files from Hosenøyan

Import files from the IMU

```
% Imports data from the txt-files of the IMU's.
clear all
clc

txtFiles = dir( '*.txt' ) ;
numfiles = length( txtFiles ) ;
mydata = cell (1 , numfiles ) ;

numFiles = 645; %Number of txt-files to import .
startRow = 2; %Exclude column headings
endRow = inf ; %Include all rows
myData = cell (1 , numFiles) ;

for fileNum = 1: numFiles
    fileName = sprintf('data%01d.txt', fileNum) ;
    myData{fileNum} = FileToMatrixFromHosenoyan( fileName , startRow ,endRow);

end

M8= myData;
%M9 = myData;

save('netPen.mat' , 'C8', '-append') %Saves the data in a .mat file
```

B.2 Convert txt-file to matrix

Make matrix of the IMU data.

```
function data1 = FileToMatrixFromHosenoyan(fileName, startRow , endRow)
%% IMPORTFILE Import numeric data from a text file as a matrix .
% DATA1 = IMPORTFILE(FILENAME) Reads data from text file FILENAME for the
% default selection .
%
% DATA1 = IMPORTFILE(FILENAME, STARTROW, ENDROW) Reads data from rows
% STARTROW through ENDROW of text file FILENAME.
% Example :
%   data1 = importfile ( 'data1.txt' , 2 , 35539) ;
% Auto-generated by MATLAB

%% Set variables .
delimiter = { ',' , ' ' };
if nargin<=2
    startRow = 2;
    endRow = inf ;
end

%% Format for each line of text :
% column 12 : double (%f )
% column 13 : double (%f )
% column 14 : double (%f )
formatSpec='%*q%*q%*q%*q%*q%*q%*q%*q%*q%*q%*q%f%f%f%*q%*q%*q%*q%*q%*q%[^\n\r]'
;
%
Open the txt-file .
fileID = fopen(fileName) ;

%% Read columns of data according to the format .
dataArray = textscan(fileID, formatSpec, newline,...
    endRow(1)-startRow(1)+1, 'Delimiter' , delimiter, newline,...
    'MultipleDelimsAsOne' , true,'TextType' , 'string' , newline,...
    'EmptyValue' , NaN, 'HeaderLines', startRow(1)-1, newline,...
    'ReturnOnError' , false , 'EndOfLine' , '\r\n');
for block=2:length(startRow)
    frewind(fileID) ;
    dataArrayBlock = textscan ( fileID , formatSpec , newline,...
        endRow( block )-startRow( block )+1, 'Delimiter' , newline,...
        delimiter , 'MultipleDelimsAsOne' , true , 'TextType' , newline,...
        'string' , 'EmptyValue' , NaN, 'HeaderLines' , newline,...
        startRow( block )-1, 'ReturnOnError' , false , newline,...
        'EndOfLine' , '\r\n' ) ;
    for col =1:length(dataArray)
        dataArray{col} = [dataArray{col}; dataArrayBlock{col}];
    end
end

%% Close the txt-file .
fclose (fileID) ;

%% Create output variable
data1 = [dataArray {1:35000}];
end
```

B.3 Integrate the measurements

Integration of the acceleration measurements

```
% This script integrates measured linear acceleration from Hosenøyan
% using the trapezoidal method.
% The script calculates mean linear velocity and mean linear position
% in time domain for fish cages 8 and 9

clear all
clc

%Load data
load('netPen.mat')
LA.M8 = M8;
LA.M9 = M9;

clear M9; clear M8;

dt = 0.1;
Fs = 1/dt ;

for r=1:645
    for s=1:4
    LV.M8{s,r}=zeros(35000,1);
    LV.M9{s,r}=LV.M8{s,r};
    LD.M8{s,r}=LV.M8{s,r};
    LD.M9{s,r}=LV.M8{s,r};
    end
end


fields = fieldnames (LA) ;

 for k=1:length( fields )
     categoryname=fields{k};

     for m = 1: length(LA.(categoryname) )
         %Load data
         data = LA.(categoryname){1 ,m}(:,3);
         %Convert to m/s^2
        data =  cellfun(@(x) x*9.81,data,'un',0);
         %Remove offset
         data = cell2mat(data);
         data=data-mean(data);
          %% Bingham filtering, providing output variable dataW
         BinghamWindow;



          %% Band pass Butterworth filtering
dt = 0.1;
Fs = 1/dt ;
```

```
nyq = Fs/2; % Nyquist frequency
cutL = 0.1; % Low cut-off frequency
cutH = 4 ;  % High cut-off frequency
wnL = cutL/nyq; % Normalized low cut-off frequency
wnH = cutH/nyq; % Normalized high cut-off frequency
[filtb,filta ]=butter (5 ,[wnL wnH] ) ;
dataFW=filtfilt(filtb,filta,dataW) ; %Filter signal after Bingham window

   %% Band-pass filter only
dataBP=filtfilt(filtb,filta,data);


%% Calculate cumulative velocity of windowed and filtered IMU data

% Unfiltered data
Vacc = trapz(data);
LV.(categoryname){1,m} = cumtrapz(data)*(1/Fs);
LV.(categoryname){1,m}= detrend(LV.(categoryname){1,m},1);

%Windowed data
VaccW=trapz(dataW);
LV.(categoryname){2,m}=cumtrapz(dataW)*(1/Fs);

%Band-pass filtered data
VaccBP=trapz(dataBP);
LV.(categoryname){3,m}=cumtrapz(dataBP)*(1/Fs);

%Band-pass filtered and windowed data
VaccFW=trapz(dataFW);
LV.(categoryname){4,m}=cumtrapz(dataFW)*(1/Fs);
LV.(categoryname){4,m}=detrend(LV.(categoryname){4,m},1);

%% Calculate cumulative displacement of calculated velocity data

%Unfiltered data
Dacc = trapz(LV.(categoryname){1,m});
LD.(categoryname){1,m} = cumtrapz(LV.(categoryname){1,m})*(1/Fs);

%Windowed data
DaccW = trapz(LV.(categoryname){2,m});
LD.(categoryname){2,m} = cumtrapz(LV.(categoryname){2,m})*(1/Fs);

%High-pass filtered data
DaccBP = trapz(LV.(categoryname){3,m});
LD.(categoryname){3,m} = cumtrapz(LV.(categoryname){3,m})*(1/Fs);

%High passed filtered and windowed data
DaccFW = trapz(LV.(categoryname){4,m});
LD.(categoryname){4,m} = cumtrapz(LV.(categoryname){4,m})*(1/Fs);


    end
 end
%Save data in a .mat file

 save('netPenTrapz.mat' , 'LD', '-append')
```

B.4 Bingham Window

Bingham window

```
N = length(data) ;

N101 = round(N*0.1) ; % 0 to 10% of the measurements will
%be attenuated
N901 = round(N*0.9) ; % The last 10% of the measurements will be
 attenuated

N10 = 1:N101;
N90 = N901:N;

D10 = 0.5*(1-cos((10*pi.*N10)./N) ) ; %for 0 < i < N/10
D = ones (1 ,round(N*0.8) ) ;
D90 = 0.5*(1+cos((10*pi*(N90-0.9*N) )/N) ) ; %for 0.9N < i < N

DW = [D10, D, D90 ]';

if length(data)< length(DW)
    DW(length(data)+1:end) =[]; %remove last index if size does not
 match
    dataW =  times(data,DW);
elseif length(data)> length(DW)
    DW(numel(data) ) = 0;
    dataW = data.*DW;
else
    dataW = data.*DW;
end

clear N; clear N101; clear N901; clear N10; clear N90;
clear D10; clear D; clear D9
```

Published with MATLAB® R2019a

B.5 Calculate spectral moments

Calculate spectral moment and fish cage elevation

```
% The script plots mean linear position in time domain for fish cages
% 8 and 9 and calculates m0 for all sea states.
% It further calculates the resulting fish cage elevations.
clear all
clc

%Load data
load('netPenTrapz.mat')
%load('netPenSimpsD.mat')



%% FREQUENCY DOMAIN ANALYSIS
% Find the zero-th moment of the spectrum for all signals within
% a frequency band for every hour, corresponding to one txt-
% file, or one cell in netPenTrapz

dt = 0.1;
Fs = 1/dt ;

MomentLD = zeros (646 ,2) ;
MomentLDBP = MomentLD;
MomentLDFW = MomentLD;
MomentLDW = MomentLD;

fields = fieldnames (LD) ;

 for k=1:length(fields)
     categoryname=fields{k};

     for m = 1: length(LD.(categoryname) )
         %Load data
         data = LD.(categoryname){1 ,m} ;
         % {1,m} unfiltered integrated data
         % {2,m} Windowed integrated data
         % {3,m} Band pass filtered integrated data
         % {4,m} Band pass filtered and windowed integrated data

         % Remove offset (mean)/ detrend )
           data=detrend(data,1);
         % Convert from amplitude to total height, linear theory
         %   data=2*data;


         %% Bingham window, providing output variable dataW
         BinghamWindow;
         %% Band pass Butterworth filter
dt = 0.1;
Fs = 1/dt ;
```

```
nyq = Fs/2; % Nyquist frequency
cutL = 0.3; % Low cut-off frequency
cutH = 3;   % High cut-off frequency
wnL = cutL/nyq; %Normalized low cut-off frequency
wnH = cutH/nyq; % Normalized high cut-off frequency

[filtb,filta ]=butter(5 ,[wnL wnH]) ;
dataFW=filtfilt(filtb,filta,dataW) ; %Filter signal after Bingham window

%% Band-pass filtered only
dataBP=filtfilt ( filtb , filta , data) ;

%% Calculating the zero-crossings for the different data sets
zeroC=0;
for j=1:(length(dataFW)-1)
    if dataFW(j+1)>0 && dataFW(j)<0
        zeroC = zeroC+1;
        PosZeroC(zeroC,1)=j;
    end
end
for i=1:(zeroC-1)
    dataFW(i,1)=max(dataFW(PosZeroC(i):PosZeroC(i+1)));
end

%% Frequency domain analysis - Bingham window + band-pass filter
YFW = fft (dataFW) ; %Fast Fourier transform of linear position
LFW = length(dataFW) ;
P2FW = (abs(YFW).^2)/LFW ;
P1FW = P2FW(1:LFW/2+1) ;
P1FW(2:end-1) = 2*P1FW(2: end-1); %One sided spectrum

fvFW = Fs*(0:(LFW/2))/LFW;

%% Frequency domain analysis - Bingham window only
YW = fft (dataW) ; %Fast Fourier transform of linear position
LW = length(dataW) ;
P2W = (abs(YW).^2)/LW ;
P1W = P2W(1:LW/2+1) ;
P1W(2:end-1) = 2*P1W(2:end-1); %One sided spectrum

fvW = Fs *(0:(LW/2) )/LW;

%% Frequency domain analysis - unfiltered data
Y = fft (data) ; %Fast Fourier transform of linear position
L = length(data) ;
P2 = (abs(Y).^2)/L ;
P1 = P2(1:L/2+1) ;
P1(2: end-1) = 2*P1(2: end-1); %One sided spectrum

fv = Fs *(0:(L/2))/L;

%% Frequency domain analysis - Band pass filtered data
YBP= fft (dataBP) ; %Fast Fourier transform of linear position
LBP = length(dataBP) ;
P2BP= (abs(YBP).^2)/LBP ;
P1BP = P2BP(1:LBP/2+1) ;
P1BP(2: end-1) = 2*P1BP(2: end-1); %One sided spectrum
```

```
fvBP = Fs *(0:(LBP/2) )/LBP;

%% Calculate spectral moment using Parseval's theorem

% Bingham windowed + band pass filtered
SwFW = zeros ((( length(fvFW)-1)) ,1) ;
for r = 1:( length(fvFW)-1)
    dwFW = fvFW( r+1)-fvFW( r ) ;
    SwFW=P1FW( r )*dwFW;
    MomentLDFW(m,k) = MomentLDFW(m,k)+SwFW;
    clear SwFW
end

clear r

%Unfiltered
Sw = zeros ((( length( fv )-1)) ,1) ;
for r = 1:( length( fv )-1)
    dw = fv ( r+1)-fv ( r ) ;
    Sw=P1( r )*dw;
    MomentLD(m,k) = MomentLD(m,k) + Sw;
    clear Sw
end

clear r
% Band pass filtered only
SwBP = zeros ((( length(fvBP)-1)) ,1) ;
for r = 1:( length(fvBP)-1)
    dwBP = fvBP(r+1)-fvBP(r) ;
    SwBP =P1BP(r)*dwBP;
    MomentLDBP(m,k) = MomentLDBP(m,k) +SwBP;

clear SwHP
end

clear r

%Windowed only
SwW = zeros ((( length(fvW)-1)) ,1) ;
for r = 1:( length(fvW)-1)
    dwW = fvW( r+1)-fvW( r ) ;
    SwW =P1W( r )*dwW;
    MomentLDW(m,k) = MomentLDW(m,k) +SwW;
    clear SwW
end
clear r
%% Clear all variables
clear data ; clear dataFW ; clear dataW; clear Y; clear YW; clear YBP; clear
LBP;
clear L; clear LW; clear P1; clear P2; clear fv ; clear P1W; clear P2W;
clear fvW; clear rF ; clear P1F; clear P2F; clear fvF ; clear dw; clear dwBP;
clear P1BP; clear P2BP; clear fvBP; clear dwFW; clear LFW; clear YBP
     end
 end

 %% Plot data in time domain
```

```
 L = 1:644; %Do not include any end effects
 % t1 = datetime (2018 ,4 ,11 ,11 ,0 ,0) ;
 % t2 = datetime (2018 ,5 ,8 ,6 ,0 ,0) ;
 % time = ( t1 : hours (1) : t2 ) ';
 time = datestr (( datetime (2018 ,4 ,11,11,0,0)+hours (1:644) ) ) ;
 time = datenum(time , 'dd-mm-yyyy HH:MM:SS' ) ;
 figure ()
 subplot(3 ,1 ,1)
 plot(time ,MomentLDFW(L,1) )
 datetick ( 'x' , 'mmm-dd' , 'keepticks' , 'keeplimits' )
 hold on
plot(time ,MomentLDFW(L,2) )
datetick ( 'x' , 'mmm-dd' , 'keepticks' , 'keeplimits' )
hold on
legend(  'Fish cage 8' , 'Fish cage 9' , 'location' , 'eastoutside' )
title ({['\fontsize{12} m_0 of linear position for every hour' , newline,...
    '\fontsize{8} Bingham window and 5-th ord. Butterworth band-
pass',newline,...
    ' filter with normalized low cutoff frequency ' num2str(wnL) ' and'
,newline,...
    ' high cut-off frequency ' num2str(wnH) ' applied']})
xlabel( 'Time' )
ylabel('m0')
axis ([ time(1) time(end) -inf inf ])

subplot(3 ,1 ,2)
plot(time ,MomentLD(L,1) )
datetick ( 'x' , 'mmm-dd' , 'keepticks' , 'keeplimits' )
hold on
plot(time ,MomentLD(L,2) )
datetick ( 'x' , 'mmm-dd' , 'keepticks' , 'keeplimits' )
hold on
legend( 'Fish cage 8' , 'Fish cage 9' , 'location' , 'eastoutside' )
title ({'\fontsize{8} Unfiltered data'})
xlabel( 'Time' )
ylabel('m0')
axis ([ time(1) time(end) -inf inf ])

subplot(3 ,1 ,3)
plot(time ,MomentLDBP(L,1))
datetick ( 'x' , 'mmm-dd' , 'keepticks' , 'keeplimits' )
hold on
plot(time ,MomentLDBP(L,2) )
datetick ( 'x' , 'mmm-dd' , 'keepticks' , 'keeplimits' )
hold on
legend( 'Fish cage 8' , 'Fish cage 9' , 'location' , 'eastoutside' )
title ({['\fontsize{8} 5-th ord. Butterworth band-pass filter
with',newline,...
    ' normalized low cutoff frequency ' num2str(wnL) ' and' ,newline,...
    ' high cut off frequency ' num2str(wnH) ' applied']})
xlabel( 'Time' )
ylabel('m0')
axis ([ time(1) time(end) -inf inf ])
hold off


%% Calculate eta_m0 using eta_m0=4sqrt(m0)
```

```
%Comparison with wave buoy data (Wave buoy data not shown in the script)

for r=1:length(MomentLDFW)
    hm08(r,1)=4*sqrt(MomentLDFW(r,1));
    hm09(r,1)=4*sqrt(MomentLDFW(r,2));
end

 figure ()
 subplot(3 ,1 ,1)
 plot(time ,hm08(L,1) )
 datetick ( 'x' , 'mmm-dd' , 'keepticks' , 'keeplimits' )
 hold on
plot(time ,hm09(L,1) )
datetick ( 'x' , 'mmm-dd' , 'keepticks' , 'keeplimits' )
hold on
plot(time, bolgeboye)
datetick ( 'x' , 'mmm-dd' , 'keepticks' , 'keeplimits' )
hold on
legend(  'Fish cage 8' , 'Fish cage 9' , 'location' , 'eastoutside' )
title ({'\fontsize{12} Calculated fish cage elevation for all ' newline...
    'sea states normalized low cut-off freq.' num2str(wnL) newline...
    'and high cut-off freq. ' num2str(wnH) })
xlabel( 'Time' )
ylabel('Fish cage elevation/Wave elevation [m]')
axis ([ time(1) time(end) -inf inf ])
```

B.6 Calculate elevations directly

Calculate fish cage elevations and period

```
% Calculate eta_s, the mean of the highest one third of the measurements.
% for every txt-file/every hour.
% Calculate the mean of T_z, the zero-crossing period

clear
clc

%Load data
load('netPenTrapz.mat')
%load('netPenSimpsD.mat')

HsPen = zeros (646 ,2);
Hsdata =HsPen;
HsPenFW= HsPen;


fields = fieldnames (LD) ;

 for k=1:length(fields)
     categoryname=fields{k};

     for m = 1: length(LD.(categoryname) )
         %Load data
         data = LD.(categoryname){1 ,m} ;
         % {1,m} unfiltered integrated data
         % {2,m} Windowed integrated data
         % {3,m} Filtered integrated data
         % {4,m} High pass filtered and windowed integrated data

         % Remove offset (mean)/ detrend )
         % data=data-mean(data);
         data=detrend(data,1);
         % absolute value
          % data=abs(data);
         % Convert from amplitude to height, linear theory
          %  data=2*data;

        % Bingham window
         BinghamWindow;

          % Band pass Butterworth filter
dt = 0.1;
Fs = 1/dt ;
nyq = Fs/2; % Nyquist frequency
cutL = 0.125; % Low cut-off frequency
cutH = 3 ;  % High cut-off frequency
wnL = cutL/nyq; % Normalized low cut off frequency
wnH = cutH/nyq; % Normalized high cut off frequency
[filtb,filta ]=butter (5 , [wnL wnH] ) ;
dataFW=filtfilt(filtb,filta,dataW) ; %Filter signal after Bingham window
```

```
%% Calculate eta_s and T_z from filtered data

clear PosZeroC;
clear HsPotFw;
clear HsdataFW;
zeroC=1;
PosZeroC(1,1)=1;

% Determining the number and position of the zero crossings of each txt-file
for j=1:(length(dataFW)-1)
    if  dataFW(j+1)>0 && dataFW(j)<0     %Localize zero up-crossing
        zeroC = zeroC+1;
        PosZeroC(zeroC,1)=j;
        TzFw(zeroC-1,1)=0.1*(PosZeroC(zeroC)-PosZeroC(zeroC-1));
    end
end
for i=1:(zeroC-1)
    HsPotFW(i,1)=max(dataFW(PosZeroC(i):PosZeroC(i+1)));
end

%   Calculating eta_s and Tz
 HsPotFW = sort(HsPotFW,'descend');
 HsdataFW = HsPotFW(1:length(HsPotFW)/3);
 HsPenFW(m,k) = mean(HsdataFW);
 TzPenFW(m,k)=mean(TzFw);


         %% Calculate eta_s and Tz from unfiltered data
zeroCu=1;
PosZeroCu(1,1)=1;
for j=1:(length(data)-1)
    if data(j+1)>0 && data(j)<0
        zeroCu = zeroCu+1;
        PosZeroCu(zeroCu,1)=j;
        Tz(zeroCu,1)=0.1*(PosZeroCu(zeroCu)-PosZeroCu(zeroCu-1));
    end
end
for i=1:(zeroCu-1)
    HsPotU(i)=max(data(PosZeroCu(i):PosZeroCu(i+1)));
end

         HsPotU = sort(HsPotU,'descend');
         Hsdata = HsPotU(1:length(HsPotU)/3);
         HsPen(m,k) = mean(Hsdata);
         TzPen(m,k)=mean(Tz);
     end
 end

 %% Plot figures

 L = 1:644; %Do not include any end effects
 % t1 = datetime (2018 ,4 ,11 ,11 ,0 ,0) ;
 % t2 = datetime (2018 ,5 ,8 ,6 ,0 ,0) ;
 % time = ( t1 : hours (1) : t2 ) ';
 time = datestr (( datetime (2018 ,4 ,11,11,0,0)+hours (1:644) ) ) ;
 time = datenum(time , 'dd-mm-yyyy HH:MM:SS' ) ;
 figure ()
```

```
 subplot(2 ,1 ,1)
 plot(time ,HsPenFW(L,1) )
 datetick ( 'x' , 'mmm-dd' , 'keepticks' , 'keeplimits' )
 hold on
plot(time ,HsPenFW(L,2) )
datetick ( 'x' , 'mmm-dd' , 'keepticks' , 'keeplimits' )
hold on
legend(  'Fish cage 8' , 'Fish cage 9' , 'location' , 'eastoutside' )
title ({['\fontsize{12} Calculated fish cage elevation for all ' newline...
    'sea states, cut off freq. ' num2str(wnL) ' Hz and ' num2str(wnH) ' Hz']})
xlabel( 'Time')
ylabel('Fish cage elevation [m]')
axis ([ time(1) time(end) -inf inf ])

subplot(2 ,1 ,2)
 plot(time ,HsPen(L,1) )
 datetick ( 'x' , 'mmm-dd' , 'keepticks' , 'keeplimits' )
 hold on
plot(time ,HsPen(L,2) )
datetick ( 'x' , 'mmm-dd' , 'keepticks' , 'keeplimits' )
hold on
legend(  'Fish cage 8' , 'Fish cage 9' , 'location' , 'eastoutside' )
title ({'\fontsize{12} Calculated fish cage elevation for all ' newline...
    'sea states, unfiltered data after integration'})
xlabel( 'Time' )
ylabel('Fish cage elevation [m]')
axis ([ time(1) time(end) -inf inf ])

 figure ()
 subplot(2 ,1 ,1)
 plot(time ,TzPenFW(L,1) )
 datetick ( 'x' , 'mmm-dd' , 'keepticks' , 'keeplimits' )
 hold on
plot(time ,TzPenFW(L,2) )
datetick ( 'x' , 'mmm-dd' , 'keepticks' , 'keeplimits' )
hold on
legend(  'Fish cage 8' , 'Fish cage 9' , 'location' , 'eastoutside' )
title ({['\fontsize{12} Calculated Tz for all sea states, ' newline...
    'cut off freq. ' num2str(wnL) ' and ' num2str(wnH)]})
xlabel( 'Time')
ylabel('Tz [s]')
axis ([ time(1) time(end) -inf inf ])

subplot(2 ,1 ,2)
 plot(time ,TzPen(L,1) )
 datetick ( 'x' , 'mmm-dd' , 'keepticks' , 'keeplimits' )
 hold on
plot(time ,TzPen(L,2) )
datetick ( 'x' , 'mmm-dd' , 'keepticks' , 'keeplimits' )
hold on
legend(  'Fish cage 8' , 'Fish cage 9' , 'location' , 'eastoutside' )
title ({'\fontsize{12} Calculated Tz for all sea states, ' newline...
    'unfiltered data after integration'})
xlabel( 'Time' )
ylabel('Tz [s]')
axis ([ time(1) time(end) -inf inf ])
```

B.7 Calculate elevations for each wave direction

Plotting calculated fish cage elevation and Hs from the wave buoy

```
% data for every wave direction (N, NE, E...). The directions are
% calculated within 45 degrees angle
% Example: East is between 67.5 degrees and 112.5 degrees.

clear all
clc

% bHs=Wave buoy data
% Hs8=Elevation data for fish cage 8
% Hs9=Elevation data for fish cage 9

NEcount=0;
Ncount=0;
NWcount=0;
Wcount=0;
SWcount=0;
Scount=0;
SEcount=0;
Ecount=0;

for i=1:length(WD)
    if 22.5<WD(i) && WD(i)<67.5
        NEcount=NEcount+1;
        NEM8(NEcount)=HsM8(i);
        NEM9(NEcount)=HsM9(i);
        NEB(NEcount)=bHs(i);
    elseif 67.5 < WD(i)&& WD(i)< 112.5
        Ecount=Ecount+1;
        EM8(Ecount)=HsM8(i);
        EM9(Ecount)=HsM9(i);
        EB(Ecount)=bHs(i);
    elseif 112.5 < WD(i) && WD(i)< 157.5
        SEcount=SEcount+1;
        SEM8(SEcount)=HsM8(i);
        SEM9(SEcount)=HsM9(i);
        SEB(SEcount)=bHs(i);
    elseif 157.5< WD(i) && WD(i) < 202.5
        Scount=Scount+1;
        SM8(Scount)=HsM8(i);
        SM9(Scount)=HsM9(i);
        SB(Scount)=bHs(i);
    elseif 202.5 < WD(i) && WD(i) <247.5
        SWcount=SWcount+1;
        SWM8(SWcount)=HsM8(i);
        SWM9(SWcount)=HsM9(i);
        SWB(SWcount)=bHs(i);
    elseif 247.5<WD(i) && WD(i) <292.5
        Wcount=Wcount+1;
        WM8(Wcount)=HsM8(i);
```

```
        WM9(Wcount)=HsM9(i);
        WB(Wcount)=bHs(i);
    elseif 292.5<WD(i) && WD(i) <337.5
        NWcount=NWcount+1;
        NWM8(NWcount)=HsM8(i);
        NWM9(NWcount)=HsM9(i);
        NWB(NWcount)=bHs(i);
    else
        Ncount=Ncount+1;
        NM8(Ncount)=HsM8(i);
        NM9(Ncount)=HsM9(i);
        NB(Ncount)=bHs(i);
    end
end
%% Plot figure

 figure ()
 subplot(3 ,1 ,1)
 plot(1:NWcount ,NWM8)
 hold on
plot(1:NWcount ,NWM9 )
hold on
plot(1:NWcount,NWB)
hold on
legend(  'Fish cage 8' , 'Fish cage 9' ,'Wave buoy', 'location' ,
'eastoutside' )
title ({'\fontsize{12} Comparison of fish cage elevation and incident waves
coming from north west direction'})
xlabel( 'Occurence no.')
ylabel('Fish cage elevation/wave elevation [m]')

 subplot(3 ,1 ,2)
 plot(1:Ncount ,NM8)
 hold on
plot(1:Ncount ,NM9 )
hold on
plot(1:Ncount, NB)
hold on
legend(  'Fish cage 8' , 'Fish cage 9' , 'Wave buoy', 'location' ,
'eastoutside' )
title ({['\fontsize{12} Comparison of fish cage elevation and incident waves
coming from north direction']})
xlabel( 'Occurence no.')
ylabel('Fish cage elevation/wave elevation [m]')


subplot(3 ,1 ,3)
plot(1:NEcount ,NEM8)
hold on
plot(1:NEcount ,NEM9 )
hold on
plot(1:NEcount, NEB)
hold on
legend(  'Fish cage 8' , 'Fish cage 9' , 'Wave buoy', 'location' ,
'eastoutside' )
title ({'\fontsize{12} Comparison of fish cage elevation and incident waves
coming from north east direction'})
```

```
xlabel( 'Occurence no.')
ylabel('Fish cage elevation/wave elevation [m]')


figure()
subplot(3 ,1 ,1)
 plot(1:Wcount ,WM8)
 hold on
plot(1:Wcount ,WM9 )
hold on
plot(1:Wcount,WB)
hold on
legend(  'Fish cage 8' , 'Fish cage 9' ,'Wave buoy', 'location' ,
'eastoutside' )
title ({'\fontsize{12} Comparison of fish cage elevation and incident waves
coming from west direction'})
xlabel( 'Occurence no.')
ylabel('Fish cage elevation/wave elevation [m]')


subplot(3 ,1 ,2)
 plot(1:SWcount ,SWM8)
 hold on
plot(1:SWcount ,SWM9 )
hold on
plot(1:SWcount, SWB)
hold on
legend(  'Fish cage 8' , 'Fish cage 9' , 'Wave buoy', 'location' ,
'eastoutside' )
title ({'\fontsize{12} Comparison of fish cage elevation and incident waves
coming from south west direction'})
xlabel( 'Occurence no.')
ylabel('Fish cage elevation/wave elevation [m]')


subplot(3 ,1 ,3)
 plot(1:Scount ,SM8)
 hold on
plot(1:Scount ,SM9 )
hold on
plot(1:Scount, SB)
hold on
legend(  'Fish cage 8' , 'Fish cage 9' , 'location' , 'eastoutside' )
title ({'\fontsize{12} Comparison of fish cage elevation and incident waves
coming from south direction'})
xlabel( 'Occurence no.')
ylabel('Fish cage elevation/wave elevation [m]')

figure()
subplot(2 ,1 ,1)
 plot(1:SEcount ,SEM8)
 hold on
plot(1:SEcount ,SEM9 )
hold on
plot(1:SEcount, SEB)
hold on
```

```
legend(  'Fish cage 8' , 'Fish cage 9' , 'Wave buoy','location' ,
'eastoutside' )
title ({'\fontsize{12} Comparison of fish cage elevation and incident waves
coming from south east direction'})
xlabel( 'Occurence no.')
ylabel('Fish cage elevation/wave elevation [m]')


subplot(2 ,1 ,2)
 plot(1:Ecount ,EM8)
 hold on
plot(1:Ecount ,EM9 )
hold on
plot(1:Ecount, EB)
hold on
legend(  'Fish cage 8' , 'Fish cage 9' , 'Wave buoy','location' ,
'eastoutside' )
title ({'\fontsize{12} Comparison of fish cage elevation and incident waves
coming from east direction'})
xlabel( 'Occurence no.')
ylabel('Fish cage elevation/wave elevation [m]')
```

B.8 Transfer functions for each wave direction

```
%% Calculate transfer functions for each wave direction
% Plotting the calculated transfer functions for every wave direction
% (N, NE, E....)
% The directions are calculated within 45 degrees angle
% Example: East is between 67.5 degrees and 112.5 degrees.

clear all
clc

% a=Wave buoy data
% b=Transfer function fish cage 8
% c= Transfer function cage 9

NEcount=0;
Ncount=0;
NWcount=0;
Wcount=0;
SWcount=0;
Scount=0;
SEcount=0;
Ecount=0;

for i=1:length(a)
    if 22.5<a(i) && a(i)<67.5
        NEcount=NEcount+1;
        NEM8(NEcount)=b(i);
        NEM9(NEcount)=c(i);
    elseif 67.5 < a(i)&& a(i)< 112.5
        Ecount=Ecount+1;
        EM8(Ecount)=b(i);
        EM9(Ecount)=c(i);
    elseif 112.5 < a(i) && a(i)< 157.5
        SEcount=SEcount+1;
        SEM8(SEcount)=b(i);
        SEM9(SEcount)=c(i);
    elseif 157.5< a(i) && a(i) < 202.5
        Scount=Scount+1;
        SM8(Scount)=b(i);
        SM9(Scount)=c(i);
    elseif 202.5 < a(i) && a(i) <247.5
        SWcount=SWcount+1;
        SWM8(SWcount)=b(i);
        SWM9(SWcount)=c(i);
    elseif 247.5<a(i) && a(i) <292.5
        Wcount=Wcount+1;
        WM8(Wcount)=b(i);
        WM9(Wcount)=c(i);
    elseif 292.5<a(i) && a(i) <337.5
        NWcount=NWcount+1;
        NWM8(NWcount)=b(i);
        NWM9(NWcount)=c(i);
    else
        Ncount=Ncount+1;
        NM8(Ncount)=b(i);
        NM9(Ncount)=c(i);
    end
end
```

```
  figure ()
  subplot(3 ,1 ,1)
 plot(1:NWcount ,NWM8)
 hold on
plot(1:NWcount ,NWM9 )
hold on
legend(  'Fish cage 8' , 'Fish cage 9' , 'location' , 'eastoutside' )
title ({'\fontsize{12} Calculated transfer function for waves coming from
north-west direction'})
xlabel( 'Occurence no.')
ylabel('Transfer function')

 subplot(3 ,1 ,2)
 plot(1:Ncount ,NM8)
 hold on
plot(1:Ncount ,NM9 )
hold on
legend(  'Fish cage 8' , 'Fish cage 9' , 'location' , 'eastoutside' )
title ({['\fontsize{12} Calculated transfer function for waves coming from
north direction']})
xlabel( 'Occurence no.')
ylabel('Transfer function')

subplot(3 ,1 ,3)
plot(1:NEcount ,NEM8)
hold on
plot(1:NEcount ,NEM9 )
hold on
legend(  'Fish cage 8' , 'Fish cage 9' , 'location' , 'eastoutside' )
title ({'\fontsize{12} Calculated transfer function for waves coming from
north-east direction'})
xlabel( 'Occurence no.')
ylabel('Transfer function')


figure()
subplot(3 ,1 ,1)
 plot(1:Wcount ,WM8)
 hold on
plot(1:Wcount ,WM9 )
hold on
legend(  'Fish cage 8' , 'Fish cage 9' , 'location' , 'eastoutside' )
title ({'\fontsize{12} Calculated transfer function for waves coming from west
direction'})
xlabel( 'Occurence no.')
ylabel('Transfer function')


subplot(3 ,1 ,2)
 plot(1:SWcount ,SWM8)
 hold on
plot(1:SWcount ,SWM9 )
hold on
legend(  'Fish cage 8' , 'Fish cage 9' , 'location' , 'eastoutside' )
```

```
title ({'\fontsize{12} Calculated transfer function for waves coming from
south-west direction'})
xlabel( 'Occurence no.')
ylabel('Transfer function')


subplot(3 ,1 ,3)
 plot(1:Scount ,SM8)
 hold on
plot(1:Scount ,SM9 )
hold on
legend(  'Fish cage 8' , 'Fish cage 9' , 'location' , 'eastoutside' )
title ({'\fontsize{12} Calculated transfer function for waves coming from
south direction'})
xlabel( 'Occurence no.')
ylabel('Transfer function')

figure()
subplot(2 ,1 ,1)
 plot(1:SEcount ,SEM8)
 hold on
plot(1:SEcount ,SEM9 )
hold on
legend(  'Fish cage 8' , 'Fish cage 9' , 'location' , 'eastoutside' )
title ({'\fontsize{12} Calculated transfer function for waves coming from
south-east direction'})
xlabel( 'Occurence no.')
ylabel('Transfer function')


subplot(2 ,1 ,2)
 plot(1:Ecount ,EM8)
 hold on
plot(1:Ecount ,EM9 )
hold on
legend(  'Net pen 8' , 'Net pen 9' , 'location' , 'eastoutside' )
title ({'\fontsize{12} Calculated transfer function for waves coming from east
direction'})
xlabel( 'Occurence no.')
ylabel('Transfer function')
```

Robert Hanssen

Spatial variations in wave conditions at aquaculture sites

NTNU
Norwegian University of
Science and Technology